Targeting Blood-Brain-Barrier Invasion in Cryptococcal Meningoencephalitis: Discovery of a Novel Antifungal Peptide and Identification of an EphA2-Dependent Transcellular Pathway

By

AMELIA BRIE BENNETT

DISSERTATION

Submitted in partial satisfaction of the requirement for the degree of

DOCTOR OF PHILOSOPHY

in

Microbiology

in the

OFFICE OF GRADUATE STUDIES

of the

UNIVERSITY OF CALIFORNIA

DAVIS

Approved:

_____

Angela Gelli, Chair

_____

Reneé Tsolis

_____

Bennett Penn

Committee in Charge

2026

DEDICATION

First and foremost, I would like to thank Dr. Angela Gelli for constantly challenging me to think critically, pushing me beyond my limits, and encouraging me to strive for excellence. Your high standards and dedication to science shaped me into a more confident, independent researcher. I am incredibly grateful that you provided me with the opportunity to start fresh, train in your lab and build a strong scientific and professional foundation.

Next, I am profoundly thankful to my parents, Ethell and Samuel Bennett, for their endless sacrifices, love, and steadfast support throughout my life. You worked tirelessly to create opportunities that you did not have, ensuring that I could pursue higher education and achieve my dreams. Being the first in our family to attend college and earn a doctoral degree is a testament to your resilience, faith, and belief in me. Earning this doctorate transcends my own ambition; this accomplishment belongs to my family as much as it does to me.

I would also like to sincerely thank my mentors, Dr. Avery August and Dr. Ruth Diana Lee. Dr. August, thank you for giving me my very first research opportunity and introducing me to the world of scientific discovery in your laboratory. You taught me how to read scientific literature critically, how to ask meaningful questions, and how to present research with clarity and confidence—skills that have guided me throughout my academic journey. Furthermore, your support did not end when I graduated college. Throughout graduate school, you have always been just one email or zoom call away and for that, I am immensely grateful. Dr. Lee, thank you for your constant support during graduate school—for troubleshooting experiments with patience, providing thoughtful and constructive feedback on my writing and presentations, and for the immense emotional encouragement you offered during challenging times. Your mentorship extended far beyond the bench, and your unwavering support was my lifeline when I felt like giving up. I am grateful for the gift of knowing you and calling you a close friend.

To my students that I have taught and mentored—thank you. Getting to know each and every one of you has been nothing short of a privilege. I learned so much from the personal stories that you shared with me and I developed a toolbox of instructional techniques that I will carry with me. Furthermore, mentoring underrepresented students in programs like MESA, Ronald E. McNair scholars program and SACNAS has had a particularly profound impact on me throughout graduate school. These programs helped me pursue graduate school when I was in college and being on the other side of the experience working with students in these programs helped me gain deeper self-awareness and perspective on my own journey. My only hope is that you continue to help those that are in need of support whether you think you are “qualified enough“ or not (you will surprise yourself with the wisdom and insights you have to share).

Finally, I want to acknowledge Dr. Vernessa Roberts, Dr. Milagros Copara, my godmother, Deborah Calhoun, Darlene Rodriguez, Chenell McBean, Dr. Nathaniel Pineda and Anna Watkins for the profound personal growth you helped foster during my graduate training. Despite attending school almost 3000 miles away from home, you all were my community and
my chosen family. Thank you for endless laughs, three to four hour facetime calls, the trivia nights and most importantly, challenging me to reflect, grow, and lead with intention. Your guidance, conversations, and encouragement helped me develop not only as a scientist but as a person.

To everyone who supported me throughout this journey—thank you. This milestone represents years of mentorship, sacrifice, growth, and perseverance, and I carry each of you with me as I move forward.

ABSTRACT

Cryptococcus neoformans (*Cn*) is an opportunistic, neuroinvasive fungal pathogen that causes life-threatening meningoencephalitis and frequently results in long-term cognitive impairment despite antifungal treatment. *Cn* gains access to the central nervous system (CNS) by traversing the blood–brain barrier (BBB), yet the molecular mechanisms governing fungal entry into brain endothelial cells remain incompletely understood. The disproportionate global burden of Cryptococcal meningoencephalitis (CM) underscores the need to define the host-pathogen signaling events that enable BBB infiltration and to develop improved therapeutic strategies.

In this thesis, I first establish the cellular and molecular architecture that regulates trafficking across the BBB and outline canonical mechanisms of microbial entry, focusing on *Cn* as a clinically urgent model of fungal neuroinvasion. I then demonstrate, using both human three-dimensional BBB organoids and conventional two-dimensional in vitro BBB models, that *Cn* exploits macropinocytosis as its primary mode of endothelial internalization. Mechanistically, I show that capsular hyaluronic acid engages CD44, which functions in concert with the receptor tyrosine kinase EphA2 as a functional receptor complex to drive macropinocytotic uptake of *Cn*. Structural modeling identified two predicted binding regions on EphA2 that may cooperatively regulate signaling events required for fungal internalization.

In parallel, a complementary therapeutic strategy targeting the fungal membrane is discussed. Using a one-bead, one-compound high-throughput screening strategy, we identified LBF127, a peptide that selectively binds fungal giant unilamellar vesicles over mammalian giant unilamellar vesicles and exhibits antifungal activity with limited hemolytic and cytotoxic effect. Structure–activity relationship optimization yielded K-oLBF127, a shorter, derivative with enhanced fungal membrane selectivity, increased anti-fungal potency, and reduced toxicity toward mammalian cells. In a murine model of cryptococcal infection, K-oLBF127 significantly reduced lung fungal burden, demonstrating in vivo efficacy.

Together, these findings define a host receptor axis regulating *Cn* traversal of the BBB and advance the development of selective antifungal membrane-active peptides. By integrating mechanistic insight into endothelial invasion with rational antifungal design, this work provides complementary strategies to better understand and therapeutically target cryptococcal disease.

TABLE OF CONTENTS

CHAPTER 1

INTRODUCTION

1. Microbial traversal of the Blood-Brain-Barrier (BBB)

The central nervous system (CNS) is a metabolically demanding, highly specialized organ system whose function depends on tightly regulated exchange with the systemic circulation. [1] To preserve homeostasis while permitting nutrient and gas exchange, the brain is protected by three anatomically and functionally distinct barriers: (1) the arachnoid barrier, (2) the cerebrospinal fluid (CSF), and (3) the BBB. [2,3] Of those three barriers, the BBB is considered the principal interface governing blood-CNS exchange and serves as the dominant structural and biochemical checkpoint safeguarding the brain parenchyma. Rather than a passive wall, the BBB is considered a highly selective, dynamic and complex structural/ biochemical interface that is responsible for supplying the brain parenchyma with oxygen and nutrients while also removing waste products. Maintenance of BBB integrity is therefore fundamental to neuronal survival.

Outside of regulating exchange, one of the primary roles of the BBB is to protect the brain from infection and damage by shielding the brain from toxins, pathogens and harmful fluctuations in blood chemistry. [4–6] Despite the tightly regulated, multicellular architecture of the BBB which is maintained by coordinated interactions among endothelial cells, pericytes, astrocytic end feet, and associated components of the neurovascular unit (NVU), neurotropic pathogens have evolved sophisticated mechanisms to exploit or disrupt these elements, enabling traversal of the BBB and subsequent establishment of central nervous system infection. Infections of the CNS are especially critical as they often lead to irreversible neurological damage, and diagnosis and treatment of these infections remain difficult due to the intricate nature of the BBB. Consequently, CNS infections carry higher mortality and morbidity rates compared to other infections.

A mechanistic understanding of how the BBB regulates permeability under physiological conditions–and how pathogens subvert these regulatory mechanisms–is therefore essential. Identifying the molecular pathways that mediate microbial traversal of the BBB provides a critical foundation for the development of targeted host-directed and pathogen-directed therapeutics.

Accordingly, this chapter first outlines the cellular architecture that confers BBB restriction, then summarizes canonical routes of microbial entry, and finally narrows to *Cryptococcus neoformans* as a clinically urgent model organism in which key host receptors (CD44 and EphA2) and a candidate endocytic pathway (macropinocytosis) provide a mechanistic framework for BBB traversal.

The NVU: Structural and Functional Regulation of BBB Transport

The restrictive properties of the BBB arise not from endothelial cells alone, but from the integrated function of the NVU.[4] The specialized cells that make up the NVU include brain microvascular endothelial cells (BMECs), pericytes, astrocytes and microglia. Each cell plays a vital role in regulating transport in and out of the brain, but together, these cells establish a coordinated regulatory network that preserves barrier integrity while permitting precisely controlled molecular exchange. BMECs form the physical and functional backbone of the BBB and are therefore the first cells to come in contact with molecules in the blood. Unlike peripheral endothelial cells, BMECs strictly regulate molecule paracellular transport via specialized tight junction (TJ) proteins and molecule transcellular transport due to its low pinocytic activity.[7,8] Specialized TJ proteins, including claudins, occludin, and junctional adhesion molecules, seal the intercellular space, limiting nonspecific paracellular transport. These features collectively establish the highly restrictive endothelial phenotype unique to the CNS.

Pericytes, embedded in the vascular basement membrane, are critical for vascular stability and directly influence endothelial tight junction formation and maintenance. Pericytes reinforce endothelial barrier function by regulating BBB-specific gene expression patterns and promoting polarization of astrocyte end-feet (another cell type found in the NVU).

Astrocytes contribute to basement membrane formation and upregulate endothelial transporters and metabolic enzymes that define BBB identity. Astrocyte end-feet envelop nearly the entire basolateral surface of BMECs (nearly 99%), providing both the structural support and paracrine signaling necessary to sustain the BBB .[9,10] Additionally, perivascular astrocytes provide an additional barrier against the passage of molecules in and out of the brain by producing a 40-50 nm thick basal lamina.[11]

Microglia, the other glial cell found in the NVU and resident immune cells of the CNS, provide immunological surveillance while modulating inflammatory responses that influence barrier permeability. Under pathological conditions, microglial activation can either preserve or disrupt BBB integrity, depending on the inflammatory milieu. [12–14]

Altogether, the NVU represents a tightly regulated system that enforces the selective permeability of the BBB. However, neurotropic pathogens have developed mechanisms to circumvent these strategies, exploiting host cellular processes to initiate CNS invasion.

Mechanisms of Pathogen Infiltration of the Blood-Brain-Barrier (BBB)

Neurotropic Pathogens including bacteria, amoebae, viruses and fungi employ three principal mechanisms to cross the BBB: the “Trojan horse” method, paracellular entry and/or transcellular migration.[15,16]

In the Trojan horse mechanism, pathogens hijack peripheral immune cells that typically cross the arachnoid barrier.[17] Rather than directly invading endothelial cells, microbes survive within host immune cells and exploit their migratory capacity to gain CNS access. This route of entry has been demonstrated with *Listeria monocytogenes* [18], *Burkholderia psuedomallei* [19], *Streptococcus suis* [20] and *Mycobacterium tuberculosis.* [21]

Paracellular traversal involves disruption of tight junction integrity. Pathogen-derived toxins, proteases, or host inflammatory responses destabilize junctional complexes, permitting

intercellular passage into the brain parenchyma. [22] Paracellular migration has been demonstrated for *Escherichia coli K1* [23], *Streptococcus pneumonia* [24] and *Haemophilus influenza type B* [25,26], *Trypanosoma spp*. [27,28] and *Borrelia spp.* [29,30]

Transcellular migration, in contrast, requires direct interaction with endothelial surface receptors. Pathogens adhere to BMECs, trigger receptor-mediated signaling cascades, and induce endocytic internalization, traversing the endothelial cytoplasm before exiting on the abluminal side. This mechanism is particularly relevant for pathogens that depend on host receptor engagement to drive cytoskeletal remodeling and vesicular trafficking, like *E. coli* [32], *H. influenzae* [33], *S. suis* [34], *L. monocytogenes* [35], *Group B streptococcus* [36], *M. tuberculosis* [37], *Trypanosoma spp*. [28], *Borrelia spp.* [30], *Streptococcus agalactiae* [38], *S. pneumoniae* [39], *Neisseria meningitidis* [40] and *C. albicans.* [41]

Although a variety of pathogens have been noted to breach the BBB and cause infection, infections of the CNS by fungi have the highest morbidity and mortality when compared to other causative agents of CNS infections.[42] Among these, *Cryptococcus neoformans (Cn)* is the leading cause of fatal fungal meningoencephalitis worldwide. The disproportionate clinical burden motivates a focused mechanistic discussion of how *Cn* serves as a dominant and tractable model for understanding host–pathogen signaling at the brain endothelium.

2. Cryptococcal Meningoencephalitis (CM): Clinical Burden and Therapeutic Limitations

Fungal Infections of the CNS

Fungal infections of the CNS are the most difficult to treat because (1) it is nearly impossible to completely eradicate the fungus once it is discovered in the brain and (2) fungal infections of the CNS tend to occur primarily in individuals that are immunocompromised, like AIDS patients,

individuals taking immunosuppressive therapy, organ transplant recipients and patients undergoing cancer treatment. [43] *Cryptococcus neoformans* (*Cn*), *Candida albicans*, and *Aspergillus spp*., *Mucor, Coccidioides spp*., and *Histoplasma capsulatum* are the most common causes of fungal brain infections. Once they have infected the CNS they replicate profusely resulting in a chronic meningoencephalitis, or inflammation of the brain tissue and its protective membranes. [43,44] The most common and fatal form of fungal meningoencephalitis is Cryptococcal Meningoencephalitis (CM). [45] CM causes neurological sequelae including visual loss, cranial palsies, neurologic deficit or mental impairment in both treated and untreated patients. If left untreated, it is 100% fatal, and even with treatment, mortality rates remain high (often 10-70%) depending on the region. [46–50] Despite current treatment protocols, to date, CM is the cause of 15–20% of global AIDS-related mortality. [51]

Current therapeutics of CM

The current recommended treatment plan for an individual with CM involves three stages - induction therapy (to rapidly reduce fungal load), consolidation therapy (to eradicate remaining fungi), and maintenance therapy (long-term, low dose therapy to prevent relapse). For the induction phase of treatment, it is recommended that patients are administered 1-2 weeks of liposomal Amphotericin B combined with oral flucytosine.[52,53] Amphotericin B is a polyene antifungal agent that binds to ergosterol and forms pores that disrupt fungal membranes.[54,55] Flucytosine enters through these pores and inhibits DNA and protein synthesis. [56,57] Following successful induction, consolidation is typically 8 weeks of fluconazole, which inhibits ergosterol synthesis.[57] After consolidation, maintenance entails lower-dose fluconazole for 6 months to lifelong depending on patient factors. [56] Despite this regimen, two major problems persist: (1) inaccessibility to treatment where CM burden is highest, and (2) *Cn's* increasing antifungal resistance.

Issues with the current antifungal drugs

CM continues to have a large global impact despite the roll out of Antiretroviral therapy and pre-exposure prophylaxis, because the current antifungal drugs used in the CM treatment plan are not available to those that need it most. In resource-limited settings, intravenous administration of liposomal amphotericin B (which has been determined as the most effective administration of this drug) is too expensive, making it unattainable for many patients. Instead, individuals are administered the conventional amphotericin deoxycholate (AmBd) which can cause significant kidney damage and lead to electrolyte imbalances. Additionally, these same regions also do not have access to flucytosine, undermining induction therapy. As a result, patients may require repeated lumbar punctures to manage intracranial pressure until they succumb to disease. Hence, there is a striking global disparity in CM morbidity and mortality between high and low-income countries; in the U.S., there are approximately 3,400 new cases of CM and 700 deaths annually, whereas globally, 223,100 cases occur yearly with approximately ¾ of those cases occurring in Africa. [52,58–60] Mortality in resource-limited settings approaches ~70%, with ~135,900 deaths annually in sub-Saharan Africa alone.[61]

In parallel, *C. neoformans* is showing increased resistance to azoles such as fluconazole via mechanisms including chromosomal aneuploidy, upregulation of efflux pumps, mutations in sterol 14α-demethylase, and heteroresistance. [62–64] These challenges create a critical unmet need for better treatments; therefore, it is imperative that we investigate the molecular mechanisms of *Cn* traversal across the BBB to identify novel therapeutic targets and focus our efforts on developing improved antifungal drugs.

Because CNS disease is the lethal endpoint of cryptococcosis and because current therapies are limited by BBB penetration, toxicity, access, and resistance, defining the host–pathogen mechanisms that enable BBB crossing becomes a high-yield point of intervention.

3. Pathogenesis of *Cn*, from exposure to CNS tropism

Cryptococci species and their environmental niches

The global burden of CM is in large part due to the basidiomycetes fungi, *C. neoformans*. *Cn* spores are present across the globe and associated with various tree species, excreta of feral pigeons, and soil inhabitants such as amoebae and soil nematodes. [65] Of the 30 *Cryptococcus* species found in the environment, *Cn* accounts for over 95% of cryptococcal infections, causing disease in both immunocompromised and immunocompetent hosts. [65–67] Interestingly, *Cn* is considered to be an accidental pathogen, meaning that it has not been under direct selection for virulence within a mammalian host, but has evolved traits in response to selection pressures within environmental and animal niches that were ultimately advantageous to *Cn* infection of mammals. [68–70] Despite this, *Cn* proves to be a highly virulent, stealthy and lethal pathogen.

Pathogenesis of *Cn*

To establish infection within a human host, *Cn* spores must first be inhaled and infect the lungs. Given the ubiquitous nature of *Cn* and the fact that every human inhalation contains 1-10 fungal spores, human exposure to *Cn* spores is predicted to be near universal, first occurring in early childhood.[70] Once inhaled by immunocompromised patients, *Cn* may persist asymptomatically for indefinite periods of time within granulomas (benign clusters of immune cells). [70] While being sequestered by granulomas, *Cn* is then capable of operating as a facultative intracellular pathogen where control of *Cn* is reliant on robust cell-mediated immunity, characterized broadly by a T-helper 1 (Th1) profile. Thus, in HIV/AIDS patients who have lower Th1 cells and reduced production of Th1 associated cytokines, either persistent or newly acquired *Cn* can proliferate within the lungs and disseminate to any organ in the body. Of all the organs in the body, *Cn* has a predilection for infecting the CNS. [70]

Mechanism of *Cn* infiltration of the BBB

As previously mentioned, researchers have identified three mechanisms by which *Cn* can penetrate the BBB and subsist in the CNS: “Trojan horse”, paracellular and transcellular crossing. In the “Trojan horse” mechanism, *Cryptococcus*- engulfing phagocytes breach the BBB, and *Cn* exits via nonlytic exocytosis (vomocytosis). [71,72] *Cn* can also travel freely in the bloodstream, lodge in capillaries, and cross the BBB directly via paracellular or transcellular mechanisms. [73–75] During paracellular crossing, *Cryptococcus* migrates through the specialized tight junctions between BMECs. [73] To facilitate paracellular entry, several studies suggest that *Cn* uses phospholipase B1 (PLB1) and several enzymes, including urease and a metalloprotease (Mpr1). [76–78] It is thought that *Cn* uses PLB1 and urease to damage BMECs and weaken the endothelial vessel wall to promote fungal entry into the brain parenchyma; PLB1 can degrade host phospholipids and urease can generate toxic ammonia. Mpr1 targets BBB surface components triggering the reorganization of actin cytoskeleton elements. [76]

During transcellular crossing, cryptococci use capsular hyaluronic acid (HA) to adhere to and become internalized by brain endothelium, transmigrating through BMEC cytoplasm to exit basolaterally and invade the parenchyma. [75]

Extensive evidence has demonstrated that the NVU permits and even facilitates the regulated entry of phagocytes across the BBB during injury, infection or neuroinflammation; therefore it is logical that *Cn*-infected phagocytes will readily penetrate brain parenchyma.[79] However, despite the growing knowledge about fungal gene products that play a role in the transcytosis of *Cn* across the BBB, the identity and details of key signaling pathways in the brain endothelium that mediate the transcellular and paracellular movement of cryptococci into the CNS have yet to be fully elucidated.

Among host factors implicated in cryptococcal transcytosis, CD44 and EphA2 have emerged as a receptor axis that plausibly links fungal adhesion to endothelial cytoskeletal

remodeling — a connection with direct implications for both transcellular uptake and barrier permeability.

4. The Eph-ephrin signaling pathway and its role in *Cn* pathogenesis

The role of CD44 in Cryptococcal adherence and internalization

The molecular mechanisms that facilitate *Cn* breach of the BBB are just beginning to be identified. Multiple studies have determined that a host glycoprotein, CD44, plays a key role in the adherence of *Cn* to BMECs. [76,80] The CD44 receptor binds to the capsule-bound hyaluronic acid (HA) on the surface of cryptococcal cells, leading to attachment, actin remodeling and fungal engulfment. [80,81] High levels of inositol in the brain triggers this CD44-HA process by increasing expression of HA on fungal cells. [86] One study demonstrated that knockdown of CD44 in human

BMECs significantly reduced the adherence of *Cn* while another study showed that CD44 knockout mice showed improved survival and less brain fungal burden. [76,80,82] Recently, another host protein has proved to be important in the transcellular crossing of *Cn*. A tyrosine kinase receptor called EphA2 has been shown to mediate the migration of *Cn* across the BBB in a CD44-dependent manner. [8]

Structure and physiological roles of the tyrosine kinase receptor, EphA2

The Erythropoietin- producing hepatocellular (Eph) family of receptor tyrosine kinases (RTKs) and their membrane-tethered ligands, known as ephrins, constitute the largest RTK sub-family; almost one fourth of the 59 human RTKs, with at least 14 receptors and nine ligands [84–86]. Eph receptors are grouped into EphA and EphB classes based on binding preferences and structural features. [87] There are nine different functional EphA receptors in mammals known to date (EphA1-EphA9) that can bind to five different GPI- tethered class A ephrins (ephrin A1- ephrin A5) and there are five class B receptors (EphB1,2,3,4,and 6) that can bind to three transmembrane-tethered B class ephrins (ephrin B1- ephrin B3). [84] Both classes of receptors

include (1) an extracellular portion that consists of an N-terminal glycosylated ligand-binding domain, a region rich in cysteines and two fibronectin type III repeats, (2) a transmembrane linker segment and (3) a cytosolic portion that mediates protein-protein interactions through the SAM motif, a PDZ binding motif and its kinase domain. [84]

Eph receptors and their ligands have been known to regulate development, synaptic connectivity, and plasticity in the CNS. [95,104,106] The EphA2 receptor in particular is highly expressed on BMECs and other NVU cells, including pericytes, astrocytes, and microglia. However, despite the high expression of EphA2 on the cells involved in regulating transport in and out of the brain, the role that EphA2 plays in this BBB maintenance during neuropathogenesis has yet to be fully understood. [96]

Role of EphA2 in pathogenesis and cryptococcal BBB traversal

The role of the Eph/ephrin system in development and homeostasis is reliant on its ability to induce alterations to the cytoskeletal system of a cell. [84,85,87] As a consequence, the Eph/ephrin system has been exploited by a number of pathogens to gain intracellular and intercellular entry into cells and organ systems to establish infection. [85,97] The EphA2 receptor in particular has been shown to play a role in the pathogenesis of: Kaposi's sarcoma associated herpes virus in endothelial and fibroblast cells, *Chlamydia trachomatis* in uterine epithelial cells, *Epstein-Barr* Virus in epithelial cells, *Human Cytomegalovirus* in glioblastoma cells, *Candida albicans* in epithelial cells and neutrophils, and *Helicobacter pylori* in gastric cells.[98–102] Given the high expression of EphA2 receptors in the brain, the role of these receptors in neuropathology has been of great interest more recently. One study found that EphA2 was upregulated in cerebral malaria , and in an EphA2 knockout mouse model improved survival and BBB integrity were observed throughout the progression of the infection. [96]

In 2018, we established that during cryptococcal infection of the CNS, EphA2 activation is required for *Cn* migration across immortalized BMECs (iBMECs). We determined that (1) EphA2

was activated during the transcellular crossing of *Cn* across iBMECs, (2) activation of EphA2 with its ligand, ephrinA1, or with an agonist, doxazosin, resulted in a significant increase in the number of *Cn* able to cross iBMECs, (3) alternatively, siRNA knockdown of EphA2 or blocking of EphA2 with monoclonal antibodies or treating EphA2 with the inhibitor, dasatinib, prevented the migration of *Cn* across iBMECs, and (4) overexpression of EphA2 in a mammalian cell line that does not typically internalize *Cn*, Hek293T cells, promoted the internalization of *Cn.* [83]

Receptor cross talk between CD44 and EphA2

Despite evidence demonstrating that both EphA2 and CD44 are involved in the transcytosis of *Cn*, whether and how these proteins interact has not been fully elucidated. Data gathered thus far implies that the two receptors work together to facilitate the engulfment of *Cn* by BMECs. A direct interaction between *Cn* and host glycoprotein CD44 on BMECs to aid in adherence has been established, but CD44 signaling alone is not clearly sufficient to trigger engulfment of a cryptococcal-sized particle.[76,80] Conversely, despite the lack of evidence of direct *Cn*-EphA2 binding, it has also been established that (1) EphA2 is required for *Cn* transcytosis and (2) EphA2 has induced signaling pathways that lead to the engulfment of other pathogens.[83]

Chapter 2 of this thesis demonstrates receptor cross talk between CD44 and EphA2 during cryptococcal infection. We first employed Alphafold3, and found two plausible binding sites, CD44 and another located in the ligand binding domain of EphA2. Next, we used biochemical assays including proximity dependent ligation assay and co-immunoprecipitation to confirm that EphA2 and CD44 interact in iBMECs and HEK293 cells (exposed to *Cn*) respectively. We show that EphA1 downstream signaling does not occur during infection with an HA-deficient mutant (∆cps1), suggesting CD44 activation is required. Altogether, these data support a model in which *Cn* activates CD44 via HA and activated CD44 transactivates EphA2 to facilitate BBB crossing. However, despite previous studies providing extensive evidence that EphA2 is required for the transcytosis of *Cn*, we have yet to investigate how EphA2 activation facilitates the traversal of *Cn* across the BBB.

Downstream signaling pathway of EphA2

EphA2 signaling engages effectors including Src family kinases and Ras/Rho family GTPases, which regulate actin organization and cell adhesion. [85,103] In response to extracellular cues through cell surface receptors (such as the Eph receptors), Rho family GTPases are activated by GEFs and inactivated by GAPs, enabling rapid, spatially controlled cytoskeletal remodeling. [84,104] Eph receptors use this machinery to drive cell repulsion, adhesion, and migration. In fact, EphA2 activation has been shown to elevate GTP-Rac1 via Vav GEFs in vascular endothelium.[105–107] Eph signaling effects on the cytoskeleton can also alter junctional proteins, redistributing E-cadherin and destabilizing claudins. A previous study determined that Eph forward signaling induces redistribution of E-cadherin to the cell surface while destabilizing claudins in mammalian epithelial cells, while another study determined that EphA2 overexpression destabilized adherens junction proteins. [104,108,109]

Given that *Cn* depends on EphA2 to cross BMECs, and that EphA2 induces cytoskeletal and junctional remodeling, EphA2 activation could plausibly promote a transcellular endocytic mechanism and/or junctional permissiveness facilitating paracellular passage.

5. BMECs engulf *Cn* via Macropinocytosis

Endocytic pathways

Endocytosis describes the internalization of particles, molecules, and fluids via plasma membrane invagination to form internal vesicles. Endocytosis allows for cells to (1) adapt to varying nutrient availability by internalizing necessary materials for growth and survival, (2) perform cellular defense by engulfing cytokines and/or immune receptors and destroying pathogens and (3) communicate with other cells in the body by engulfing external signals for growth, migration and differentiation. [110,111] Most major types of endocytosis require actin, which provides force for membrane protrusions/invaginations and vesicle trafficking. [112]Given EphA2's

role in actin remodeling through Rho GTPases, it is well-positioned to regulate pathogen internalization.[85,103]

Why is clathrin-mediated endocytosis insufficient?

The canonical endocytic route for internalization of various cargoes is clathrin-mediated endocytosis (CME).[113] CME internalizes cargo via clathrin-coated pits and vesicles typically ~60-100nm in diameter. [114,115] Although EphA2 can stimulate CME in some infections (e.g., during Kaposi's Sarcoma-associated Herpesvirus (KSHV) entry into human foreskin fibroblast cells), CME cannot engulf *Cn* given the typical diameter of *Cn* is 4-10 μm. [116,117] Given that *Cn* is dependent on EphA2 to achieve transcellular crossing of BMECs, it is likely that EphA2 plays a role in inducing another type of endocytic event.

The endocytic mechanism, Macropinocytosis

Macropinocytosis is a nonspecific endocytic pathway capable of rapidly internalizing large amounts of membrane and extracellular fluid. It is transiently triggered by signaling pathways that induce global actin polymerization, producing membrane ruffles that collapse into macropinosomes. The vesicle size, typically 5-10 μm in diameter, makes macropinocytosis compatible with fungal uptake.[120–122]

Multiple pathogens exploit macropinocytosis, and several studies note ruffling in BMECs infected with *Cn*. Investigating macropinocytosis in cryptococcal neuroinvasion could clarify molecular mechanisms of transcellular crossing, reveal BMEC-specific features of this pathway, and inform therapeutic delivery strategies into the CNS.

Evidence supporting macropinocytosis in *Cn* pathogenesis

There are several reasons why macropinocytosis has been investigated as a promising endocytic pathway for the transcytosis of *Cn* across BMECs. [123] (1) Macropinocytosis is commonly initiated downstream of receptor tyrosine kinase signaling that drives global actin polymerization. Because EphA2 activation engages Rho GTPases and reorganizes the cytoskeleton, it is well

positioned to initiate the actin dynamics required for macropinocytic uptake. (2) The nonselective nature and large vesicle size (5–10 μm) of macropinosomes would confer a clear advantage for a 4–10 μm fungal cell. (3) Many pathogens exploit this pathway, including bacteria (*Salmonella* [125], *Shigella* [126], *Mycobacterium* [127], *Legionella* [128], *Brucella* [129] and *Burkholderia cenocepacia* [130]), protozoa (*Leishmania mexicana* [131], *L. donovani* [131]and *Trypansoma cruzi* [132]) and viruses (*Ebola* [133], *HIV-1* [134], *Vaccinia* [135], *Adenovirus 3* [136], *Echovirus 1* [137], *Coxsackievirus B* [138] and *SARS-CoV-2* [139]).

The nonspecific nature and lack of unique cellular markers of macropinocytosis can make it difficult to study.[124,142] As a result, several requirements must be met to support the conclusion that macropinocytosis mediates engulfment of *Cn.*

First, there should be evidence that *Cn* induces cytoskeletal rearrangements to form membrane ruffling. In addition to multiple studies of *Cn* pathogenesis that have noted a distinct ruffled morphology in BMECs infected with *Cn*, a hallmark feature of macropinocytosis; in a previous study, we used confocal light microscopy to demonstrate that during infection, *Cn* colocalizes with F actin during engulfment. [68,140,141]

Second, engulfment of *Cn* should be dependent on amiloride, an inhibitor of sodium proton exchangers. The inhibition of sodium proton exchangers alters intracellular pH and impairs Rho GTPases.[143] Studies have demonstrated that amiloride specifically inhibits macropinosome formation with no detectable impact on other endocytic pathways.[144] In chapter 2, we demonstrate that the transcytosis of *Cn* is reliant on amiloride using a transwell assay: pretreatment or cotreatment with amiloride significantly decreased transcytosis, and this reduction was not attributable to decreased fungal viability or altered virulence factor expression.

Third, engulfment of *Cn* should be reliant on either Rac1 or Cdc42 GTPase activation. There are three main types of Rho family GTPases including RhoA, Rac1 and Cdc42. The RhoA GTPase primarily regulates stress fibers and focal adhesions, whereas Rac1 and Cdc42

GTPases drive protrusive structures such as lamellipodia and filopodia, respectively. [117] Using an ELISA-based assay to quantify GTP-bound versus GDP-bound Rho GTPases, we found a significant increase in GTP-bound Cdc42 during *Cn* infection. In contrast, EphA2-/- iBMECs or iBMECs infected with the HA-deficient mutant (Δcps1) failed to activate this GTPase.

Finally, macropinocytosis should be associated with increased fluid-phase uptake. Because macropinocytosis internalizes extracellular fluid as ruffles collapse and seal, it results in substantial fluid uptake — in contrast to phagocytosis, where close apposition of membrane to cargo limits unoccupied volume.[120] We demonstrate that *Cn* induces fluid uptake in iBMECs using confocal microscopy: *Cn* promoted uptake of a fluorescent fluid-phase marker and colocalized with this marker in the perinuclear region, consistent with co-localization within the same intracellular vesicle. This was not observed in amiloride-treated iBMECs or in EphA2-/- iBMECs.

Collectively, our studies identify EphA2 as the key molecular driver of macropinocytosis during *Cn* infection of the BBB, supporting EphA2 as a potential therapeutic target to inhibit transcellular crossing into the CNS.

6. Novel antifungal peptide to treat CM

Benefits of antimicrobial peptides

While host targets are promising, the mortality of CM also motivates development of novel antifungals that are more efficacious and less toxic than current drugs. Antifungal peptides are particularly attractive due to multi-target mechanisms, lower likelihood of resistance, and potential for *de novo* fungal targets with reduced host toxicity.[145–148,152] Because fungi are evolutionarily close to humans, antifungal drug development is constrained by toxicity and limited unique targets. Antifungal peptides that target cell wall features offer an accessible therapeutic strategy distinct from mammalian cells.

Challenges of developing peptide drugs

Peptide drugs face pharmacokinetic limitations including low metabolic stability and rapid clearance. These limitations arise from peptide structure and susceptibility to proteases. [153] However, strategies such as cyclization, D-amino acid substitution, PEGylation, and nanoparticle encapsulation can improve stability and half-life, making peptide therapeutics increasingly feasible.[154,155]

Antimicrobial peptide usage

Antimicrobial peptides (AMPs) have been used to combat a variety of pathogens including bacteria, viruses and fungi. [156,157] Despite the vast majority of AMP research and development primarily focusing on bacterial and viral pathogens, there has been an increased effort in expanding antifungal peptide drugs. The *de novo* antifungal peptide drugs that have been developed, primarily target membrane integrity leading to leakage and cell death and target chitin or glucan synthesis, inhibiting formation of the cell wall. [158] Antifungal peptide drugs have been designed to target *Candida albicans* (Protegrins 1-5, Protonectin and Lactoferricin), *Aspergillus fumigatus* (Thanatin) and *Candida glabrata* (Protonectin). [159–162] Despite these developments, there are no AMP drugs approved and, on the market, specifically targeting *Cn*. Given the benefits of developing antifungal peptides, if we were to focus our efforts on developing and AMP against *Cn*, we could potentially have a significant impact on the rates of mortality due to CM. [63,64]

One-bead, one-compound (OBOC) combinatorial library is an effective antifungal screening method

To address the shortage of effective and non-toxic antifungal agents, one-bead, one-compound (OBOC) combinatorial libraries enable rapid screening of millions of peptides (including unnatural and D-amino acids), discovery of non-obvious motifs, and direct sequencing of active peptides. In chapter 3, we propose the use of one-bead, one-compound (OBOC) combinatorial library methods to develop new membrane active, fungicidal peptides that

demonstrate selectivity toward fungal membranes over mammalian membranes. [163] Specifically, we applied this method to identify a novel membrane-active peptide (LBF127) and we optimized it to increase antifungal potency and to reduce hemolysis and we demonstrate its activity against *Cn* in vitro and in vivo.

7. Summary

Focusing our efforts on developing novel therapeutics and identifying novel targets is vital to decreasing the mortality of CM. Understanding how *Cn* invades the BBB can identify host molecules responsible for entry and motivate prophylactic strategies to prevent CNS disease. While exact mechanisms of transcellular and paracellular invasion are not fully elucidated, EphA2 is established as a host receptor necessary for BBB invasion, and evidence in upcoming studies implicates EphA2 as a key regulator of pathways enabling traversal. In parallel, current antifungals remain inaccessible in high-burden regions and are threatened by increasing resistance, motivating development of novel antifungal agents including antifungal peptides.

This thesis advances a model in which capsular HA-driven activation of CD44 initiates receptor crosstalk that transactivates EphA2 at the brain endothelium. EphA2 activation then drives Rho GTPase–dependent actin remodeling, enabling macropinocytosis as a size-appropriate route for cryptococcal transcellular uptake. Together, these mechanisms define a host-signaling axis that can be therapeutically targeted to limit BBB traversal while novel antifungal peptides address limitations of current drug regimens.

References:

1. Banerjee D, Das PK, Mukherjee J. Nervous System. In: Das PK, Sejian V, Mukherjee J, Banerjee D, eds. *Textbook of Veterinary Physiology*. Springer Nature; 2023:265-293. doi:10.1007/978-981-19-9410-4_11

2. Abbott NJ. Prediction of blood–brain barrier permeation in drug discovery from *in vivo*, *in vitro* and *in silico* models. *Drug Discov Today Technol*. 2004;1(4):407-416. doi:10.1016/j.ddtec.2004.11.014

3. Lampron A, ElAli A, Rivest S. Innate Immunity in the CNS: Redefining the Relationship between the CNS and Its Environment. *Neuron*. 2013;78(2):214-232. doi:10.1016/j.neuron.2013.04.005

4. Abbott NJ. Blood–brain barrier structure and function and the challenges for CNS drug delivery. *J Inherit Metab Dis*. 2013;36(3):437-449. doi:10.1007/s10545-013-9608-0

5. Wolak DJ, Thorne RG. Diffusion of Macromolecules in the Brain: Implications for Drug Delivery. *Mol Pharm*. 2013;10(5):1492-1504. doi:10.1021/mp300495e

6. Broadwell RD. Transcytosis of macromolecules through the blood-brain barrier: a cell biological perspective and critical appraisal. *Acta Neuropathol (Berl)*. 1989;79(2):117-128. doi:10.1007/BF00294368

7. Findley MK, Koval M. Regulation and roles for claudin-family tight junction proteins. *IUBMB Life*. 2009;61(4):431-437. doi:10.1002/iub.175

8. Adil MS, Narayanan SP, Somanath PR. Cell-cell junctions: structure and regulation in physiology and pathology. *Tissue Barriers*. 9(1):1848212. doi:10.1080/21688370.2020.1848212

9. Mishra A. Binaural blood flow control by astrocytes: listening to synapses and the vasculature. *J Physiol*. 2017;595(6):1885-1902. doi:10.1113/JP270979

10. Sobral AF, Costa I, Teixeira V, Silva R, Barbosa DJ. Molecular Motors in Blood–Brain Barrier Maintenance by Astrocytes. *Brain Sci*. 2025;15(3):279. doi:10.3390/brainsci15030279

11. Hayden MR. Protoplasmic Perivascular Astrocytes Play a Crucial Role in the Development of Enlarged Perivascular Spaces in Obesity, Metabolic Syndrome, and Type 2 Diabetes Mellitus. *Neuroglia*. 2023;4(4):307-328. doi:10.3390/neuroglia4040021

12. Kisler K, Nikolakopoulou AM, Zlokovic BV. Microglia have a grip on brain microvasculature. *Nat Commun*. 2021;12:5290. doi:10.1038/s41467-021-25595-3

13. Pallarés-Moratalla C, Bergers G. The ins and outs of microglial cells in brain health and disease. *Front Immunol*. 2024;15. doi:10.3389/fimmu.2024.1305087

14. Evilsizor MN, Ray-Jones HF, Ellis TW, Lifshitz J, Ziebell JM. Microglia in Experimental Brain Injury: Implications on Neuronal Injury and Circuit Remodeling. In: Kobeissy FH, ed. *Brain Neurotrauma: Molecular, Neuropsychological, and Rehabilitation Aspects*. Frontiers in

Neuroengineering. CRC Press/Taylor & Francis; 2015. Accessed February 7, 2026. http://www.ncbi.nlm.nih.gov/books/NBK299191/

15. Dando SJ, Mackay-Sim A, Norton R, et al. Pathogens Penetrating the Central Nervous System: Infection Pathways and the Cellular and Molecular Mechanisms of Invasion. *Clin Microbiol Rev*. 2014;27(4):691-726. doi:10.1128/CMR.00118-13

16. Kim KS. Mechanisms of microbial traversal of the blood–brain barrier. *Nat Rev Microbiol*. 2008;6(8):625-634. doi:10.1038/nrmicro1952

17. Santiago-Tirado FH, Doering TL. False friends: Phagocytes as Trojan horses in microbial brain infections. *PLoS Pathog*. 2017;13(12):e1006680. doi:10.1371/journal.ppat.1006680

18. Drevets DA. Dissemination of Listeria monocytogenesby Infected Phagocytes. *Infect Immun*. 1999;67(7):3512-3517. doi:10.1128/iai.67.7.3512-3517.1999

19. Liu PJ, Chen YS, Lin HH, et al. Induction of Mouse Melioidosis with Meningitis by CD11b+ Phagocytic Cells Harboring Intracellular B. pseudomallei as a Trojan Horse. *PLoS Negl Trop Dis*. 2013;7(8):e2363. doi:10.1371/journal.pntd.0002363

20. Williams AE, Blakemore WF. Pathogenesis of meningitis caused by Streptococcus suis type 2. *J Infect Dis*. 1990;162(2):474-481. doi:10.1093/infdis/162.2.474

21. Thwaites G. The pathophysiology of tuberculous meningitis. In: *Meningitis: Cellular and Molecular Basis*. Advances in Molecular and Cellular Microbiology. 2013:153-167. doi:10.1079/9781780641621.0153

22. Zhao Y, Gan L, Ren L, Lin Y, Ma C, Lin X. Factors influencing the blood-brain barrier permeability. *Brain Res*. 2022;1788:147937. doi:10.1016/j.brainres.2022.147937

23. Mittal R, Prasadarao NV. Nitric oxide/cGMP signalling induces Escherichia coli K1 receptor expression and modulates the permeability in human brain endothelial cell monolayers during invasion. *Cell Microbiol*. 2010;12(1):67-83. doi:10.1111/j.1462-5822.2009.01379.x

24. Nizet V, Kim KS, Stins M, et al. Invasion of brain microvascular endothelial cells by group B streptococci. *Infect Immun*. 1997;65(12):5074-5081. doi:10.1128/iai.65.12.5074-5081.1997

25. Krishnan S, Fernandez GE, Sacks DB, Prasadarao NV. IQGAP1 mediates the disruption of adherens junctions to promote Escherichia coli K1 invasion of brain endothelial cells. *Cell Microbiol*. 2012;14(9):1415-1433. doi:10.1111/j.1462-5822.2012.01805.x

26. Wispelwey B, Hansen EJ, Scheld WM. Haemophilus influenzae outer membrane vesicleinduced blood-brain barrier permeability during experimental meningitis. *Infect Immun*.
1989;57(8):2559-2562. doi:10.1128/iai.57.8.2559-2562.1989

27. Grab DJ, Nikolskaia O, Kim YV, et al. African trypanosome interactions with an in vitro model of the human blood-brain barrier. *J Parasitol*. 2004;90(5):970-979. doi:10.1645/GE-287R

28. Masocha W, Rottenberg ME, Kristensson K. Migration of African trypanosomes across the blood-brain barrier. *Physiol Behav*. 2007;92(1-2):110-114. doi:10.1016/j.physbeh.2007.05.045
29. Sethi N, Sondey M, Bai Y, Kim KS, Cadavid D. Interaction of a neurotropic strain of Borrelia turicatae with the cerebral microcirculation system. *Infect Immun*. 2006;74(11):6408-6418. doi:10.1128/IAI.00538-06

30. Grab DJ, Perides G, Dumler JS, et al. Borrelia burgdorferi, Host-Derived Proteases, and the Blood-Brain Barrier. *Infect Immun*. 2005;73(2):1014-1022. doi:10.1128/IAI.73.2.10141022.2005

31. Kim KS. Mechanisms of microbial traversal of the blood-brain barrier. *Nat Rev Microbiol*. 2008;6(8):625-634. doi:10.1038/nrmicro1952

32. Stins MF, Badger J, Sik Kim K. Bacterial invasion and transcytosis in transfected human brain microvascular endothelial cells. *Microb Pathog*. 2001;30(1):19-28. doi:10.1006/mpat.2000.0406

33. Al-Obaidi MMJ, Desa MNM. Mechanisms of Blood Brain Barrier Disruption by Different Types of Bacteria, and Bacterial–Host Interactions Facilitate the Bacterial Pathogen Invading the Brain. *Cell Mol Neurobiol*. 2018;38(7):1349-1368. doi:10.1007/s10571-0180609-2

34. Charland N, Nizet V, Rubens CE, Kim KS, Lacouture S, Gottschalk M. Streptococcus suis Serotype 2 Interactions with Human Brain Microvascular Endothelial Cells. *Infect Immun*. 2000;68(2):637-643. doi:10.1128/iai.68.2.637-643.2000

35. Greiffenberg L, Goebel W, Kim KS, et al. Interaction of Listeria monocytogenes with human brain microvascular endothelial cells: InlB-dependent invasion, long-term intracellular growth, and spread from macrophages to endothelial cells. *Infect Immun*. 1998;66(11):52605267. doi:10.1128/IAI.66.11.5260-5267.1998

36. Banerjee A, Kim BJ, Carmona EM, et al. Bacterial Pili exploit integrin machinery to promote immune activation and efficient blood-brain barrier penetration. *Nat Commun*. 2011;2(1):462. doi:10.1038/ncomms1474

37. Jain SK, Paul-Satyaseela M, Lamichhane G, Kim KS, Bishai WR. Mycobacterium tuberculosis invasion and traversal across an in vitro human blood-brain barrier as a pathogenic mechanism for central nervous system tuberculosis. *J Infect Dis*. 2006;193(9):1287-1295. doi:10.1086/502631

38. Tenenbaum T, Spellerberg B, Adam R, Vogel M, Kim KS, Schroten H. Streptococcus agalactiae invasion of human brain microvascular endothelial cells is promoted by the laminin-binding protein Lmb. *Microbes Infect*. 2007;9(6):714-720. doi:10.1016/j.micinf.2007.02.015

39. Ring A, Weiser JN, Tuomanen EI. Pneumococcal trafficking across the blood-brain barrier. Molecular analysis of a novel bidirectional pathway. *J Clin Invest*. 1998;102(2):347-360. doi:10.1172/JCI2406

40. Källström H, Liszewski MK, Atkinson JP, Jonsson AB. Membrane cofactor protein (MCP or

CD46) is a cellular pilus receptor for pathogenic Neisseria. *Mol Microbiol*. 1997;25(4):639647. doi:10.1046/j.1365-2958.1997.4841857.x

41. Jong AY, Stins MF, Huang SH, Chen SH, Kim KS. Traversal of Candida albicans across human blood-brain barrier in vitro. *Infect Immun*. 2001;69(7):4536-4544. doi:10.1128/IAI.69.7.4536-4544.2001

42. Ueno N, Lodoen MB. From the blood to the brain: avenues of eukaryotic pathogen dissemination to the central nervous system. *Curr Opin Microbiol*. 2015;26:53-59. doi:10.1016/j.mib.2015.05.006

43. Williamson PR, Jarvis JN, Panackal AA, et al. Cryptococcal meningitis: epidemiology, immunology, diagnosis and therapy. *Nat Rev Neurol*. 2017;13(1):13-24. doi:10.1038/nrneurol.2016.167

44. Ungureanu A, van der Meer J, Bicvic A, et al. Meningitis, meningoencephalitis and encephalitis in Bern: an observational study of 258 patients. *BMC Neurol*. 2021;21(1):474. doi:10.1186/s12883-021-02502-3

45. Mohamed SH, Nyazika TK, Ssebambulidde K, Lionakis MS, Meya DB, Drummond RA. Fungal CNS Infections in Africa: The Neuroimmunology of Cryptococcal Meningitis. *Front Immunol*. 2022;13. doi:10.3389/fimmu.2022.804674

46. Soscia SJ, Kirby JE, Washicosky KJ, et al. The Alzheimer's disease-associated amyloid beta-protein is an antimicrobial peptide. *PloS One*. 2010;5(3):e9505. doi:10.1371/journal.pone.0009505

47. Park BJ, Wannemuehler KA, Marston BJ, Govender N, Pappas PG, Chiller TM. Estimation of the current global burden of cryptococcal meningitis among persons living with HIV/AIDS. *AIDS*. 2009;23(4):525-530. doi:10.1097/QAD.0b013e328322ffac

48. Tauber SC, Eiffert H, Kellner S, et al. Fungal encephalitis in human autopsy cases is associated with extensive neuronal damage but only minimal repair. *Neuropathol Appl Neurobiol*. 2014;40(5):610-627. doi:10.1111/nan.12044

49. Pisa D, Alonso R, Rábano A, Rodal I, Carrasco L. Different Brain Regions are Infected with Fungi in Alzheimer's Disease. *Sci Rep*. 2015;5(1):15015. doi:10.1038/srep15015

50. Kumar DKV, Choi SH, Washicosky KJ, et al. Amyloid-β peptide protects against microbial infection in mouse and worm models of Alzheimer's disease. *Sci Transl Med*. 2016;8(340):340ra72. doi:10.1126/scitranslmed.aaf1059

51. Rajasingham R, Govender NP, Jordan A, et al. The global burden of HIV-associated cryptococcal infection in adults in 2020: a modelling analysis. *Lancet Infect Dis*. 2022;22(12):1748-1755. doi:10.1016/S1473-3099(22)00499-6

52. Molloy SF, Kanyama C, Heyderman RS, et al. Antifungal Combinations for Treatment of Cryptococcal Meningitis in Africa. *N Engl J Med*. 2018;378(11):1004-1017. doi:10.1056/NEJMoa1710922

53. Ngan NTT, Flower B, Day JN. Treatment of Cryptococcal Meningitis: How Have We Got Here and Where are We Going? *Drugs*. 2022;82(12):1237-1249. doi:10.1007/s40265-02201757-5

54. Sangalli-Leite F, Scorzoni L, Mesa-Arango AC, et al. Amphotericin B mediates killing in *Cryptococcus neoformans* through the induction of a strong oxidative burst. *Microbes Infect*. 2011;13(5):457-467. doi:10.1016/j.micinf.2011.01.015

55. Barchiesi F, Schimizzi AM, Caselli F, et al. Interactions between Triazoles and Amphotericin B against Cryptococcus neoformans. *Antimicrob Agents Chemother*. 2000;44(9):2435-2441. doi:10.1128/aac.44.9.2435-2441.2000

56. Loyse A, Dromer F, Day J, Lortholary O, Harrison TS. Flucytosine and cryptococcosis: time to urgently address the worldwide accessibility of a 50-year-old antifungal. *J Antimicrob Chemother*. 2013;68(11):2435-2444. doi:10.1093/jac/dkt221

57. Nguyen MH, Barchiesi F, McGough DA, Yu VL, Rinaldi MG. In vitro evaluation of combination of fluconazole and flucytosine against Cryptococcus neoformans var. neoformans. *Antimicrob Agents Chemother*. 1995;39(8):1691-1695. doi:10.1128/aac.39.8.1691

58. Stott KE, Loyse A, Jarvis JN, et al. Cryptococcal meningoencephalitis: time for action. *Lancet Infect Dis*. 2021;21(9):e259-e271. doi:10.1016/S1473-3099(20)30771-4

59. Rhein J, Morawski BM, Hullsiek KH, et al. Efficacy of adjunctive sertraline for the treatment of HIV-associated cryptococcal meningitis: an open-label dose-ranging study. *Lancet Infect Dis*. 2016;16(7):809-818. doi:10.1016/S1473-3099(16)00074-8

60. Day JN, Chau TTH, Wolbers M, et al. Combination antifungal therapy for cryptococcal meningitis. *N Engl J Med*. 2013;368(14):1291-1302. doi:10.1056/NEJMoa1110404

61. Rajasingham R, Smith RM, Park BJ, et al. Global burden of disease of HIV-associated cryptococcal meningitis: an updated analysis. *Lancet Infect Dis*. 2017;17(8):873-881. doi:10.1016/S1473-3099(17)30243-8

62. A systematic review of fluconazole resistance in clinical isolates of Cryptococcus species - Bongomin - 2018 - Mycoses - Wiley Online Library. Accessed February 8, 2026. https://onlinelibrary.wiley.com/doi/full/10.1111/myc.12747?casa_token=KRHsFRfCg2cAAAA%3AUg3aq_G6CN3aPxW7GPVoqySI-dYz-8u7r9-8k3CqnmkZOTzc9LsgztwmFEItucTw0ox3Yw-On8Ez1g

63. Mondon P, Petter R, Amalfitano G, et al. Heteroresistance to Fluconazole and Voriconazole inCryptococcus neoformans. *Antimicrob Agents Chemother*. 1999;43(8):1856-1861. doi:10.1128/aac.43.8.1856

64. Chen YC, Chang TY, Liu JW, et al. Increasing trend of fluconazole-non-susceptible Cryptococcus neoformans in patients with invasive cryptococcosis: a 12-year longitudinal study. *BMC Infect Dis*. 2015;15(1):277. doi:10.1186/s12879-015-1023-8

65. Nascimento E, Barião PHG, Kress MR von Z, et al. Cryptococcosis by Cryptococcus neoformans/Cryptococcus gattii Species Complexes in non-HIV-Infected Patients in

Southeastern Brazil. *Rev Soc Bras Med Trop*. 54:e0169-2021. doi:10.1590/0037-86820169-2021

66. Saidykhan L, Onyishi CU, May RC. The Cryptococcus gattii species complex: Unique pathogenic yeasts with understudied virulence mechanisms. *PLoS Negl Trop Dis*. 2022;16(12):e0010916. doi:10.1371/journal.pntd.0010916

67. McDonald T, Wiesner DL, Nielsen K. Cryptococcus. *Curr Biol CB*. 2012;22(14):R554-R555. doi:10.1016/j.cub.2012.05.040

68. Casadevall A. Evolution of Intracellular Pathogens. *Annu Rev Microbiol*. 2008;62(Volume 62, 2008):19-33. doi:10.1146/annurev.micro.61.080706.093305

69. Bliska JB, Casadevall A. Intracellular pathogenic bacteria and fungi--a case of convergent evolution? *Nat Rev Microbiol*. 2009;7(2):165-171. doi:10.1038/nrmicro2049

70. Denham ST, Brown JCS. Mechanisms of Pulmonary Escape and Dissemination by Cryptococcus neoformans. *J Fungi*. 2018;4(1):25. doi:10.3390/jof4010025

71. Gaylord EA, Choy HL, Doering TL. Dangerous Liaisons: Interactions of Cryptococcus neoformans with Host Phagocytes. *Pathogens*. 2020;9(11):891. doi:10.3390/pathogens9110891

72. Cruz-Acuña M, Pacifici N, Lewis JS. Vomocytosis: Too Much Booze, Base, or Calcium? *mBio*. 2019;10(6):e02526-19. doi:10.1128/mBio.02526-19

73. Al-Huthaifi AM, Radman BA, Al-Alawi AA, Mahmood F, Liu TB. Mechanisms and Virulence Factors of Cryptococcus neoformans Dissemination to the Central Nervous System. *J Fungi*. 2024;10(8):586. doi:10.3390/jof10080586

74. Chang YC, Stins MF, McCaffery MJ, et al. Cryptococcal yeast cells invade the central nervous system via transcellular penetration of the blood-brain barrier. *Infect Immun*. 2004;72(9):4985-4995. doi:10.1128/IAI.72.9.4985-4995.2004

75. Shi M, Li SS, Zheng C, et al. Real-time imaging of trapping and urease-dependent transmigration of Cryptococcus neoformans in mouse brain. *J Clin Invest*. 2010;120(5):1683-1693. doi:10.1172/JCI41963

76. Na Pombejra S, Jamklang M, Uhrig JP, Vu K, Gelli A. The structure-function analysis of the Mpr1 metalloprotease determinants of activity during migration of fungal cells across the blood-brain barrier. *PLoS ONE*. 2018;13(8):e0203020. doi:10.1371/journal.pone.0203020

77. Olszewski MA, Noverr MC, Chen GH, et al. Urease Expression by Cryptococcus neoformans Promotes Microvascular Sequestration, Thereby Enhancing Central Nervous System Invasion. *Am J Pathol*. 2004;164(5):1761-1771. doi:10.1016/S0002-9440(10)63734-0

78. Fu MS, Coelho C, Leon-Rodriguez CMD, et al. Cryptococcus neoformans urease affects the outcome of intracellular pathogenesis by modulating phagolysosomal pH. *PLOS Pathog*. 2018;14(6):e1007144. doi:10.1371/journal.ppat.1007144

79. Presta I, Vismara MFM, Novellino F, et al. Innate Immunity Cells and the Neurovascular Unit. *Int J Mol Sci*. 2018;19(12):3856. doi:10.3390/ijms19123856

80. Jong A, Wu CH, Gonzales-Gomez I, et al. Hyaluronic Acid Receptor CD44 Deficiency Is Associated with Decreased Cryptococcus neoformans Brain Infection. *J Biol Chem*. 2012;287(19):15298-15306. doi:10.1074/jbc.M112.353375

81. Ding S, Yang J, Feng X, et al. Interactions between fungal hyaluronic acid and host CD44 promote internalization by recruiting host autophagy proteins to forming phagosomes. *iScience*. 2021;24(3):102192. doi:10.1016/j.isci.2021.102192

82. Ding S, Yang J, Feng X, et al. Interactions between fungal hyaluronic acid and host CD44 promote internalization by recruiting host autophagy proteins to forming phagosomes. *iScience*. 2021;24(3):102192. doi:10.1016/j.isci.2021.102192

83. Aaron PA, Jamklang M, Uhrig JP, Gelli A. The blood-brain barrier internalises Cryptococcus neoformans via the EphA2-tyrosine kinase receptor. *Cell Microbiol*. 2018;20(3). doi:10.1111/cmi.12811

84. Lisabeth EM, Falivelli G, Pasquale EB. Eph Receptor Signaling and Ephrins. *Cold Spring Harb Perspect Biol*. 2013;5(9):a009159. doi:10.1101/cshperspect.a009159

85. Pasquale EB. Eph-Ephrin Bidirectional Signaling in Physiology and Disease. *Cell*. 2008;133(1):38-52. doi:10.1016/j.cell.2008.03.011

86. Yamaguchi Y, Pasquale EB. Eph receptors in the adult brain. *Curr Opin Neurobiol*. 2004;14(3):288-296. doi:10.1016/j.conb.2004.04.003

87. Zhou R. The Eph Family Receptors and Ligands. *Pharmacol Ther*. 1998;77(3):151-181. doi:10.1016/S0163-7258(97)00112-5

88. Flanagan JG, Vanderhaeghen P. The ephrins and Eph receptors in neural development. *Annu Rev Neurosci*. 1998;21:309-345. doi:10.1146/annurev.neuro.21.1.309

89. Poliakov A, Cotrina M, Wilkinson DG. Diverse roles of eph receptors and ephrins in the regulation of cell migration and tissue assembly. *Dev Cell*. 2004;7(4):465-480. doi:10.1016/j.devcel.2004.09.006

90. Eph/ephrin Signaling as a Potential Therapeutic Target After Cent...: Ingenta Connect. Accessed February 8, 2026. https://www.ingentaconnect.com/content/ben/cpd/2007/00000013/00000024/art00009

91. Li X, Wang Y, Wang Y, et al. Expression of EphA2 in human astrocytic tumors: correlation with pathologic grade, proliferation and apoptosis. *Tumour Biol J Int Soc Oncodevelopmental Biol Med*. 2007;28(3):165-172. doi:10.1159/000103010

92. Puschmann TB, Turnley AM. Eph receptor tyrosine kinases regulate astrocyte cytoskeletal rearrangement and focal adhesion formation. *J Neurochem*. 2010;113(4):881-894. doi:10.1111/j.1471-4159.2010.06655.x

93. Kale S, Hanai J ichi, Chan B, et al. Microarray analysis of in vitro pericyte differentiation reveals an angiogenic program of gene expression. *FASEB J Off Publ Fed Am Soc Exp Biol*. 2005;19(2):270-271. doi:10.1096/fj.04-1604fje

94. Teichert M, Milde L, Holm A, et al. Pericyte-expressed Tie2 controls angiogenesis and vessel maturation. *Nat Commun*. 2017;8(1):16106. doi:10.1038/ncomms16106

95. Thundyil J, Manzanero S, Pavlovski D, et al. Evidence That the EphA2 Receptor Exacerbates Ischemic Brain Injury. *PLOS ONE*. 2013;8(1):e53528. doi:10.1371/journal.pone.0053528

96. Darling TK, Mimche PN, Bray C, et al. EphA2 contributes to disruption of the blood-brain barrier in cerebral malaria. *PLOS Pathog*. 2020;16(1):e1008261. doi:10.1371/journal.ppat.1008261

97. de Boer ECW, van Gils JM, van Gils MJ. Ephrin-Eph signaling usage by a variety of viruses. *Pharmacol Res*. 2020;159:105038. doi:10.1016/j.phrs.2020.105038

98. Leite M, Marques MS, Melo J, et al. Helicobacter Pylori Targets the EPHA2 Receptor Tyrosine Kinase in Gastric Cells Modulating Key Cellular Functions. *Cells*. 2020;9(2):513. doi:10.3390/cells9020513

99. Subbarayal P, Karunakaran K, Winkler AC, et al. EphrinA2 Receptor (EphA2) Is an Invasion and Intracellular Signaling Receptor for Chlamydia trachomatis. *PLOS Pathog*. 2015;11(4):e1004846. doi:10.1371/journal.ppat.1004846

100. Zhang H, Li Y, Wang HB, et al. Ephrin receptor A2 is an epithelial cell receptor for EpsteinBarr virus entry. *Nat Microbiol*. 2018;3(2):1-8. doi:10.1038/s41564-017-0080-8

101. Dong XD, Li Y, Li Y, et al. EphA2 is a functional entry receptor for HCMV infection of glioblastoma cells. *PLOS Pathog*. 2023;19(5):e1011304. doi:10.1371/journal.ppat.1011304

102. Swidergall M, Solis NV, Lionakis MS, Filler SG. EphA2 is an epithelial cell pattern recognition receptor for fungal β-glucans. *Nat Microbiol*. 2018;3(1):53-61. doi:10.1038/s41564-0170059-5

103. Pasquale EB. Eph receptors and ephrins in cancer: bidirectional signalling and beyond. *Nat Rev Cancer*. 2010;10(3):165-180. doi:10.1038/nrc2806

104. Arvanitis D, Davy A. Eph/ephrin signaling: networks. *Genes Dev*. 2008;22(4):416-429. doi:10.1101/gad.1630408

105. Sadok A, Marshall CJ. Rho GTPases. *Small GTPases*. 2014;5:e29710. doi:10.4161/sgtp.29710

106. Stankiewicz TR, Linseman DA. Rho family GTPases: key players in neuronal development, neuronal survival, and neurodegeneration. *Front Cell Neurosci*. 2014;8:314. doi:10.3389/fncel.2014.00314

107. Brantley-Sieders DM, Caughron J, Hicks D, Pozzi A, Ruiz JC, Chen J. EphA2 receptor tyrosine kinase regulates endothelial cell migration and vascular assembly through phosphoinositide 3-kinase-mediated Rac1 GTPase activation. *J Cell Sci*. 2004;117(10):2037-2049. doi:10.1242/jcs.01061

108. Fang WB, Ireton RC, Zhuang G, Takahashi T, Reynolds A, Chen J. Overexpression of EPHA2 receptor destabilizes adherens junctions via a RhoA-dependent mechanism. *J Cell Sci*. 2008;121(3):358-368. doi:10.1242/jcs.017145

109. Pasquale EB. Eph-Ephrin Bidirectional Signaling in Physiology and Disease. *Cell*. 2008;133(1):38-52. doi:10.1016/j.cell.2008.03.011

110. Endocytosis - an overview | ScienceDirect Topics. Accessed February 8, 2026. https://www.sciencedirect.com/topics/neuroscience/endocytosis

111. Alberts B, Johnson A, Lewis J, Raff M, Roberts K, Walter P. Transport into the Cell from the Plasma Membrane: Endocytosis. In: *Molecular Biology of the Cell. 4th Edition*. Garland Science; 2002. Accessed February 8, 2026. https://www.ncbi.nlm.nih.gov/books/NBK26870/

112. Doherty GJ, McMahon HT. Mechanisms of Endocytosis. *Annu Rev Biochem*. 2009;78(1):857-902. doi:10.1146/annurev.biochem.78.081307.110540

113. Kaksonen M, Roux A. Mechanisms of clathrin-mediated endocytosis. *Nat Rev Mol Cell Biol*. 2018;19(5):313-326. doi:10.1038/nrm.2017.132

114. Scott BL, Sochacki KA, Low-Nam ST, et al. Membrane bending occurs at all stages of clathrin-coat assembly and defines endocytic dynamics. *Nat Commun*. 2018;9(1):419. doi:10.1038/s41467-018-02818-8

115. Delos Santos RC, Bautista S, Lucarelli S, et al. Selective regulation of clathrin-mediated epidermal growth factor receptor signaling and endocytosis by phospholipase C and calcium. *Mol Biol Cell*. 2017;28(21):2802-2818. doi:10.1091/mbc.E16-12-0871

116. Hahn AS, Desrosiers RC. Binding of the Kaposi's Sarcoma-Associated Herpesvirus to the Ephrin Binding Surface of the EphA2 Receptor and Its Inhibition by a Small Molecule. *J Virol*. 2014;88(16):8724-8734. doi:10.1128/JVI.01392-14

117. Briner SL, Doering TL. CRYPTOCOCCUS. *Curr Biol CB*. 2025;35(11):R518-R522. doi:10.1016/j.cub.2025.04.008

118. Doherty GJ, McMahon HT. Mechanisms of endocytosis. *Annu Rev Biochem*. 2009;78:857902. doi:10.1146/annurev.biochem.78.081307.110540

119. Lin XP, Mintern JD, Gleeson PA. Macropinocytosis in Different Cell Types: Similarities and Differences. *Membranes*. 2020;10(8):177. doi:10.3390/membranes10080177

120. Mercer J, Helenius A. Virus entry by macropinocytosis. *Nat Cell Biol*. 2009;11(5):510-520. doi:10.1038/ncb0509-510

121. Yerbury JJ. Protein aggregates stimulate macropinocytosis facilitating their propagation. *Prion*. 2016;10(2):119-126. doi:10.1080/19336896.2016.1141860

122. Bloomfield G, Kay RR. Uses and abuses of macropinocytosis. *J Cell Sci*. 2016;129(14):2697-2705. doi:10.1242/jcs.176149

123. Lanser DM, Bennett AB, Vu K, Gelli A. Macropinocytosis as a potential mechanism driving neurotropism of Cryptococcus neoformans. *Front Cell Infect Microbiol*. 2023;13:1331429. doi:10.3389/fcimb.2023.1331429

124. Kerr MC, Teasdale RD. Defining Macropinocytosis. *Traffic*. 2009;10(4):364-371. doi:10.1111/j.1600-0854.2009.00878.x

125. Salmonella stimulate macrophage macropinocytosis and persist within spacious phagosomes. *J Exp Med*. 1994;179(2):601-608. doi:10.1084/jem.179.2.601

126. Weiner A, Mellouk N, Lopez-Montero N, et al. Macropinosomes are Key Players in Early Shigella Invasion and Vacuolar Escape in Epithelial Cells. *PLoS Pathog*. 2016;12(5):e1005602. doi:10.1371/journal.ppat.1005602

127. García-Pérez BE, De la Cruz-López JJ, Castañeda-Sánchez JI, et al. Macropinocytosis is responsible for the uptake of pathogenic and non-pathogenic mycobacteria by B lymphocytes (Raji cells). *BMC Microbiol*. 2012;12:246. doi:10.1186/1471-2180-12-246

128. Watarai M, Derre I, Kirby J, Growney JD, Dietrich WF, Isberg RR. Legionella pneumophila Is Internalized by a Macropinocytotic Uptake Pathway Controlled by the Dot/Icm System and the Mouse Lgn1 Locus✪. *J Exp Med*. 2001;194(8):1081-1096. doi:10.1084/jem.194.8.1081

129. Watarai M, Makino SI, Fujii Y, Okamoto K, Shirahata T. Modulation of Brucella-induced macropinocytosis by lipid rafts mediates intracellular replication. *Cell Microbiol*. 2002;4(6):341-355. doi:10.1046/j.1462-5822.2002.00195.x

130. Rosales-Reyes R, Sánchez-Gómez C, Ortiz-Navarrete V, Santos-Preciado JI. Burkholderia cenocepacia Induces Macropinocytosis to Enter Macrophages. *BioMed Res Int*. 2018;2018:4271560. doi:10.1155/2018/4271560

131. de Carvalho TMU, Barrias ES, de Souza W. Macropinocytosis: a pathway to protozoan infection. *Front Physiol*. 2015;6:106. doi:10.3389/fphys.2015.00106

132. Barrias ES, Reignault LC, De Souza W, Carvalho TMU. Trypanosoma cruzi uses macropinocytosis as an additional entry pathway into mammalian host cell. *Microbes Infect*. 2012;14(14):1340-1351. doi:10.1016/j.micinf.2012.08.003

133. Aleksandrowicz P, Marzi A, Biedenkopf N, et al. Ebola Virus Enters Host Cells by Macropinocytosis and Clathrin-Mediated Endocytosis. *J Infect Dis*. 2011;204(Suppl 3):S957S967. doi:10.1093/infdis/jir326

134. Maréchal V, Prevost MC, Petit C, Perret E, Heard JM, Schwartz O. Human Immunodeficiency Virus Type 1 Entry into Macrophages Mediated by Macropinocytosis. *J Virol*. 2001;75(22):11166-11177. doi:10.1128/JVI.75.22.11166-11177.2001

135. Mercer J, Knébel S, Schmidt FI, Crouse J, Burkard C, Helenius A. Vaccinia virus strains use distinct forms of macropinocytosis for host-cell entry. *Proc Natl Acad Sci U S A*. 2010;107(20):9346-9351. doi:10.1073/pnas.1004618107

136. Amstutz B, Gastaldelli M, Kälin S, et al. Subversion of CtBP1-controlled macropinocytosis by human adenovirus serotype 3. *EMBO J*. 2008;27(7):956-969. doi:10.1038/emboj.2008.38
137. Krieger SE, Kim C, Zhang L, Marjomaki V, Bergelson JM. Echovirus 1 Entry into Polarized Caco-2 Cells Depends on Dynamin, Cholesterol, and Cellular Factors Associated with Macropinocytosis. *J Virol*. 2013;87(16):8884-8895. doi:10.1128/JVI.03415-12

138. Coyne CB, Shen L, Turner JR, Bergelson JM. Coxsackievirus Entry across Epithelial Tight Junctions Requires Occludin and the Small GTPases Rab34 and Rab5. *Cell Host Microbe*. 2007;2(3):181-192. doi:10.1016/j.chom.2007.07.003

139. Zhang YY, Liang R, Wang SJ, et al. SARS-CoV-2 hijacks macropinocytosis to facilitate its entry and promote viral spike–mediated cell-to-cell fusion. *J Biol Chem*. 2022;298(11):102511. doi:10.1016/j.jbc.2022.102511

140. Chen SHM, Stins MF, Huang SH, et al. Cryptococcus neoformans induces alterations in the cytoskeleton of human brain microvascular endothelial cells. *J Med Microbiol*. 2003;52(Pt 11):961-970. doi:10.1099/jmm.0.05230-0

141. Long M, Huang SH, Wu CH, Shackleford GM, Jong A. Lipid raft/caveolae signaling is required for Cryptococcus neoformans invasion into human brain microvascular endothelial cells. *J Biomed Sci*. 2012;19(1):19. doi:10.1186/1423-0127-19-19

142. King JS, Kay RR. The origins and evolution of macropinocytosis. *Philos Trans R Soc B Biol Sci*. 2018;374(1765):20180158. doi:10.1098/rstb.2018.0158

143. Koivusalo M, Welch C, Hayashi H, et al. Amiloride inhibits macropinocytosis by lowering submembranous pH and preventing Rac1 and Cdc42 signaling. *J Cell Biol*. 2010;188(4):547-563. doi:10.1083/jcb.200908086

144. Swanson JA, Watts C. Macropinocytosis. *Trends Cell Biol*. 1995;5(11):424-428. doi:10.1016/S0962-8924(00)89101-1

145. Li Y, Ambati S, Meagher RB, Lin X. Developing mRNA lipid nanoparticle vaccine effective for cryptococcosis in a murine model. *Npj Vaccines*. 2025;10(1):24. doi:10.1038/s41541025-01079-z

146. Specht CA, Lee CK, Huang H, et al. Vaccination with Recombinant Cryptococcus Proteins in Glucan Particles Protects Mice against Cryptococcosis in a Manner Dependent upon Mouse Strain and Cryptococcal Species. *mBio*. 2017;8(6):e01872-17. doi:10.1128/mBio.01872-17

147. Chen Y, Li Y, Nahar KS, et al. New Generation Modified Azole Antifungals against Multidrug-Resistant Candida auris. *J Med Chem*. 2025;68(13):14054-14071. doi:10.1021/acs.jmedchem.5c01253

148. Chen Y, Li Y, Hind C, et al. New generation modified azole antifungals against multidrugresistant Candida auris. *ChemRxiv*. 2024(0923). doi:10.26434/chemrxiv-2024-r0fzq

149. Khan M. Peptide Therapy: The Future of Targeted Treatment? News-Medical. February 17,

2025. Accessed February 8, 2026. https://www.news-medical.net/health/Peptide-Therapy-The-Future-of-Targeted-Treatment.aspx

150. Fosgerau K, Hoffmann T. Peptide therapeutics: current status and future directions. *Drug Discov Today*. 2015;20(1):122-128. doi:10.1016/j.drudis.2014.10.003

151. Fernández de Ullivarri M, Arbulu S, Garcia-Gutierrez E, Cotter PD. Antifungal Peptides as Therapeutic Agents. *Front Cell Infect Microbiol*. 2020;10:105. doi:10.3389/fcimb.2020.00105

152. Cecropin - an overview | ScienceDirect Topics. Accessed February 8, 2026. https://www.sciencedirect.com/topics/immunology-and-microbiology/cecropin

153. Lamers C. Overcoming the Shortcomings of Peptide-Based Therapeutics. *Future Drug Discov*. 2022;4(2):FDD75. doi:10.4155/fdd-2022-0005

154. Pereira AJ, de Campos LJ, Xing H, Conda-Sheridan M. Peptide-based therapeutics: challenges and solutions. *Med Chem Res*. 2024;33(8):1275-1280. doi:10.1007/s00044-02403269-1

155. Purva Patel. Innovative Strategies In Peptide Therapeutics: Stability Challenges And Advanced Analytical Methods. *Int J Pharm Sci*. 2024;02(08). doi:10.5281/zenodo.13629324

156. Duarte-Mata DI, Salinas-Carmona MC. Antimicrobial peptides´ immune modulation role in intracellular bacterial infection. *Front Immunol*. 2023;14:1119574. doi:10.3389/fimmu.2023.1119574

157. Roque-Borda CA, Primo LMDG, Franzyk H, Hansen PR, Pavan FR. Recent advances in the development of antimicrobial peptides against ESKAPE pathogens. *Heliyon*. 2024;10(11):e31958. doi:10.1016/j.heliyon.2024.e31958

158. Mazu TK, Bricker BA, Flores-Rozas H, Ablordeppey SY. The Mechanistic Targets of Antifungal Agents: An Overview. *Mini Rev Med Chem*. 2016;16(7):555-578. doi:10.2174/1389557516666160118112103

159. Steinberg DA, Hurst MA, Fujii CA, et al. Protegrin-1: a broad-spectrum, rapidly microbicidal peptide with in vivo activity. *Antimicrob Agents Chemother*. 1997;41(8):1738-1742. doi:10.1128/aac.41.8.1738

160. Wang K, Dang W, Xie J, et al. Antimicrobial peptide protonectin disturbs the membrane integrity and induces ROS production in yeast cells. *Biochim Biophys Acta*. 2015;1848(10 Pt A):2365-2373. doi:10.1016/j.bbamem.2015.07.008

161. Lactoferricin - an overview | ScienceDirect Topics. Accessed February 8, 2026. https://www.sciencedirect.com/topics/biochemistry-genetics-and-molecularbiology/lactoferricin

162. Dash R, Bhattacharjya S. Thanatin: An Emerging Host Defense Antimicrobial Peptide with Multiple Modes of Action. *Int J Mol Sci*. 2021;22(4):1522. doi:10.3390/ijms22041522

163. Bansal S, Vu K, Liu R, et al. Discovery and Characterization of a Potent Antifungal Peptide through One-Bead, One-Compound Combinatorial Library Screening. *ACS Infect Dis*.

2022;8(7):1291-1302. doi:10.1021/acsinfecdis.2c00019
164. Lam KS, Sroka T, Chen ML, et al. Application of “one-bead one-compound” combinatorial library methods in signal transduction research. *Life Sci*. 1998;62(17):1577-1583. doi:10.1016/S0024-3205(98)00110-6

165. Lam KS, Liu R, Miyamoto S, Lehman AL, Tuscano JM. Applications of one-bead onecompound combinatorial libraries and chemical microarrays in signal transduction research. *Acc Chem Res*. 2003;36(6):370-377. doi:10.1021/ar0201299

166. Godinho-Pereira J, Garcia AR, Figueira I, Malhó R, Brito MA. Behind Brain Metastases Formation: Cellular and Molecular Alterations and Blood–Brain Barrier Disruption. *Int J Mol Sci*. 2021;22(13):7057. doi:10.3390/ijms22137057

167. Hawkins BT, Davis TP. The Blood-Brain Barrier/Neurovascular Unit in Health and Disease. *Pharmacol Rev*. 2005;57(2):173-185. doi:10.1124/pr.57.2.4

Chapter 2

Macropinocytosis mediates neurotropism of *Cryptococcus neoformans* in a human organoid model of the blood-brain barrier.

Authors: Amelia B. Bennett[1£], Dylan M. Lanser[1,£], Kiem Vu[1], Amita R. Sahoo[2], Matthias Buck[2], Angie Gelli[1*]

Affiliations:

1 Department of Pharmacology, School of Medicine, University of California, Davis, CA, 95616, USA.

2
Department of Physiology and Biophysics, Case Western Reserve University, Cleveland, OH, 44106-4970, USA.

£
Shared first-authorship, names listed alphabetically

*Corresponding author: Angie Gelli, PhD
Department of Pharmacology, School of Medicine
451 Health Sciences Dr
Davis, CA, 95616, USA email: acgelli@ucdavis.edu; phone: 530-754-6446

Conflict of interest: The authors have declared that no conflict of interest exists.

Key words: Ephrin receptor tyrosine kinase, EphA2, *Cryptococcus neoformans*, *Cryptococcus deuterogattii,* CD44, macropinocytosis, BBB organoid, brain endothelial cells, Cdc42, amiloride.

Abstract

The opportunistic and neuroinvasive fungus, *Cryptococcus neoformans* (*Cn*), causes a life-threatening brain infection that despite treatment can cause long-term cognitive deficiencies. Studies have shown that *Cn* can infiltrate the central nervous system (CNS) through a transcellular route across the brain endothelium, however the molecular process that drives brain endothelial cells to internalize *Cn* remains poorly defined. Here we examine the molecular interactions between fungal cells and the brain endothelium by utilizing a human 3D organoid model of the blood-brain barrier (BBB). We show that *Cn* exploits the process of macropinocytosis as the mechanism of endocytosis into brain endothelial cells by recruiting CD44 and EphA2 as a molecular complex. We identified two predicted binding sites on EphA2, suggesting that the two

structurally distinct regions may provide a molecular basis for cooperative signaling in brain endothelial cells that stimulate macropinocytosis as the mode of entry for *Cn*.

Introduction

In a healthy brain, components of circulating blood that could damage the central nervous system (CNS) are excluded by the blood-brain barrier (BBB). The tightly connected endothelial cells, the low rate of vesicular transport and the highly-selective permeability of the BBB collectively ensure a protective environment for the CNS.[1] Despite this, *Cryptococcus neoformans* (*Cn*), a neurotropic fungal pathogen and leading cause of meningoencephalitis in immunosuppressed adults[2], has developed adaptations that promote its entry[3] into- and proliferation within the CNS.[4,5]Several lines of evidence support multiple routes of CNS invasion, including: (i) "Trojan Horse," in which *Cn* infiltrates the BBB via infected phagocytes[6-12], (ii) paracellular crossing of free *Cn* via the disruption of the BBB endothelial cell junction proteins[12,15], and (iii) direct fungal interaction with brain endothelial cells leading to endocytosis and transcytosis of free *Cn*.[16-22] The molecular mechanistic details of these routes, the propensity of *Cn* using one route versus another and whether all three routes are used during infection remains largely unresolved.

Utilization of endothelial cells and exploitation of endocytosis to cross the BBB via a transcellular path is central to *Cn*'s ability to infiltrate and survive within the CNS. Several *in vitro* and *in vivo* studies have demonstrated transcytosis as the primary mechanism driving *Cn* across the BBB.[3,16,23,24] Evidence includes observational studies that found cryptococci moving freely through the bloodstream and crossing the brain endothelium independently of phagocytes[14], and quantitative analyses that established a direct association between brain endothelial cells and *Cn* *in vivo*.[16,23]Collectively, these data support recruitment of a transcellular pathway for BBB

crossing, however the molecular process by which brain endothelial cells internalize *Cn* remains poorly understood.

One form of endocytosis is macropinocytosis, an actin-driven endocytic process that internalizes extracellular cargo -via large vesicles referred to as macropinosomes.[25-27] In contrast to other forms of endocytosis such as clathrin-mediated endocytosis and phagocytosis where specific cargoes trigger local alterations of cytoskeleton dynamics that lead to their engulfment; macropinocytosis is typically stimulated by activated by epidermal growth factors or tyrosine kinase receptors that induce a global change in actin dynamics within a cell, leading to the nonspecific uptake of extracellular fluid and extracellular components that vary greatly in size. [AB1] Based on previously observed indicators of macropinocytosis, such as actin-supported membrane ruffles in brain endothelial cells infected with *Cn*[16,21], actin disruptors preventing BBB crossing[13,21,28] and the lack of evidence for other processes, we questioned whether *Cn* might exploit macropinocytosis as the mechanism of entry to the CNS.[29]

To investigate this, we utilized a human organoid model of the BBB. Multicellular BBB organoids have been used as a reliable and predictive platform that recapitulate features of the native BBB.[30] The present study examines the molecular interaction between *Cn* and the brain endothelium. We previously found that *Cn* induced the non-canonical, ligand-free activation of the ephrin tyrosine kinase receptor, EphA2, in human brain endothelial cells.[21] Eph receptors and their ligands have been known to be highly expressed in the central nervous system and studies have established that they play a crucial role in the development and maintenance of the brain. While we demonstrated that transcytosis of *Cn* across the BBB relied on the phosphorylationdependent activity of EphA2[21], the mechanistic details of the endocytic process remained unresolved. It was also unclear whether EphA2 played a role in recruiting CD44, the glycoprotein receptor for hyaluronic acid, and a known contributor to the transcellular pathway co-opted by *Cn* to cross the brain endothelium.[31-33]

Results

Cellular organization and validation of a human blood-brain barrier (BBB) organoid model of neural cryptococcosis.

To examine whether macropinocytosis is the mechanism facilitating *Cn* internalization by the brain endothelium and transcytosis of *Cn* across the BBB, we constructed a 3D human organoid model of the BBB (Supp. Fig. 1a).[34,35] To our knowledge, this is the first study that used a 3D BBB organoid model in the context of neurocryptococcosis. BBB organoids were generated by combining human immortalized brain endothelial cells (iBMECs) or primary brain endothelial cells, astrocytes and pericytes in a 1:1:1 ratio in commercially purchased low-adhesion 96-well plates specially designed to encourage the formation of unitary and uniformly sized (~200 μm) organoids (Akura microplates, InSphero, Brunswick, ME, USA, Supp. Fig. 1b and inset). Approximately 1000 cells of each neurovascular cell type were combined to generate organoids, which formed spontaneously within 2-3 days and remained viable and static for at least 2 weeks. Scaffold support was not required as each cell type spontaneously self-arranged into a recapitulation of the cellular organization of the BBB.[34]

Immunofluorescence was used to examine expression of cellular markers of BBB organoids that were fixed and cryo-sectioned (Supp. Fig. 2). Surface-localized brain endothelial cells spontaneously established tight junctions, indicated by Claudin-5 expression, a transmembrane protein that is key to the physical establishment of the BBB through prevention of paracellular leakage (Supp. Fig. 2c, 2d, merge). Astrocytes and pericytes concentrated in the core of the organoids (Supp. Fig. 2e, 2f). Under these conditions, the size of the organoids remained unchanged over 14 days of culture, suggesting that endothelial cells appeared to regulate the proliferation of the pericytes and astrocytes encapsulated within the organoids. As

the data supported the expected orientation of the three cell types in the organoids, we next examined the integrity of the endothelial barrier.

Using transmission electron microscopy (TEM), we assessed the integrity of the organoid endothelium and observed structures indicative of tight junctions between endothelial cells (Fig. 1a). The inability of the FITC-dextran (70 kDa) macromolecule to cross brain endothelial cells and infiltrate the organoid interior demonstrated BBB impermeability and confirmed an intact endothelial barrier encapsulating the organoid (Fig. 1c). In contrast, FITC alone, which is a much smaller molecule, freely crossed the endothelial barrier as expected (Fig. 1c). BBB organoids showed strong expression of Claudin-5 co-localized with the outer layers of the organoid, further confirming an intact barrier and also illustrating the precise location of the endothelial cell layer along the surface of the organoid (Fig. 1c). TEM analysis of BBB spheroids exposed to a high inoculum of fungal (*Cn*) cells revealed extensive plasma membrane ruffling confined to the endothelial cells that was in close proximity to *Cn* (Fig. 1d, 1e), consistent with cytoskeleton remodeling and in agreement with similar morphological changes observed in previous studies.[13,16,28] BBB organoids consisting of either immortalized or primary human brain endothelial cells (Fig. 1f, 1g) were similar in organization and function.

Treatment of the BBB with an inhibitor of macropinocytosis prevented *Cn* crossing of the BBB.

Next, we assessed whether the BBB organoids permitted *Cn* crossing to a degree that could be robustly analyzed. *Cn*, labeled in green with an antibody to the GXM of the polysaccharide capsule, appeared to penetrate the Claudin-5-labeled endothelial layer of BBB organoids (Fig. 2a-c). Numerous *Cn* were observed within endothelial cells and near DAPIstained astrocytes or pericytes that were closest to the endothelial layer but appeared to be largely excluded from the astrocyte core (Fig. 2a (inset), 2b). We also observed sloughing off of *Cn* capsule, indicated by green puncta (Fig. 2c), consistent with earlier studies that found remnants of the polysaccharide capsule with reactive astrocytes adjacent to cryptococcomas during

infection.[36-38] We found that *Cn* was readily internalized by BBB organoids, in contrast to the sibling species, *Cryptococcus deuterogattii* (*Cd*), and to the negative control, *Saccharomyces cerevisiae* (*Sc*) (Fig. 2d, 2e). Collectively, these results suggest that the BBB organoids are highly functional entities able to distinguish neuroinvasive pathogens from others and could serve as a suitable model to examine the mode of *Cn* entry.

Macropinocytosis is uniquely susceptible to amiloride (AML), a chemical inhibitor of Na^+/H^+ exchange that inhibits macropinocytosis by lowering endomembrane pH and thereby inhibiting actin polymerization.[39] Treating BBB organoids with AML prior to *Cn* exposure significantly reduced the number of fungal cells internalized, in contrast to the vehicle treated control (Fig. 2e; Supp. Fig. 3). Fungal cell viability was not impacted at the concentration of AML used in these assays (Fig. 2g). To confirm this result and by extension the BBB organoid-based model, we used a well-established 2D transwell-based model of the BBB[40,41] to investigate *Cn* crossing of AML-treated cultured human brain microvascular endothelial cells (HBMECs)[41] (Fig. 2f). In this model, HBMECs (similar to the cells used in the organoids), were grown on a transwell resulting in an intact, impermeable endothelial barrier that separated the bottom well (abluminal/basolateral) from the upper chamber (luminal/apical side).[21,40,42] AML treatment was administered to the top chamber either before exposure to *Cn* or added to the fungal cell inoculum. The number of fungal cells crossing the endothelial barrier was reduced by ~3-fold with AML compared to the vehicle treatment, and the data were consistent with the results from the BBB organoids (Fig. 2h). Employing the same 2D transwell model of the BBB, the crossing of transferrin - used here as a previously validated negative control for macropinocytosis-dependent transcellular crossing[43] - was examined 8 h, 12 h and 16 h post treatment with AML. The relative fluorescence unit (RFU) ratios of transferrin in the upper chamber versus the bottom well were not significantly different at all time points, suggesting that clathrin-mediated endocytosis of transferrin was not inhibited by AML (Fig. 2i). The AML-mediated inhibition of *Cn* internalization

and crossing in both 2D and 3D *in vitro* BBB models was strongly indicative of macropinocytosis involvement.

Brain microvascular endothelial cells challenged with *Cn* induced the internalization of a macromolecule, further implicating macropinocytosis.

Serum starvation of cells can induce macropinocytosis thereby enabling cells to engulf extracellular cargo including macromolecules.[44,45] To visualize the process of macropinocytosis in brain endothelial cells exposed to *Cn,* we examined the fate of a 70 kDa FITC-labeled dextran macromolecule (Fig. 3).[46] Brain endothelial cells were either starved of serum or fed with medium containing serum (non-serum starved) for 24 h and subsequently exposed to *Cn* for 1 h in the presence of FITC-dextran. We observed a *Cn*-induced uptake of dextran in cells that was independent of serum starvation (Fig. 3d). Distinct peri-nuclear puncta (green), indicative of dextran uptake, observed in serum starved (Fig. 3a) and *Cn*-treated (Fig. 3b, 3d) were found in close proximity to cryptococci (red) (Fig. 3d). Quantification of the internalized dextran signal suggested that *Cn* induced significant uptake of the dextran macromolecule in non-serum starved cells to levels comparable to serum starvation in cells not exposed to *Cn* (Fig. 3e). Moreover, the uptake of FITC-dextran induced by *Cn* in non-serum starved cells was significantly diminished by AML-treatment, further implicating macropinocytosis (Fig. 3f).

***Cn* crossing of the BBB in the organoid model was contingent on EphA2 activity.**

We next examined the contribution of the ephrin receptor tyrosine kinase, EphA2, to the neuroinvasion of *Cn* in BBB organoids that were genetically modified with the CRISPR/Cas9 system to knock out EphA2 in brain endothelial cells. The EphA2 knockout (KO) cells expressing Red Fluorescence Protein (RFP) exhibited the same peripheral localization as wild type (WT)

endothelial cells (Fig. 4a). Western blot analysis of EphA2 KO cells confirmed the lack of EphA2 protein expression (Fig. 4b).

Organoids constructed with EphA2 KO endothelial cells were exposed to *Cn* for 24 h, after which the number of endocytosed fungal cells was quantified (Fig. 4c). Significantly fewer fungal cells were internalized by the organoids deficient in EphA2. Conversely, over-expression of EphA2 resulted in an increased rate of *Cn* crossing (Supp. Fig. 4). These results were consistent with our prior study using the 2D BBB transwell model showing that EphA2 is required for *Cn* to cross the brain endothelium.[21] This also further demonstrated that the lack of EphA2 may not have compromised the integrity of the organoid endothelium to the extent that it permitted *Cn* crossing.

To assess whether organoid astrocytes were affected by the absence of EphA2 in endothelial cells, GFAP, a marker of astrocyte activation and indication of neuroinflammation, was quantified in intact organoids. The intensity of GFAP expression was significantly higher in organoids deficient in EphA2 when compared to wild type (EphA2+) organoids (Fig. 4d). Notably, GFAP expression increased significantly when organoids were exposed to *C. deuterogattii*(*Cd*) a fungal species known to cause disease primarily in immunocompetent individuals.[47,48] This result was contrary to the levels of GFAP expression in organoids challenged with *Cn*, which were similar to control (Fig. 4e). These data are consistent with numerous studies that have reported a milder neuroinflammatory response associated with *Cn* brain burden compared to other neurotrophic pathogens, and further underscore the ability of BBB organoids to discern differences that the more commonly used 2D transwell BBB models overlook.[49,50]

_Cn_-induced activity of GTP-bound Cdc42 is dependent on both EphA2 and CD44.

Eph receptors and their ligands are most notably known for their prominent role in embryonic development. They typically act as guidance cues by mediating contact- dependent communication between cells of the same or different types to control: cell morphology, adhesion,

movement, proliferation, survival and differentiation. The role of the Eph/ephrin system in development and homeostasis is reliant on its ability to induce alterations to the cytoskeletal system of a cell. Both class A and class B eph receptors and ephrins use some common signaling effectors, such as Src family kinases and Ras/Rho family GTPases (Rho, Rac1 and Cdc42), which are particularly important for the organization of the actin cytoskeleton and cell adhesion. Studies have shown that during development, the EphA2 receptor activation specifically leads to an elevation of GTP-Rac1 via Vav GEFs in vascular endothelial cells to regulate angiogenesis. Macropinocytosis, initiated by actin-polymerization and plasma membrane folding, produces cell surface ruffles that encapsulate extracellular cargo into macropinosomes. The entire process is regulated by signaling pathways, including small Rho GTPases such as Cdc42.[51] To test the hypothesis that EphA2 promotes macropinocytosis of fungal cells by influencing actin remodeling through downstream signaling of Rho Gtpases, we employed an activation assay to examine Rho Gtpase activity. While we did not see an increase in GTP-bound (active) Rac1, GTP-bound (active) Cdc42 was detected in brain endothelial cells exposed to *Cn* with high levels of Cdc42 activity relative to unexposed cells (Fig. 5a). EphA2 KO endothelial cells that had been exposed to the same *Cn* inoculum had significantly reduced GTP-bound Cdc42 (Fig. 5a), suggesting that *Cn* stimulation of active Cdc42 was dependent on EphA2 activity. We confirmed by western blot analysis that Cdc42 protein expression levels were comparable in all endothelial cell lysates (Fig. 5c).

Next, we sought to examine whether adherence of *Cn* to brain endothelial cells via CD44 was required for the EphA2-mediated macropincytosis of *Cn*. Previous studies found that a hyaluronic acid-deficient strain of *Cn*, which lacks the gene encoding hyaluronic synthase (*CPS1*), failed to bind CD44, a transmembrane glycoprotein receptor for hyaluronic acid, and was defective at crossing the BBB.[31-33] Employing the same Cdc42 activation assay as performed above, we detected significantly reduced levels of active GTP-bound Cdc42 in wild type (EphA2+) and EphA2 KO brain endothelial cells exposed to the *CPS1* deletion strain of *Cn* (Fig. 5b). The

lack of activity was not due to reduced or absent expression of Cdc42 in cell lysates as evidenced by western blot analysis (Fig. 5d). Collectively, the data suggest that *Cn* engages both CD44 and EphA2 to promote Cdc42-mediated signaling and thereby induce macropinocytosis.

_Cn_ recruits CD44 and EphA2 as a complex in brain endothelial cells.

The dependence of *Cn* on both EphA2 and CD44 to adapt macropinocytosis and cross the BBB, led us to question whether EphA2 could form a molecular complex with CD44 in brain endothelial cells. To probe this possibility, we employed AlphaFold3 (AF3) [52] to predict potential interaction interfaces between the EphA2 extracellular region and CD44. The structural predictions suggested two plausible binding sites for CD44: one located in the EphA2 ligandbinding domain (LBD) and a second in the fibronectin domains (FN1–FN2) positioned proximal to the plasma membrane (Fig. 6a). The predicted models yielded ptm scores of 0.49 and iptm scores of 0.13/ 0.11, indicating relatively low confidence in the inter-protein interface. Such low iptm values are not unexpected, as no structural evidence for EphA2–CD44 interactions currently exists in structural databases, making it challenging for AF3 to accurately capture the interface.

Nevertheless, AlphaFold models can still serve as useful hypotheses for exploring possible binding modes. To test whether the predicted complexes could form stable assemblies, we carried out molecular dynamics (MD) simulations on the LBD:CD44 and FN:CD44 models independently. As a positive control, we simulated the EphA2 LBD bound to ephrinA5, using the crystal structure as the starting model.[53] In all cases, the complexes remained stable throughout 200 ns of simulation in solution. The backbone RMSD profiles (Supplementary Fig. 5. a–c) exhibited minimal fluctuations, indicating that both CD44-binding modes are structurally compatible with EphA2 and can persist on the relevant timescale. We next clustered the simulation trajectories, using an RMSD cutoff of 5 Å for LBD:CD44 and FN:CD44 complexes, and 2 Å for the LBD:

ephrinA5 control system. The dominant conformation of the LBD:CD44 complex (Fig. 6b) highlighted specific EphA2 residues, including Q56, Y65, D61, and F156, that formed stable contacts with CD44. Interestingly, the same EphA2 residue Q56 also mediates interactions with ephrinA5, together with R103, D53, and G39, in the LBD: ephrinA5 complex (Supplementary Fig. 5d). This overlap suggests that CD44 and ephrinA5 may compete for binding to the same functional interface of EphA2. By contrast, the dominant FN:CD44 conformation (Fig. 5c) revealed interactions involving both FN1 and FN2 domains, suggesting that CD44 can also engage EphA2 through a distinct, membrane-proximal site. To gain deeper mechanistic insights, we analyzed intermolecular contacts over the course of the simulations (Supplementary Fig. 6a-c). The interaction analysis confirmed that CD44 engages the LBD of EphA2 at an interface overlapping with ephrinA5 binding, while also being capable of forming a secondary, non-overlapping interaction with the FN domains. The ability of CD44 to bind EphA2 at two structurally distinct regions may provide a molecular basis for cooperative signaling in endothelial cells. In particular, competition with ephrin ligands at the LBD could modulate canonical EphA2 signaling, whereas FN-mediated interactions may stabilize CD44 association near the membrane to facilitate macropinocytic uptake.

To visualize the CD44 and EphA2 protein-protein complex, we used an *in-situ* fluorescence-based proximity ligation assay (PLA, DuoLink) in both primary and immortalized brain endothelial cells challenged with *Cn.* The detected fluorescent signal, evidenced by the red puncta in brain endothelial cells challenged with *Cn*, were indicative of a molecular interaction between EphA2 and CD44 (Fig. 5g, 5h). Quantification of the fluorescence signal detected in mouse primary brain endothelial cells (Fig. 5e) and in immortalized human brain endothelial cells (Fig. 5f) revealed stimulation of the EphA2-CD44 protein interaction by *Cn* in both cell types, which was not observed in brain endothelial cells exposed to *Cd*.

Discussion

A key innovation of the current study is the use of the 3D human BBB organoid model for the first time to elucidate mechanistic details by which *Cn* engages and crosses the BBB. A crucial feature of the organoid, vital to replicating the functionality of the BBB, is the direct contact of endothelial cells, pericytes and astrocytes, which collectively maintain the barrier integrity.[30] Despite some limitations, human BBB organoids are a highly versatile and translational tool that overcome many of the constraints posed by 2D *in vitro* BBB models.[30] By leveraging human BBB organoids in our studies, we determined that *Cd* and *Cn* elicit distinct responses from endothelial cells and astrocytes, which would have been difficult to discern in other BBB models. We also demonstrated that the BBB organoids are amenable to genetic manipulation. We engineered BBB organoids with endothelial cells that lacked EphA2 and detected a concomitant increase in GFAP+ astrocytes that likely acted in a compensatory manner to reinforce the barrier, as evidenced by the inability of *Cn* to cross the BBB.[54,55] These results provide mechanistic insight into *in vivo* studies that found EphA2 deficiency preserved BBB integrity.[56,57]

In the present study we have made several compelling observations of the endocytic mechanism responsible for internalizing *Cn* and driving transcytosis across the brain endothelium. Despite the challenging nature of demonstrating the engulfment and transport of a pathogen by macropinocytosis, due to the non-specificity of this endocytic pathway, the data presented here strongly implicate macropinocytosis as the mechanism of entry. Exploitation of this process by *Cn* is of particular interest because the paucity of fluid phase endocytosis (i.e., macropinocytosis) is a distinguishing feature of the brain endothelium.[58-60] At the same time, other pathogens have also adapted this mode of entry into non-phagocytic cells,[61-68] which may have evolved from interactions either with innate immune cells that utilize macropinocytosis to survey and internalize the bulk extracellular milieu, or from single-celled eukaryotes that use macropinocytosis as a feeding-mechanism.[69] Unlike other endocytic processes,

macropinocytosis[70-73] is not triggered by cargo binding or direct contact with large particles. Moreover, the larger size of macropinosomes (0.2-10 μm in diameter) would be the appropriate size for *Cn* (4-6 μm), unlike canonical endocytic pathways that typically produce vesicles less than 0.1 μm in diameter.[26,69] While macropinocytosis is considered to be essentially nonselective (receptor-independent), recent evidence suggest that ligand-bound integrins and receptor tyrosine kinases may provide some degree of selectivity to this process.[74]

The role of the Eph/ephrin system in development and homeostasis is reliant on its ability to induce alterations to the cytoskeletal system of a cell. As a consequence, the Eph/ephrin system has been exploited by a number of pathogens to gain intracellular and intercellular entry into cells and organ systems to establish infection. Dutta et al, found that Kaposi's sarcoma associated herpes virus activates EphA2 to initiate clathrin-mediated endocytosis and knocking down EphA2 inhibits viral entry into endothelial and fibroblast cells. Additionally, EphA2 is required for Chlamydia trachomatis entry into uterine epithelial cells and its recruitment of PI3 kinase is required for effective replication of chlamydia. With there being such a high expression of EphA2 receptors in the brain, more recently, the role of these receptors in neuropathology has been of great interest. Darling et al, established that EphA2 was upregulated during cerebral malaria infection and that EphA2-/- mice that were infected had improved survival and a more intact bloodbrain-barrier (BBB) throughout the progression of infection. As previously aforementioned, we have established that EphA2 must be present and activated on brain microvascular endothelial cells for the direct neuroinvasion of the BBB by *Cryptococcus neoformans* to establish cryptococcal meningoencephalitis. The mechanisms by which Eph receptors/ ephrins mediate their downstream signaling, are crucial to gaining an understanding of various mechanisms of pathogenesis and are rapidly being unveiled.

In a previous study, we demonstrated that transcytosis of *Cn* is mediated by a *Cn*- induced, ligand-independent activation of EphA2, potentially initiated by CD44, but the underlying

mechanism had not been determined.[21] Moreover, no studies have linked EphA2 and CD44 in the context of fungal neuroinvasion, although multiple lines of evidence have implicated their individual roles.[18,21,32,33] In the present study, we found that CD44 and EphA2 are both critical for the successful entry and transcytosis of free *Cn.* Collectively our data support a model in which *Cn* has adapted macropinocytosis as the mechanism of entry to the CNS by recruiting both EphA2 and CD44 (Fig. 7). This is based on two key observations: (i) we detected a molecular interaction between EphA2 and CD44 in both human and primary mouse brain endothelial cells that is stimulated by *Cn*; and (ii) the absence of EphA2 or a failure to engage CD44 via hyaluronic acid-binding prevented the downstream activation of Cdc42, a key activator of macropinocytosis.[75,76] Our model is further supported by the established independent roles of CD44 and EphA2 in *Cn* adherence to- and crossing of the brain endothelium, both of which require cytoskeleton remodeling, and activation of Rho-GTPase signaling cascades - activities attributed to both CD44 and EphA2.[77] Our model suggests that the *Cn*-induced phosphorylation of EphA2 we previously reported as a required event for transcytosis[21], is mediated by the association of EphA2 with CD44 upon binding *Cn*. This transactivation of EphA2 may involve PKC, a serine threonine kinase required for transcytosis of *Cn*[18] and known to phosphorylate EphA2 independent of ligand binding (non-canonical signaling).[78,79] The culmination of EphA2-CD44 complex formation would activate Cdc42-mediated signaling, and thereby trigger macropinocytosis. Our *in vitro* data is further supported by the *in-silico* prediction of a molecular interaction between EphA2 and CD44 such that CD44 may modulate canonical signaling of EphA2 via the LBD domain, while the FNmediated interaction with CD44 may serve to stabilize the CD44-EphA2 complex near the cell surface and facilitate *Cn* entry.

Consistent with macropinocytosis as the mode of entry, we found that amiloride treatment prevented the internalization of *Cn* by brain endothelial cells in both the BBB organoid model and the monoculture transwell BBB model. Amiloride is known to inhibit macropinocytosis by reducing

endomembrane pH and preventing Cdc42 signaling, which is required for the actinpolymerization/remodeling needed to form the membrane ruffles and maturation of macropinosomes.[39,76] Our results further demonstrate that brain invasion by *Cn* does not damage tight junctions or proceed through lytic death of the brain endothelium, at least initially.[22] Despite their advantages, certain tradeoffs associated with BBB organoids must be noted. While the BBB organoid model recapitulates the cell-to-cell contact required for BBB function and barrier integrity, it still cannot recapitulate all the relevant *in vivo* conditions, such as the directional shear forces from blood flow. Also, the organoid core appears to be solid, unlike the “less compact” organization of pericytes and astrocytes observed in brain tissue, which likely impedes the penetration of *Cn* deep into the organoid interior. Our organoid model does not yet include neurons, oligodendrocytes, and microglia, which are likely to respond to internalized fungal cells and further impact the integrity of the BBB.[4,5] However, we emphasize that our organoid model readily captures other important interactions between cells of the neurovascular unit and cryptococci; we found that astrocytes were especially activated upon exposure to *Cd*, and yet *Cd* had lower crossing rates than *Cn*, meaning that the effect of *Cd* on astrocytes is much stronger than *Cn* given that relatively few astrocytes were in direct contact with *Cd* as compared to *Cn*. This suggests that secreted factors from *Cd* may be responsible for the astrocyte activity observed in our studies.

Astrocyte activation can occur as a result of BBB dysfunction, with tight junctions breaking down completely and allowing macromolecules (e.g., albumin) to come into direct contact with astrocytes, eliciting inflammation.[80,81] However, if this had occurred in our study, it did not occur to the extent that permitted *Cd* to infiltrate between endothelial cells. This implies an A2 type astrocytic response, in which astrocytes act to reinforce the BBB [82-84] and further suggests that *Cn* is entering the brain with the cooperation of brain endothelial cells, while *Cd* lacking this cooperation, elicits an astrocytic response, and is thwarted from crossing. However, further

studies would be required to fully differentiate A1 and A2 astrocytes in the context of fungal neuroinvasion.[84] That *Cd* has reduced BBB crossing relative to *Cn* in the BBB organoid model, is consistent with epidemiological studies demonstrating that *Cd* causes significantly fewer CNS infections compared to *Cn*.[85,86] However, when *Cd* does infect the brain it often causes severe neurological complications likely due to a strong immune response that leads to inflammation.[87]

It is well known that capsule components of *Cn* downregulate the mammalian host immune response.[4,88] The secreted *Cn* capsule component glucuronoxylomannan (GXM) in particular has been shown to influence the response of microglia to CNS-resident *Cn*, with cryptococcomaproximal microglial cells adopting a non-phagocytic cell morphology near fungal cells producing a wild-type capsule.[4] In the mouse model, GXM also reduces overall infiltration of microglia into cryptococcomas by directly reducing microglia motility, and skews the composition of circulating immune cells extravasating to sites of infection away from macrophages and B cells in favor of neutrophils and T-cells.[4] The capsules of *Cn* and *Cd* differ in terms of capsule composition and average length of polysaccharides, with *Cd* expressing shorter GXM chains, and provoking a greater immune response in certain tissues,[49] although *Cd* may have a certain advantage over *Cn* in immune evasion in the lung.[89] Secreted capsule components that differ between *Cn* and *Cd* may therefore account for the differences in the astrocytic response observed in our BBB organoid model. Utilizing a human brain organoid model generated from human embryonic stem cells infected with *Cn* and *Cd* may provide further insight, as would expanding the human BBB organoid

model to include additional cell types.[90]

Methods

Organoid model

Human brain microvascular endothelial cells (HBMEC/D3 endothelial cells; also referred to as immortalized BMECs or iBMECs) were a gift from Babette Weksler.[40] These iBMECs were maintained in collagen-coated flasks with Endothelial Growth Media (EGM, Lonza) containing 0.25% FBS, 1 ng/μL Fibroblast Growth Factor, and Penicillin/Streptomycin. Human primary astrocytes and brain vascular pericytes were purchased from ScienCell (Cat. #1800 and Cat. #1020 respectively, Carlsbad, California). Astrocytes and pericytes were maintained in poly-Llysine coated flasks with their respective growth media (ScienCell, Carlsbad, California). In some experiments, primary human brain microvascular endothelial cells (Cat. #1000, ScienCell), maintained in the supplier-provided media (Cat. #1001, ScienCell) were used. Organoids were formed as previously described.[34] Briefly, astrocytes and pericytes were cultured separately in 2D cultures before being trypsinized in 0.025% Trypsin-EDTA, seeded at $1x10^3$ per well each in lowadhesion polymer-coated 96-well plates (InSphero, Brunswick, Maine) inclined at 30 degrees to foster the formation of single organoids in each well for 48 h (37ºC, 5% CO_2). Brain endothelial cells were then split and seeded at $1x10^3$ cells per well on top of the astrocytes and pericytes.

Baseline Permeability with FITC-dextran

Organoid permeability was established using low (FITC) versus high (FITC-dextran, 70 kDa) molecular weight fluid-phase fluorescent markers. FITC-dextran was diluted in EGM-2 media to a working concentration of 14.3 nM (10 μg/mL) and FITC to 500 nM (0.2 μg/mL) because it was empirically determined that these concentrations were approximately equivalent in relative fluorescence. Organoids were incubated in either FITC-dextran or FITC for 24 h, washed twice with warm PBS and once with media, then imaged on a confocal microscope at up to 100 μm depth in 8 μm slices. Average fluorescent signal in the FITC channel inside the spheroid at 100 μm was compared to assess permeability.

Fixation and sectioning of organoids

Following treatment, organoids were removed from 96-well plates using flame-polished glass aspirators and placed in conical tubes containing immunofluorescence buffer (IF buffer: 0.15 M NaCl, 5 mM EDTA, 20 mM HEPES pH 7.5) and washed thrice, with intervals to settle to the bottom of tubes between washes. PBS was replaced with 4% PFA (pH 7.4 in PBS) and fixed overnight at 4ºC with agitation. Organoids were then washed in IF buffer thrice before being placed in a 30% sucrose solution for cryoprotection, which was left to diffuse into organoids for 3 h at 4ºC. DAPI was included in the cryoprotectant solution to aid visibility in a subsequent step. Flame-polished glass aspirators in combination with a stereoscope were used to transfer organoids to embedding molds and subsequently flash-frozen in a dry-ice ethanol bath and stored at -80ºC. OCT blocks were sectioned at 15 µm in a cryostat under near-UV illumination in order to distinguish DAPI-stained organoids against the white OCT background. In experiments not requiring antibody staining, slides were rehydrated in IF buffer and sealed with aqueous mountant beneath coverslips.

Live-cell membrane dye

An Invitrogen CellTracker fluorescent probe (Green, cat#: C7025) was used to stain pericytes prior to organoid formation to confirm the expected layering of cells in organoids. Staining procedure was done per the recommended manufacturer's protocol. Briefly, the dye was dissolved in DMSO at 10 mM, then diluted in serum-free media to 15 µM. Cells were washed, trypsinized, pelleted at 200g for 3 min, and washed with warm PBS 3x. Cells were then incubated with dye-containing media for 30 min at 37ºC in 5% CO_2. Dyed cells were then washed twice with warm PBS before being combined with non-dyed cells as described above. Organoids were then

fixed and sectioned as described previously before being imaged on a Leica TCS SP8 STED 3X confocal microscope with 50 nm laterally and 150 nm axially optical sectioning.

Immunofluorescence

After sectioning, slides with spheroid-containing sections were brought up to room temperature over 30 min, then rehydrated in IF buffer for 1 min. Slides were then transferred to antigen retrieval solution (10 mM Sodium Citrate Buffer, 0.05% Tween 20, pH 6.0) for 30 min at 60ºC, washed twice with IF buffer, then permeabilized and blocked for 2 h at room temperature in 1% BSA, 0.1 Triton X-100 in IF buffer. Antibodies [rabbit anti-Claudin5 (abcam ab15106-1003), 1:250, and mouse anti-GFAP (Invitrogen MA5-12023), 1:2000] were diluted in 1% BSA-IF buffer. Slides were incubated with primary antibodies at 4ºC overnight, with rotation. Secondary antibodies (goat-anti rabbit TR ab6719, goat-anti mouse Cy5 ab6563, all used at 1:1000) were prepared in 1% BSA-IF buffer. Slides were washed five times in IF buffer, then incubated at room temperature with secondary antibodies for 2 h with gentle agitation. Sections were washed five times and nuclear stained with DAPI or Hoechst.

TEM

Organoids were immersed in primary electron microscopy fixative (2.5% glutaraldehyde, 2% paraformaldehyde, 0.1 M sodium phosphate) for 3 h, rinsed with 0.1 M sodium phosphate, then fixed in secondary electron microscopy fixative (1% osmium tetroxide, 1.5 potassium ferrocyanide) for 1 h. Fixed organoids were washed thrice in cold deionized water, dehydrated in an ethanol series, then fixed in resin (Araldite 6005-Epon 812 mixture) overnight at 70ºC. Resin blocks were then sectioned at 100 nm, transferred to copper grids, dried at 60ºC for 30 min, and stained (4% uranyl acetate, 0.1 % lead citrate, 0.1 N sodium hydroxide). Imaging was performed with a FEI Talos L120C TEM 80kv.

Generation of EphA2 knockout (KO) cell line

CRISPR/Cas9 technology was used to generate the HCMEC/D3 EphA2 KO cell line lacking expression of EphA2. Two sets of plasmids were used in the CRISPR/Cas9 method - the EphA2 CRISPR/Cas9 KO plasmids and the EphA2 HDR plasmids, both of which were ordered from Santa Cruz Biotechnology. The EphA2 CRISPR/Cas9 KO plasmids (Cat# sc-400535-KO-2) consist of a pool of three plasmids each encoding the Cas9 nuclease and a EphA2-specific 20 nt guide RNA (gRNA) designed for high knockout efficiency. Sequences of the gRNA were derived from the GeCKO (v2) library and direct the Cas9 protein to induce a site-specific double strand break (DBS) in the genomic DNA. Co-transfection with the EphA2 HDR plasmids (Cat# sc400535-HDR-2) were carried out to select for cells containing a successful Cas9-induced DSB. The HDR plasmids consist of a pool of 2-3 plasmids, each containing a homology-directed DNA repair template corresponding to the cut sites generated by the EphA2 CRISPR/Cas9 KO plasmids. Each HDR plasmid contains two 800bp homology arms designed to specifically bind to the genomic DNA surrounding the corresponding Cas9-induced DBS site, leading to insertion a puromycin resistance gene to enable selection of stable knockout cells and insertion an RFP (Red Fluorescent Protein) gene to visually verify transfection. The puromycin resistance and RFP genes are flanked by two LoxP sites to allow for further processing by Cre recombinase (Cat# sc418923) if desired. Transfection steps were carried out according to the manufacturer's instructions. Briefly, freshly passaged HCMEC/D3 cells were first grown on a collagen-coated 6well culture dish to about 50-80% confluence. The sub-confluent monolayer was then cotransfected for 48 h with 3 µg of EphA2 CRISPR/Cas9 KO plasmids and 3 µg of the EphA2 HDR plasmids in combination with 5-10 µl of the UltraCruz transfection reagent (Cat# sc-395739). After 48hours of incubation, transfected cells were grown in media containing 2.5 µg/mL of puromycin to select for successful recombination events in which a stretch of the HDR plasmid spanning the puromycin resistance gene and an RFP gene were integrated into the genomic

DNA, leading to loss of transcription and expression of EphA2. Puromycin-resistant and RFP-positive cells were further purified and enriched using FACs (UC Davis flow cytometry core).

Lentiviral Production and Transduction

To generate iBMECs overexpressing EphA2, lentiviral particles were first produced by transient transfection of HEK293T cells using a third-generation packaging system. Briefly, HEK293T cells were co-transfected with the transfer plasmid (pLenti-) and an optimized mix of packaging plasmids - pLP1, pLP2, and pLP/VSVG (ViraPower ^{TM} Lentiviral packaging mix, thermofisher scientific) using Lipofectamine 2000 (Thermo Fisher Scientific) according to the manufacturer's instructions. Viral supernatants were collected 48 and 72 h post-transfection, filtered through a 0.45 µm PVDF filter, and stored at –80°C. iBMECs were transduced with viral supernatant at an MOI of 5 and supplemented with 8 µg/mL polybrene (Sigma-Aldrich). After 48 h, the medium was replaced, and cells were allowed to recover. Transduced cells were selected using blasticidin (1.5 µg/mL) for 3 days before analyzing expression via western blot analysis (anti-V5 tag antibody, ab27671, abcam inc. dilution 1:1000).

BBB transcytosis assay iBMECs were grown on collagen-coated transwells (Transwell-24 well plate, PET membrane, 8.0 µm pore size; Corning Inc., Lowell, MA, USA) as described previously.[40] After differentiation of the cells, *Cn* at an MOI of 10 were added to the upper transwell chamber either in 1x EGM2 media to untreated cells (control treatment), in 1x EGM2 media to cells pretreated with 250 µm AML for 1 h (AML pretreatment) or in 1x EGM2 media with 250 µm AML to cells not pre-treated with AML (*Cn* and AML added together) to assess the effect of AML on the transcytosis of *Cn*. Cells were then incubated at 37°C, 5% CO_2. At 12 h post-infection, the media in the lower chambers was collected and plated onto YPD agar plates to quantify the number of *Cn* that had crossed the iBMECs.

Organoid model (GFAP probing and quantification; *C. neoformans* vs *C. deuterogattii*; amiloride treatment assays)

Fungi (*Cn, Cd, Sc* strains, respectively - *Cryptococcus neoformans* H99, *Cryptococcus deuterogattii* VGII NIH-444, *Saccharomyces cerevisiae* W303) were grown overnight in 3 mL yeast peptone dextrose (YPD) liquid media at 30ºC overnight. Second cultures were prepared 4 h prior to inoculation. Cultures were pelleted and washed in PBS 3x, diluted in PBS to $2x10^7$ cells/mL, then incubated in 500 µM CFDA-SE (10% DMSO) for 30 min at 37ºC. The CFDA-SEtreated fungi were then washed and resuspended in cell culture media. Media over the organoids replaced with 100 µL of the fungal suspension, sufficient to completely bury organoids, which were returned to the incubator for 24-72 h, depending on the experiment. In experiments involving AML treatment, 250 µM AML or 0.25% DMSO (vehicle control) was added to the cell culture media along with fungi. Organoids were subsequently sectioned and imaged, as described above. BBB crossing was quantified in a semi-automated manner, with the edge of each organoid automatically delineated in ImageJ using a custom macro applied to the DAPI (cell nuclei) channel and redrawn on the FITC (fungi) channel (see supplementary information). This provided an unbiased boundary for manual counting of internalized versus adherent fungi. Fungal cells that had entered at least as far as the first layer of endothelial cells were considered as those that breached the organoid BBB.

Tight junction protein localization in organoids

BBB organoids were created with either regular or EphA2 KO hCMEC/D3 cells, treated with *Cn* for 48 h, and sectioned as described above. Sections were probed with rabbit antiClaudin5 (1:1000, ab15106, abcam) primary antibodies and goat anti-rabbit Cy5 (1:1000, ab6565, abcam) secondary antibodies. To create a metric of protein localization within organoids,

pixel intensity in the Claudin5 (Cy5) channel across the diameter of organoid sections was measured using the Plot Profile tool in ImageJ. Values were normalized to the maximum value within each profile. The coefficient of variation for each normalized profile was then calculated in order to measure signal localization.

2D FITC-dextran uptake iBMECs were grown on 4 well chambered slides (Nunc™ Lab-Tek™ II Chamber slide™ System, Thermo Fisher Scientific Inc., Waltham, MA) as previously described.[20,21] Cells were either exposed to *Cn* (mCherry strain) at an MOI of 50 and 0.5 mg/mL of FITC-dextran or 0.5 mg/mL of FITC-dextran alone. Cells were incubated at 37°C, 5% CO_2 for 1 h. Cells were immediately placed on ice, washed in 1x PBS (pH 7.4) and then washed in 0.1M NaCl solution and 0.1M Glycine solution (pH 3.00) 3x. After another 1x PBS wash, cells were fixed in 4% PFA for 10 min and prepared for confocal imaging (Leica, TCS SP8 STED 3x). For quantification of internalized dextran, an internalization index (dextran signal/area of the cell) was taken for 10 cells per treatment group using Image J software.

Cdc42 Activation Assay

WT and EphA2 KO iBMECs were grown to confluency on 6-well plates as previously described[21] (6-well plates, Corning Inc., Lowell, MA, USA). After differentiation, iBMECs were exposed to *Cn* at an MOI of 10 on ice and then incubated at 37°C, 5% CO_2 for 1 h. To measure Cdc42 activation, the G-LISA activation kit (Kit # BK127 Cytoskeleton Inc., Denver, CO) were used per manufacturer's recommendations. This assay used Cdc42-GTP binding proteins linked to the wells of a 96-well plate. Active, GTP-bound Cdc42 in cell lysates bound to the wells while inactive GDP-bound forms were removed during wash steps. Bound GTP Cdc42 were detected by incubation with a Cdc42 specific antibody followed by a secondary antibody conjugated to HRP

and a detection reagent. The signal was quantified by measuring absorbance at 490 nm using a microplate reader (Spectramax M5, Molecular Devices Inc., San Jose, CA).

Co- immunoprecipitation assay

Hek293T cells were transiently transfected with a V5 tagged EphA2 protein and/ or a Flag tagged CD44 protein with Lipofectamine 3000 (Lipofectamine™ 3000 transfection reagent, ThermoFisher Scientific, L3000001). 48h post transfection, Hek293T cells were exposed to Cn WT for 2h and then were lysed with RIPA buffer (10X RiPA Buffer abcam Inc.) supplemented with a protease inhibitor (cOmplete mini, EDTA free cocktail protease inhibitor, Roche Inc.) and a phosphatase inhibitor (Roche PhosStop phosphatase inhibitor, Roche Inc.). The protein concentrations were measured by Bradford Assay (Quick Start™ Bradford Protein Assay; Bio-Rad Laboratories Inc.). 40 µg of the lysate was saved to confirm that EphA2 and CD44 plasmids were successfully transfected in the cells and were stored at -80°Cwhile the remaining lysate was incubated with the v5 antibody (3.0ug of Ms v5 probe antibody (C-9); Santa Cruz Biotechnology, sc-271944) for 2 h on ice. Subsequently, the lysate and antibody mix were incubated with DynaGreen™Protein A/G magnetic beads (ThermoFisher Scientific, 80104G) for 2 h at 4°C. Beads were then washed with RIPA buffer 10 times and then proteins captured by the beads and lysate that was initially saved were denatured and reduced in Laemmli buffer (Premixed 4X Laemmli protein sample Buffer; Bio-Rad Laboratories Inc.) and 2-mercaptoethanol (Bio-Rad laboratories Inc.), followed by a 10 minute incubation at 70°C. SDS-PAGE electrophoresis was performed with 10% polyacrylamide gel at 80 V for 3 h (Mini-PROTEAN Tetra Cell; Bio-Rad laboratories Inc.). The proteins on the SDS PAGE gels were transferred to nitrocellulose membranes (Nitrocellulose/ Filter paper sandwiches 0.45µm, Bio-Rad Inc.) using the wet transfer method at 4°C (Mini Trans-Blot Cell; Bio- Rad Inc.) at 100 V for 2 h. The nitrocellulose membranes were stained with Ponceau Red (PONCEAU S High Purity; VWR Inc. 0.1% wt/vol with glacial

acetic acid 5% vol/vol) to visualize polypeptide bands and then blocked with 5% milk (BlottingGrade Blocker; Bio-Rad Inc.) for 1 h at room temperature. Membranes were then incubated with primary antibody (1:800 dilution of either Ms anti-Flag probe; Santa Cruz Biotechnology, sc51590 or Ms anti V5 probe; Santa Cruz Biotechnology, sc-271944) at 4°C overnight. The membranes were washed several times with TBST buffer and then incubated in secondary antibody (1:10,000 dilution of Goat anti-Mouse IgG H&L HRP ab6789 and Goat Anti-Rabbit IgG H&L HRPab6721; Abcam Inc., Cambridge, MA, USA) at room temperature for 1 h. After additional washing with

TBST, the chemiluminescent substrate solution for HRP (Supersignal West Pico Chemiluminescent substrate; Pierce Biotechnology, Rockford, IL, USA) was added to the membranes and X-Ray films (HyBlot ES Autoradiography Film; Denville Scientific Inc., Metuchen, NJ, USA) were used to detect the expression of V5 tagged proteins (EphA2) and Flag tagged proteins (Cd44).

EphA2-CD44 Proximity Ligation Assay (PLA)

Brain endothelial cells (BECs) were seeded at 50% confluence in collagen-coated LabTek II chamber slides in EGM2 media containing 0.25% FBS and 1 ng/μL FGF (1X media). To promote the BBB phenotype, after the endothelial monolayer had reached confluency, the concentration of growth factors in media was reduced by half for 24 h, then reduced by half again for another 24 h before introduction of cryptococci (*Cn* or *Cd*). Cryptococci were grown at 30ºC overnight in YPD, then secondary cultures were prepared from overnight cultures and grown 4 h prior to experiments to ensure that fungi were in logarithmic phase growth. The secondary cultures were washed thrice in PBS, then diluted to deliver $3.5x10^5$ cryptococci per 0.7 cm^2 chamber (MOI of 5). Cryptococci and ECs were co-incubated at 37ºC, 5% $CO_2$for 90 minutes. Control chambers that

did not receive fungi were prepared as well. Cells were then washed with warm PBS and fixed with 4% PFA for 10 min at room temperature. A proximity-ligation assay (PLA) using the Duolink system (Sigma-Aldritch) was conducted following the supplier's instructions (protocol source: https://www.sigmaaldrich.com/deepweb/assets/sigmaaldrich/marketing/global/documents/154/882/introduction-duolink-pla-4383-ms.pdf). Briefly, after fixation, cells were blocked with Duolink blocking solution for 1 h at 37ºC in a humidified chamber. Slides were then incubated with mouse anti-CD44 (Abcam ab254530) and rabbit anti-EphA2 (Abcam ab185156), diluted 1:500 and 1:50, respectively, in Duolink antibody diluent (Sigma-Aldrich), and incubated at 4ºC overnight with agitation. Slides were washed twice with PBS before being incubated with anti-mouse PLUS and anti-rabbit MINUS probes diluted 1:5 in DuoLink antibody diluent and incubated for 1 h in a humidified chamber. Ligase (1:40 in ligation buffer) was then added to ligate PLUS and MINUS probes (up to 40 nm separation, per manufacturer specifications) and incubated for 30 min at 37ºC. Amplification buffer containing the red detection reagent and polymerase (1:80) were incubated with slides for 100 min at 37ºC. Control slides that did not receive primary antibodies were processed in parallel. After cover slips were added, slides were imaged using a fluorescence microscope. Quantification of fluorescence was performed in ImageJ.

Molecular Dynamics Simulations

We utilized Alphafold3[52] (ref) to model the interactions of extracellular region (ECR) of EphA2 (A24-V537) with CD44 (Q21-S180). To analyze the protein-protein interface between EphA2-CD44, we started our md simulations with two systems: first one with the LBD (K27-L205) of EphA2 with CD44 and the second one with the FN domains (C325-E530) of EphA2 with CD44. As a control system we used the LBD of EphA2 with EphrinA5 from the crystal structure (PDB: 2X11). The FN:CD44 system and the LBD:CD44/ EphrinA5 systems were encased in a box with dimensions measuring 110 × 110 × 110 $Å^3$ and 90 × 90 × 90 $Å^3$ respectively. The system was

solvated using the TIP3P water model. To ensure neutrality, Na+ ions were added and also 150mM of NaCl was introduced using the CHARMM-GUI interface.[91]Molecular dynamics simulations were performed using GROMACS 2023.3[92] with the CHARMM36m force field.[93]Production MD simulations were carried out in GROMACS using the leap-frog integrator with a 2 fs timestep and a total length of 200 ns. Non-bonded interactions were treated with the Verlet cutoff scheme, a 1.2 nm cutoff (force-switch for van der Waals), and PME for electrostatics. Temperature was maintained at 303 K using the velocity-rescale thermostat, and pressure at 1 bar with the C-rescale barostat. All bonds involving hydrogens were constrained with LINCS. A total of three replica simulations were conducted for each system. Trajectory analysis was conducted using the integrated modules within GROMACS. Subsequently, the data was visualized and plotted using Origin.

Statistical analysis

Data were analyzed for statistical significance with either GraphPad Prism 10 software or R v4.4.2. Statistical analysis of two data sets was performed using unpaired, two-sided parametric t-tests with Welch's correction. Data sets greater than two were analyzed by one-way analysis of variance (ANOVA) with Tukey's multiple comparisons test. (ns = not significant, *p<0.05, **p<0.01, ***p<0.001, ****p<0.0001).

Figure 1.

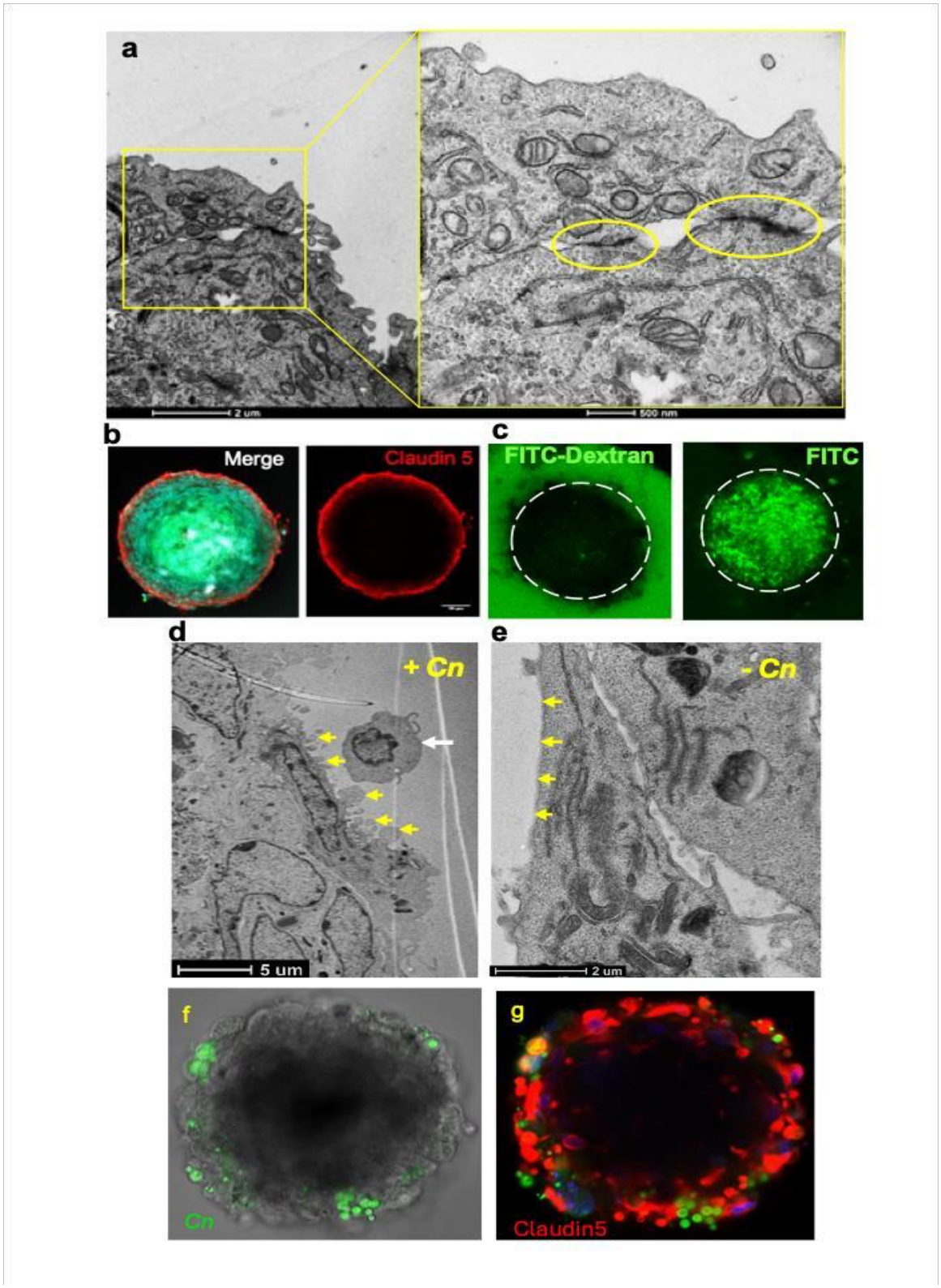
a
2 um
500 nm
b
Merge
Claudin 5
c
FITC-Dextran
FITC
d
+ Cn
5 um
e
- Cn
2 um
f
Cn
g
Claudin5

Fig 1. Human BBB organoids possess a functional endothelial barrier that is responsive to *Cn*. a TEM tight junctions between brain endothelial cells on the surface of an organoid. **b** Immunofluorescence image of the tight junction protein Claudin5 on the surface of fixed and sectioned BBB organoids, indicating the presence of tight junctions and position of endothelial cells. Interior of organoid stained with DAPI. **c** BBB organoids are not permeable to a large molecular weight dye (70 kDa FITC-Dextran, left panel), in contrast to small molecules like FITC (right panel). **d** TEM images of membrane ruffling and protrusions (yellow arrows) along the surface of brain endothelial cells exposed to *Cn* (white arrow), **e** in contrast to flat endothelial cell surface (yellow arrows) on BBB organoids not exposed to *Cn*. **f, g** Immunofluorescence image of BBB organoids consisting of primary human brain endothelial cells express Claudin-5 (red) and show infiltration of *Cn* (green) indicating similar morphology and function to organoids with immortalized brain endothelial cells.

Figure 2.

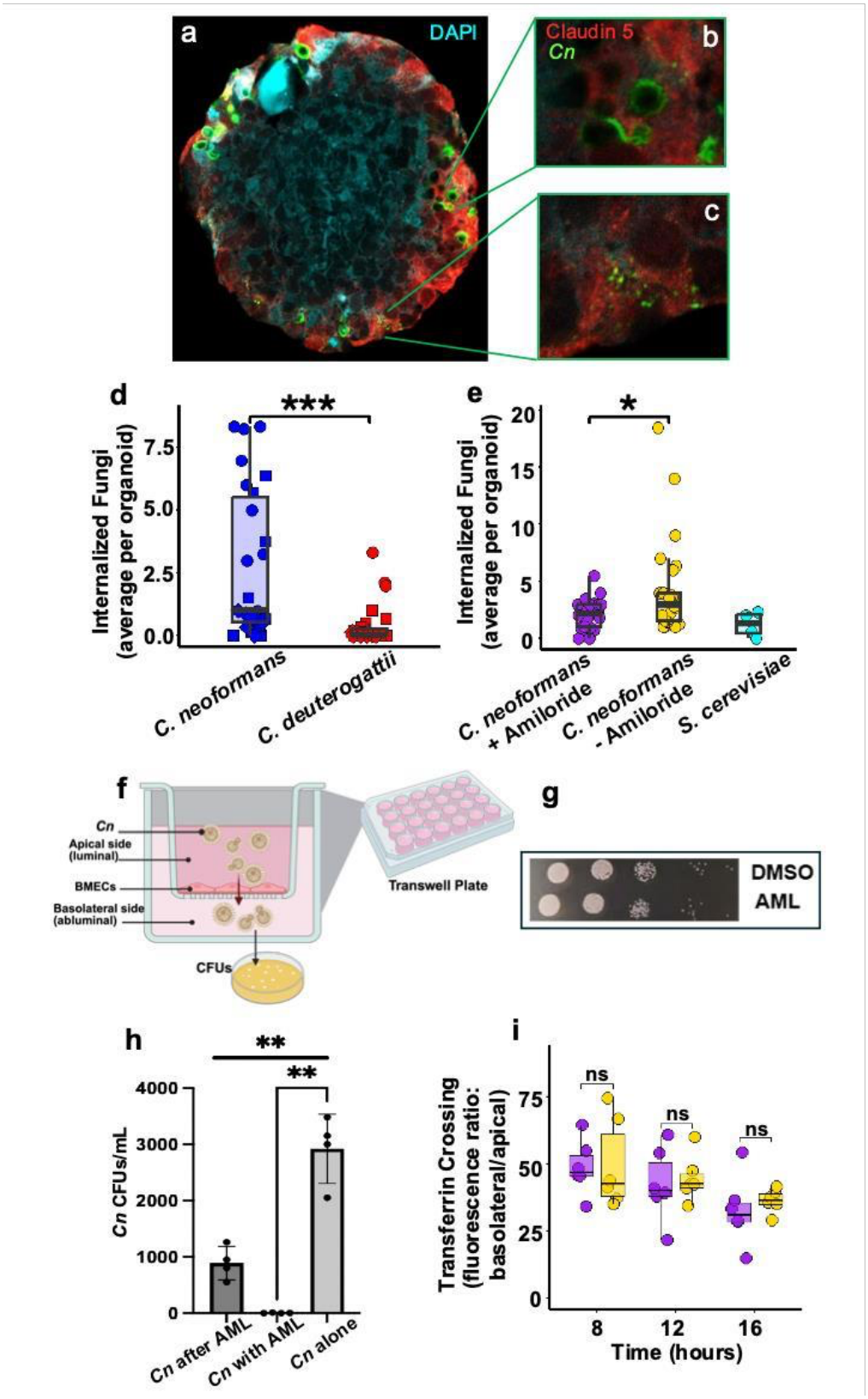
a
DAPI
Claudin 5
Cn
b
c
d
***
Internalized Fungi (average per organoid)
7.5
5.0
2.5
0.0
C. neoformans
C. deuterogattii
e
*
20
15
10
5
0
C. neoformans + Amiloride
C. neoformans - Amiloride
S. cerevisiae
f
Cn
Apical side (luminal)
BMECs
Basolateral side (abluminal)
CFUs
Transwell Plate
g
DMSO
AML
h
**
**
Cn CFUs/mL
4000
3000
2000
1000
0
Cn after AML
Cn with AML
Cn alone
i
Transferrin Crossing (fluorescence ratio: basolateral/apical)
ns
ns
ns
75
50
25
0
8
12
16
Time (hours)

Fig 2. Treatment of BBB organoids with Amiloride, a potent inhibitor of macropinocytosis, prevents fungal cells from crossing the endothelial barrier of organoids. a Fluorescent image of BBB organoid incubated with *Cn* (green) for 72 h, fixed, sectioned and imaged on a confocal microscope. *Cn* stained with anti-capsule antibody (anti-GXM 18b7, 1:300) kindly provided by A. Casadevall. Claudin-5 expression shown in red. **b** Enlarged image shows fungal cell (green) internalized by Claudin-5 (red)-expressing endothelial cells. **c** Degraded and/or released *Cn* capsule components shown in green. **d** *Cn* invades BBB organoids at a significantly higher rate than *Cd* at 48 h (two-sample t-test with Welch's correction: t = 4.01, df = 28.59, $p < 0.0004$). **e** Amiloride (250 μM) treatment significantly reduces (t = -2.46, df = 28.23, $p = 0.020$) *Cn* internalization to a level comparable to non-pathogenic *Saccharomyces cerevisiae* (t = 1.53, df = 4.50, $p = 0.194$). Each data point represents the average number of internalized fungal cells per BBB organoid across multiple images of fixed and cryo-sectioned organoids. For (d) and (e), each data point represents the average number of internalized fungal cells per BBB organoid across multiple images of fixed and cryosectioned organoids. **f** Schematic of the transwell human BBB model. To assay for BBB crossing, fungal cells or fluorescent macromolecules were first added to the upper chamber (luminal side) and then collected from the bottom well (abluminal side) for either CFU enumeration or fluorescence quantification. **g** Spot assay comparing growth of *Cn* on minimal media following incubation for 24 h with 250 μM amiloride or DMSO control in endothelial media at 37ºC, 5% CO_2. **h** Treatment of iBMECs with amiloride (250 μM) inhibits *Cn* crossing in an *in vitro* BBB transwell model. iBMECs were either pre-treated with amiloride for 30 min_or treated with amiloride along with *Cn*. Statistical analysis of the transwell assay was done using two-tailed unpaired t-test with Welches correction (t = 9.504, df = 3.00, $^{**}p = 0.0025$) or one-way ANOVA (GraphPad Prism 10 software). **i** In the transwell model, the presence of amiloride (purple) makes no significant difference in the rate of transferrin transcytosis relative to the vehicle control (yellow). The relative fluorescence ratio (RFU) was measured at 8 h, 12 h, and 16 h posttreatment. Non-significant differences were determined by Welch two-sample t-test between

treatment and control at 8 h (t = -0.12, df = 8.27, p = 0.91), 12 h (t = -0.34, df = 8.42, p = 0.74), and 16 h (t = -0.65, df = 6.13, p = 0.54) (R v4.2.2).

Figure 3.

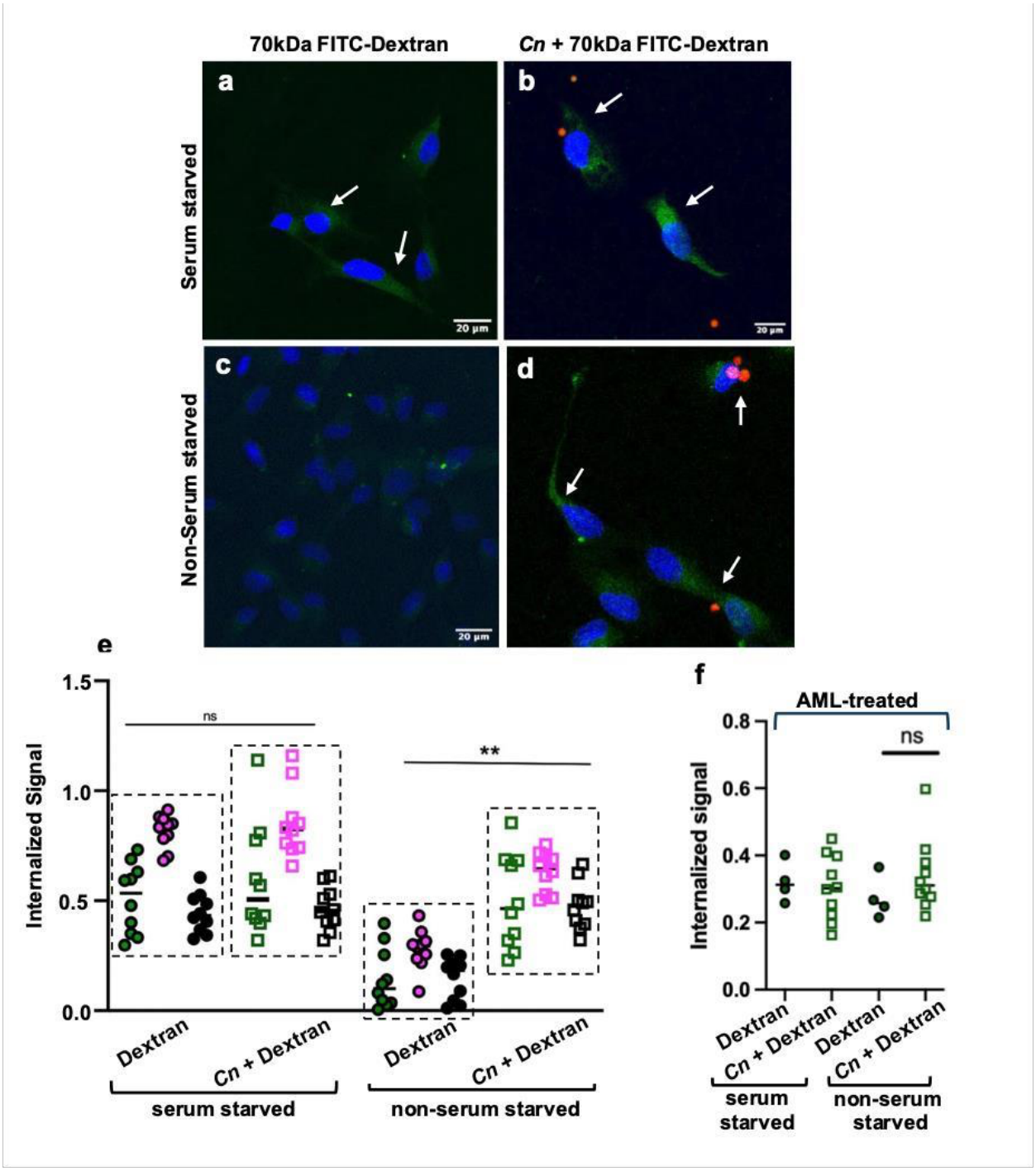

Fig 3. *Cn* induces the internalization of the macromolecule, 70kDa FITC-Dextran, by brain endothelial cells independent of serum starvation. a – d Exposure of non-serum starved human iBMECs (stained with DAPI, blue) to *Cn* promotes internalization of dextran indicated by perinuclear staining of dextran (green puncta) that co-localizes with fungal cells (*Cn,* shown in red). This is in contrast to non-serum starved iBMECs not treated with *Cn* (negative control). Serum starvation of iBMECs (positive control) leads to dextran uptake. iBMECs were serum starved for 24 h and then exposed to 0.5mg/mL FITC-Dextran (70 kDa) and treated with *Cn* (MOI 10) for 1 h. iBMECs were washed of extracellular fluorescent signal, fixed and analyzed via confocal microscopy. **e** Internalized FITC-dextran signal was quantified by determining the internalized signal of FITC-Dextran within the area of each cell (internalization index) using ImageJ.[46]Three biological replicates shown for each treatment. Each replicate is represented in a different color (green, pink or black) and filled data points represent the cells that were exposed to dextran alone while hollow data points represent the cells that were exposed to *Cn* and dextran. Each data point represents the average internalization index within one microscopic image. Statistical analysis was done using a two tailed, unpaired t test (n = 10, per group, t= 5.934, df=18, $^{**}p = 0.007$) (GraphPad Prism 10 software). **f** Amiloride inhibits FITC-dextran uptake by iBMECs. iBMECs serum starved and non- serum starved were treated with 250 μM amiloride for 1 h prior to exposure to *Cn* (MOI of 10) and 0.5 mg/mL FITC-dextran. Internalized FITC-Dextran signal was quantified by determining the internalized signal of FITC-Dextran within the area of each cell (internalization index) using Image J. Each point represents the average internalization index within one microscopic image (n > 3). Statistical analysis was done using a two tailed, unpaired t test with Welch correction (t= 1.412, df =9.5, $p = 0.1897$) (GraphPad Prism 10 software).

Figure 4.

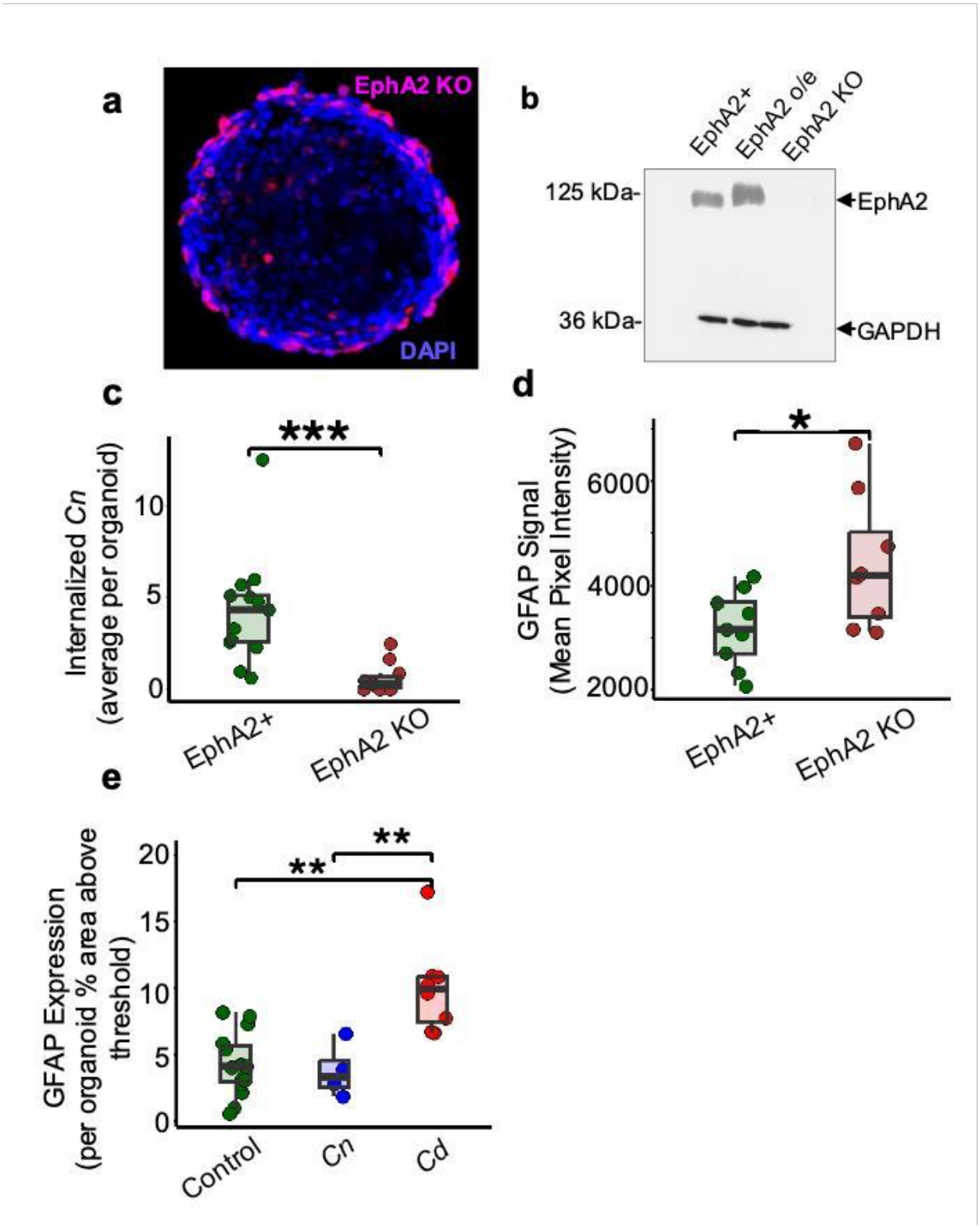
a
EphA2 KO
DAPI
b
EphA2+
EphA2 o/e
EphA2 KO
125 kDa-
EphA2
36 kDa-
GAPDH
c
***
Internalized Cn
(average per organoid)
10
5
0
EphA2+
EphA2 KO
d
*
GFAP Signal
(Mean Pixel Intensity)
6000
4000
2000
EphA2+
EphA2 KO
e
**
**
GFAP Expression
(per organoid % area above
threshold)
20
15
10
5
0
Control
Cn
Cd

Fig 4. EphA2 expression promotes barrier integrity while facilitating *Cn* Internalization. a Representative fluorescent image of BBB organoids formed from EphA2 knockout (KO) human brain endothelial cells. EphA2 KO cells express RFP (magenta) against DAPI (blue) counterstaining. **b** Western blot analysis (1:1000 dilution of rabbit anti-Human EphA2; Cell signaling technology Inc. D4A2) (1:10,000 dilution of Goat Anti-Rabbit IgG H&L HRPab6721; Abcam Inc., Cambridge, MA, USA) confirming loss of EphA2 protein expression in EphA2 KO organoids, in contrast to controls (EphA2+ and EphA2 over-expression (o/e)). **c** Internalization of *Cn* (*Cryptococcus neoformans*) by BBB organoids is dependent on EphA2 expression. Organoids (EphA2+ or EphA2 KO brain endothelial cells) were exposed to CFSE-stained *Cn* for 48 h, after which organoids were sectioned and analyzed for *Cn* invasion (Welch two-sample t-test: t = 4.28, df = 13.94, $p < 0.0008$)(R v.4.4.2). **d** Comparison of GFAP expression between BBB organoids formed with EphA2 KO versus EphA2+ brain endothelial cells. Organoids deficient in EphA2 show significantly higher levels of GFAP expression compared to EphA2+ organoids. Quantification was performed on GFAP-antibody probed organoid sections by applying a uniform threshold to images and measuring the percent area in the relevant channel above the threshold (Welch twosample t-test: t = 2.42, df = 10.68, $p = 0.0343$)(R v.4.2.2). **e** Organoids exposed to *Cd* (*Cryptococcus deuterogattii*) show increased GFAP expression in stark contrast to organoids exposed to *Cn* after 48 h of exposure (Welch two-sample t-test comparing *Cn* & *Cd* treatments: t = 3.84, df = 9.38, $p = 0.003$, comparing *Cd* & Control treatments: t = 4.25, df = 10.57, $p = 0.0015$)(R v.4.4.2). For panels c – e, each data point represents the average value for an organoid across several images.

Figure 5.

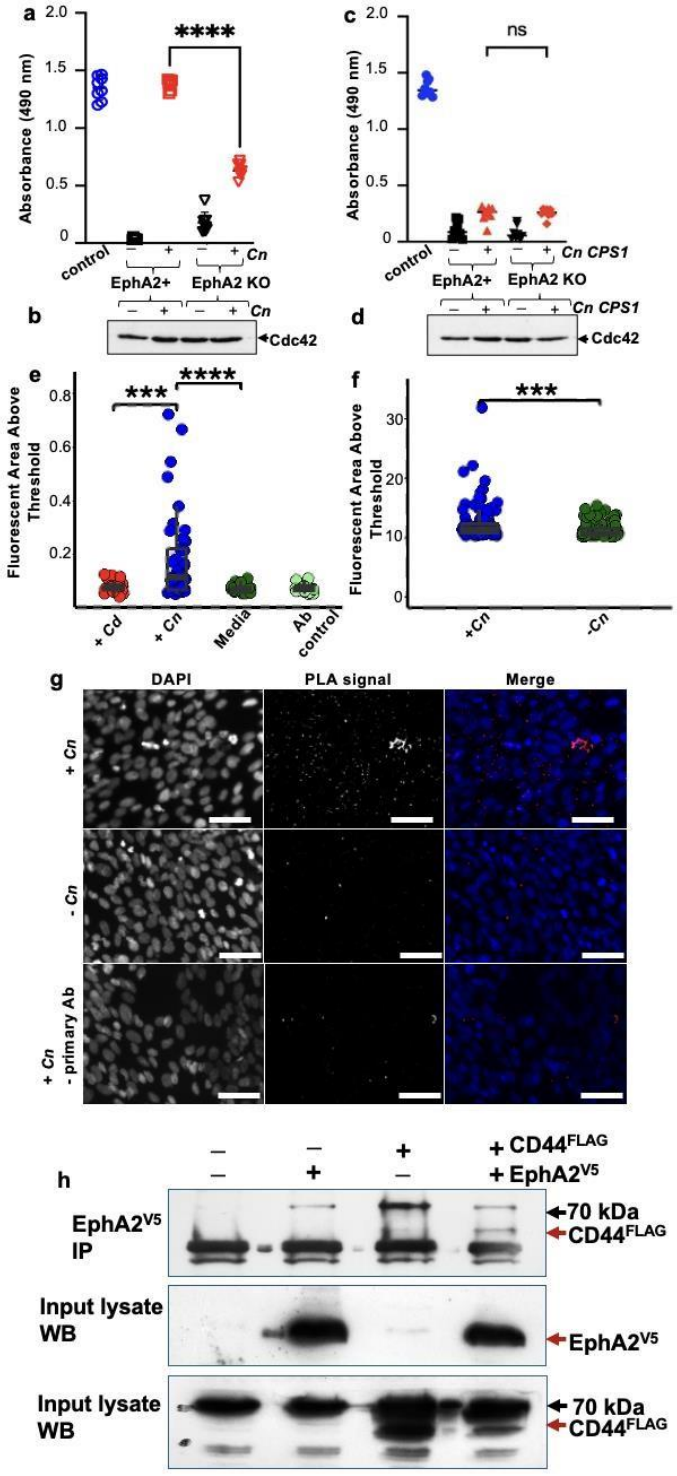
a
Absorbance (490 nm)
****
control
Cn
EphA2+
EphA2 KO
b
Cdc42
c
ns
Cn CPS1
d
e
Fluorescent Area Above Threshold
***
****
+ Cd
+ Cn
Media
Ab control
f
+Cn
-Cn
g
DAPI
PLA signal
Merge
+ Cn
- Cn
+ Cn - primary Ab
h
+ CD44FLAG
+ EphA2V5
EphA2V5 IP
70 kDa
CD44FLAG
Input lysate WB
EphA2V5

Fig 5. *Cn* activates GTP-bound Cdc42 via recruitment of a CD44-EphA2 molecular complex. **a** *Cn* induced stimulation of GTP-bound Cdc42 is contingent on EphA2 expression and **b** CD44 engagement. EphA2+ and EphA2 KO human brain endothelial cells were treated with either **a** *Cn* or **b** cps1Δ Cn deletion mutant at an MOI of 10 for 30 min and then lysed. Untreated and treated cell lysates were analyzed for GTP bound Cdc42 (active Cdc42) using the Cytoskeleton G-LISA assay. Data are expressed as a mean ± SD of three independent experiments. Statistical analysis was done using a two tailed unpaired t-test (n = 8, t = 0.2156, df = 14, ****$p < 0.0001$)(GraphPad Prism 10 software). **c, d** Expression of Cdc42 protein in lysates was confirmed by western blot analysis of nitrocellulose membrane probed with primary antibody to amino acid 150-182 of Cdc42 protein. (1:800 dilution of mouse anti-human Cdc42; cytoskeleton Inc. ACD04) (1:10,000 dilution of Goat anti-Mouse IgG H&L HRP ab6789; Abcam Inc., Cambridge, MA, USA). **e, f** *Cn* recruits a CD44-EphA2 protein complex in brain endothelial cells, detected by Proximity Labeling Assays (PLA - DuoLink) of EphA2 and CD44 in **e** mouse primary brain endothelial cells and **f** human brain endothelial cells (EphA2+, iBMEC). The *in-situ* interaction was quantified as the area in an image above a universally applied threshold. Significantly higher fluorescence was observed in *Cn* (+) versus *Cn* (-) treatments in both mouse primary cells (t = 4.40, df = 43.13, $p < 0.0001$) and human cells (t = 3.63, df = 131.88, $p = 0.0004$). In mouse primary cells, there was significantly higher signal in the *Cn* (+) compared to the *Cd* (+) treatments (t = 4.08, df = 43.63, $p < 0.0002$)(R v.4.4.2). Mouse primary brain endothelial cells were exposed to *Cd*, *Cn* media or a no primary antibody control. **g** Representative fluorescent images of PLA in human brain endothelial cells (EphA2+, iBMECs). Top row: iBMECs exposed to *Cn* for 90 min. Middle row: control panel iBMECs not exposed to *Cn*. Bottom row: control treatment in which iBMECs were exposed to *Cn* but omitting primary antibodies (anti-CD44 and anti-EphA2) Left column: Nuclear stain. Middle column: Fluorescent puncta (PLA-red probe) are indicative of target proteins (EphA2 and CD44) in proximity (within 40 nm) to each other. Right column: merged images.

Figure 6.

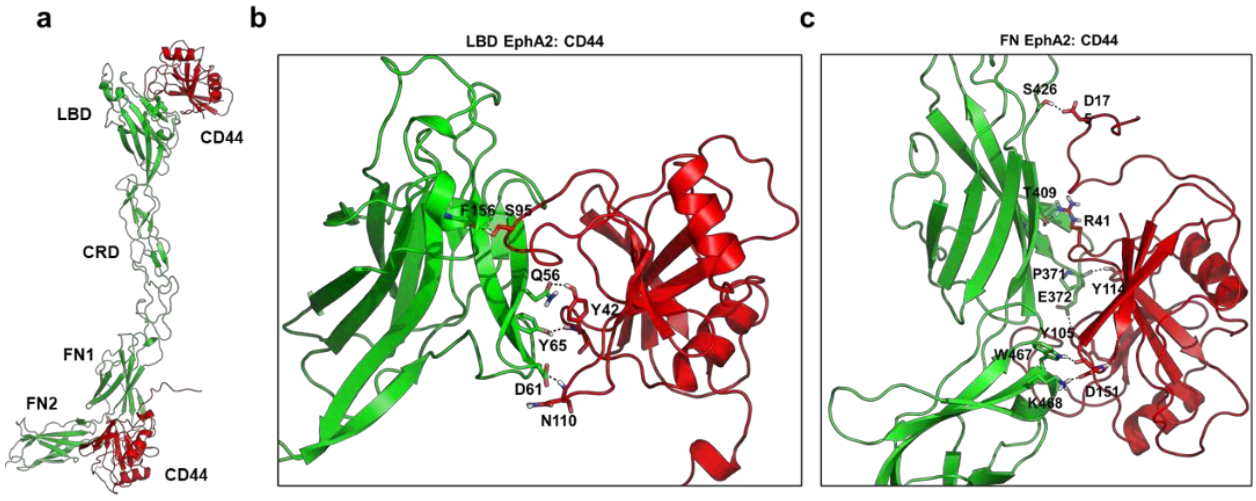

Fig 6. Alpha-Fold-Multimer structure prediction indicates reliable binding between EphA2 and CD44. **a** Cartoon representation of the AlphaFold3-predicted model of the EphA2 structure. extracellular region in complex with CD44, highlighting two distinct putative binding interfaces: the ligand-binding domain (LBD) (ipTM = 0.13; pTM = 0.49) and the fibronectin domains (FN1-FN2) (ipTM = 0.11; pTM = 0.49). **b-c** Representative binding conformations of the LBD: CD44 and FN: CD44 complexes obtained from molecular dynamics simulations. Shown here are the major conformational clusters derived from all replica trajectories. EphA2 is depicted in green and CD44 in red cartoon representations. For clarity, only the principle interfacial hydrogen bonds are displayed.

Figure 7.

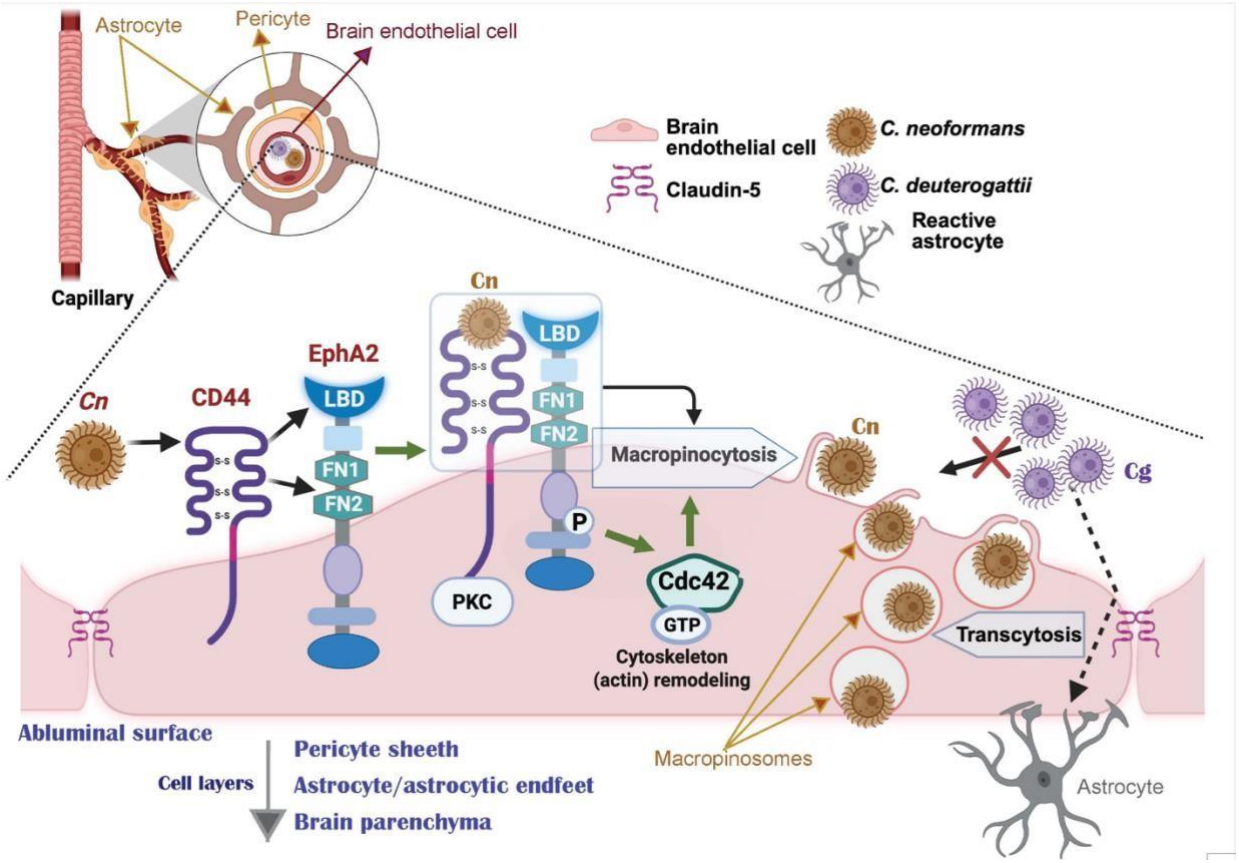

Fig 7. Conceptual model illustrating the molecular interactions that drive the transcytosis of *Cn* across the BBB. Upon binding to CD44, *Cn* promotes the association of CD44 with the ligand binding domain (LBD) and interactions involving both FN1 and FN2 domains, suggesting that CD44 can also engage EphA2 via a membrane-proximal siteand/or the fibronectin 2 domain (FN2) (black arrows). The CD44-EphA2 molecular interaction leads to a PKC-dependent phosphorylation of EphA2, and the downstream activation of GTP-bound Cdc42 (green arrows). Active Cdc42 stimulates membrane ruffling by remodeling the cytoskeleton via actin polymerization. The ensuing macropinocytosis of *Cn* is a result of macropinosomes large enough to internalize and transport *Cn* across the brain endothelium. *Cd* does not cross the brain endothelium (crossed-out black arrow) but stimulates the expression of GFAP+ astrocytes by as yet an unknown mechanism (dashed arrow). Figure created in BioRender.com.

Supplementary Fig. 1

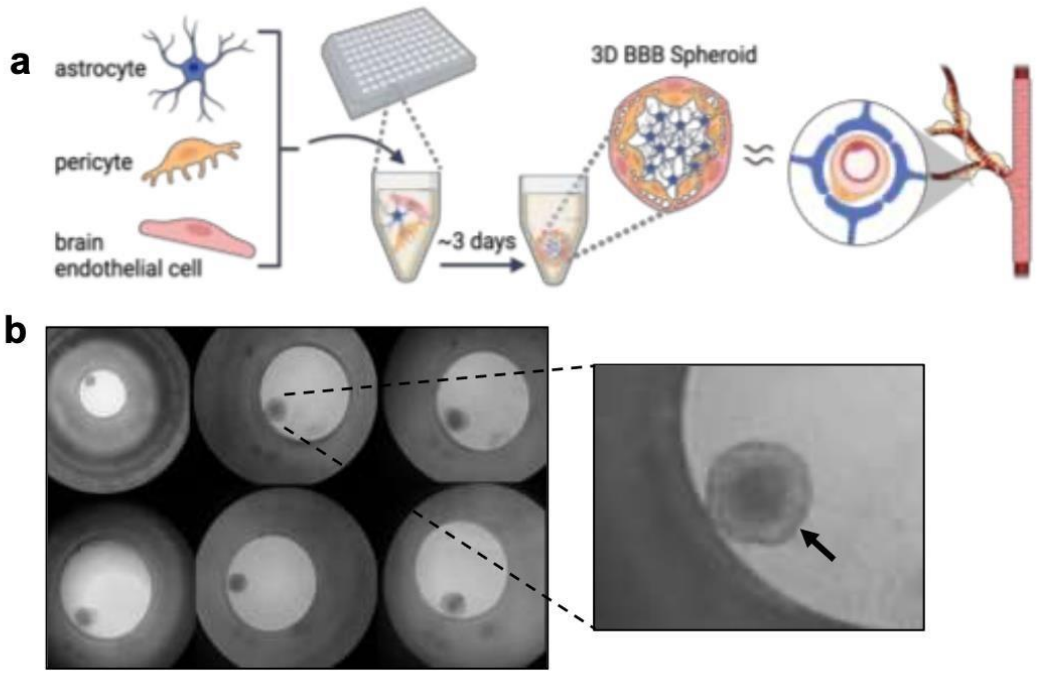

Supplementary Fig. 1. Schematics and images of 3D BBB organoid formation. **a** Organoids were formed from either primary human BMECs (passage < 6) or immortalized HCMEC/D3 cells (iBMECs, passage < 35), human primary pericytes (passage 4), and human astrocytes (passage 4). Primary cells were purchased from ScienCell (Carlsbad, California, USA). The organoids were formed by combining the three cell types in a 1:1:1 ratio, each at a concentration of 1x104 cells/mL. The combined cells were grown in 100 µL media in a 96-well plate. **b** Brightfield view of organoids formed at the bottom of flat-bottom 96-well plates with a transparent non- stick polymer coating. Organoids were relatively homogenous in size and shape.

Supplementary Fig. 2

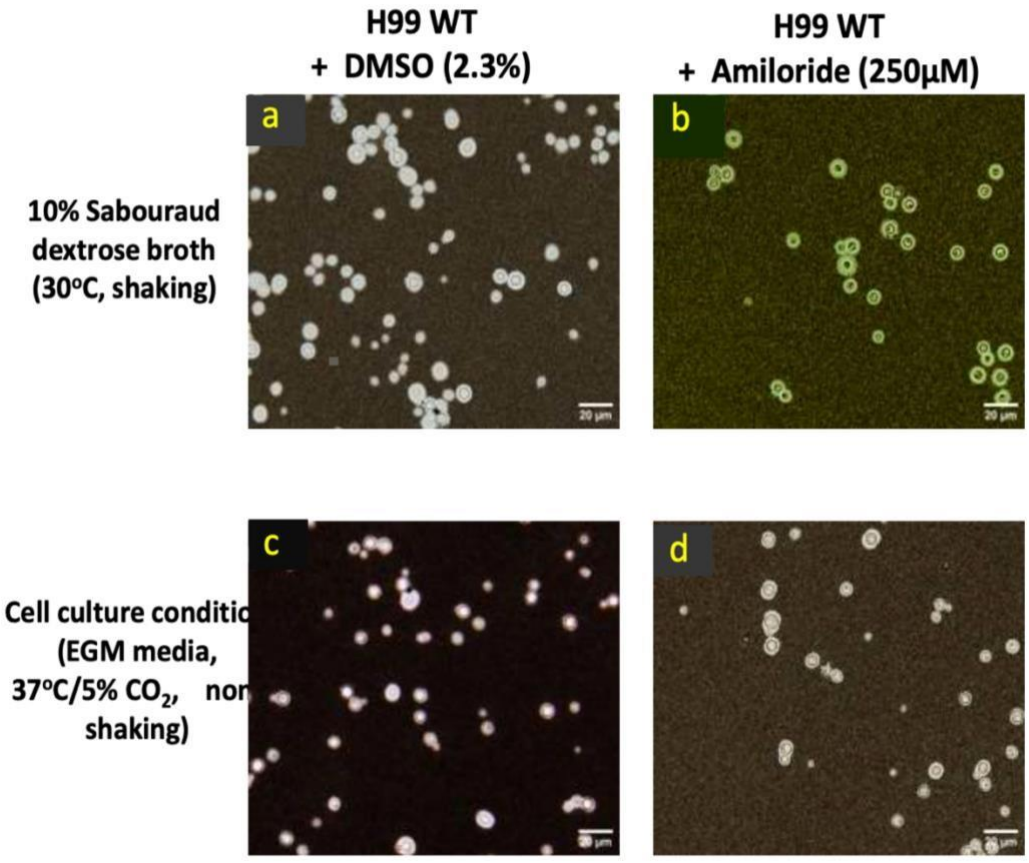

Supplementary Fig. 2. AML treatment did not alter capsule expression of the *Cn* H99 wild-type strain. (**a,b)** To induce capsule, the Cn H99 wild-type strain was grown to stationary phase under either the capsule-inducing condition (10% Sabouraud dextrose broth, 30oC, shaking) or mammalian growth condition (cell culture condition at 37oC, 5% CO2 in EGM media), respectively. DMSO vehicle control (**a,c**) or 250µM amiloride (**b,d**) were coincubated with the *Cn* H99 wild-type strain at the start of the assay. Capsules of cells were visualized using India ink (1ul ink + 3ul of cells) under a brightfield microscope.

Supplementary Fig. 3

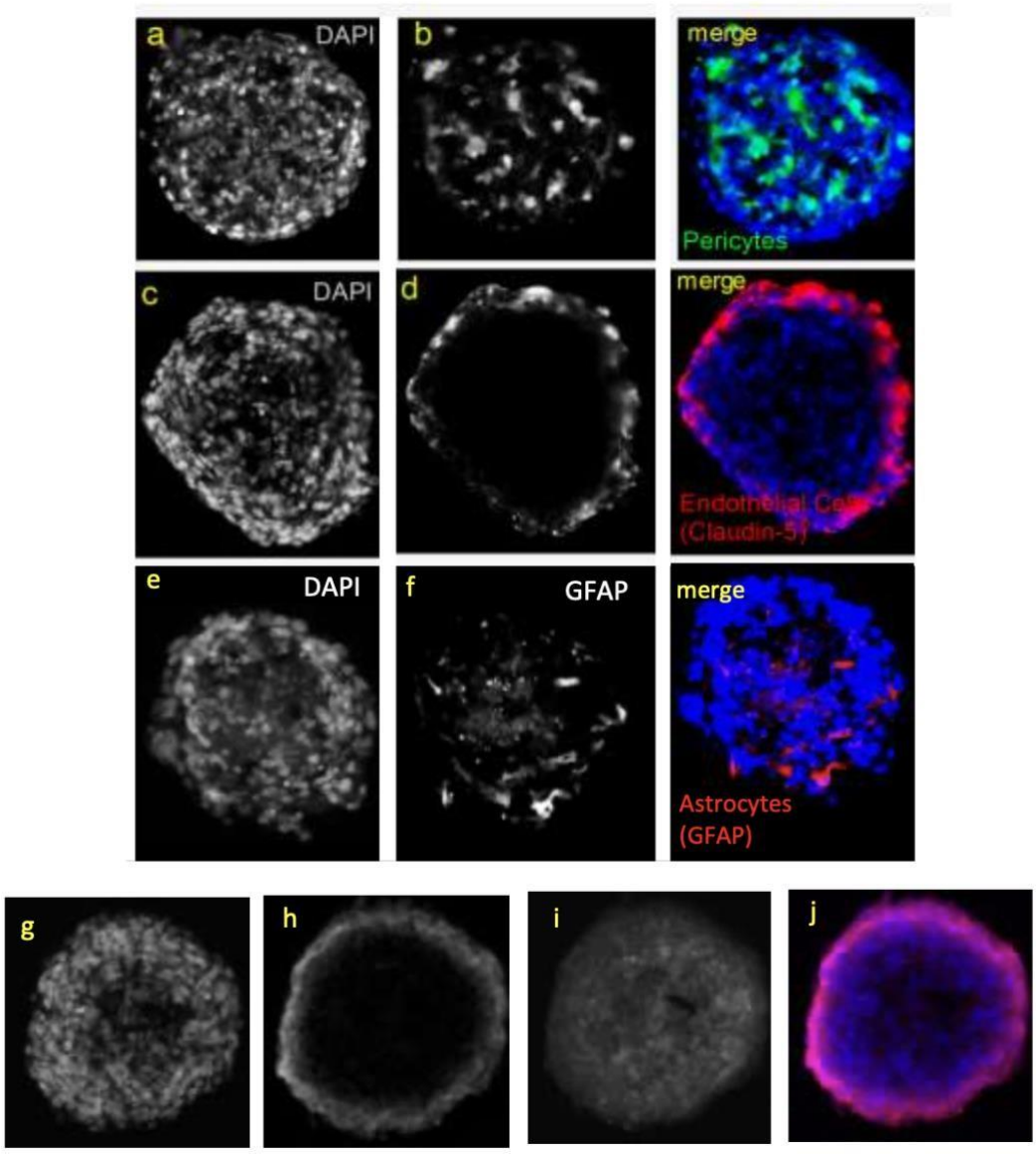

Supplementary Fig. 3. Organization of neurovascular cell types in human BBB organoids. First column **a**, **c**, **e** shows DAPI counterstaining. Second column **b**, **d**, **f** shows celltype specific staining. Third column contains merged images from column 1 and column 2. Top row: pericytes were labeled in 2D culture with CMFDA (CellTracker Green, Invitrogen) and combined with endothelial cells and astrocytes to form organoids. **a** DAPI, **b** pericytes, merged image to the right. Middle row: Organoids were probed with **d** rabbit anti-Claudin5 (1:250) and goat - anti-rabbit TexasRed, merged image (middle row, right) with DAPI **c**. Bottom row: Astrocytes were visualized with GFAP (Invitrogen MA5-12023, 1:2000) **f** with DAPI counterstaining **e**, with merged images to the right. All images were acquired from 15µm thick cryosections of PFA-fixed sections made from 1week old organoids. **g-j.** DAPI (**g**), claudin 5 (**h**), anti-*Cn* capsule (**i**) and composite (**j**) image of control (non - *Cn*-exposed) organoid section showing the expected peripheral localization of claudin 5 antibody (red) and the absence of nonspecific anti-*Cn* capsule antibody (green channel). The image in **i** shows non-specific autofluorescence, with the gain adjusted to maximum settings, indicating that the anti-capsule (18b7) antibody does not bind to specific mammalian cell components. *Cn, Cryptococcus neoformans.*

Supplementary Fig. 4

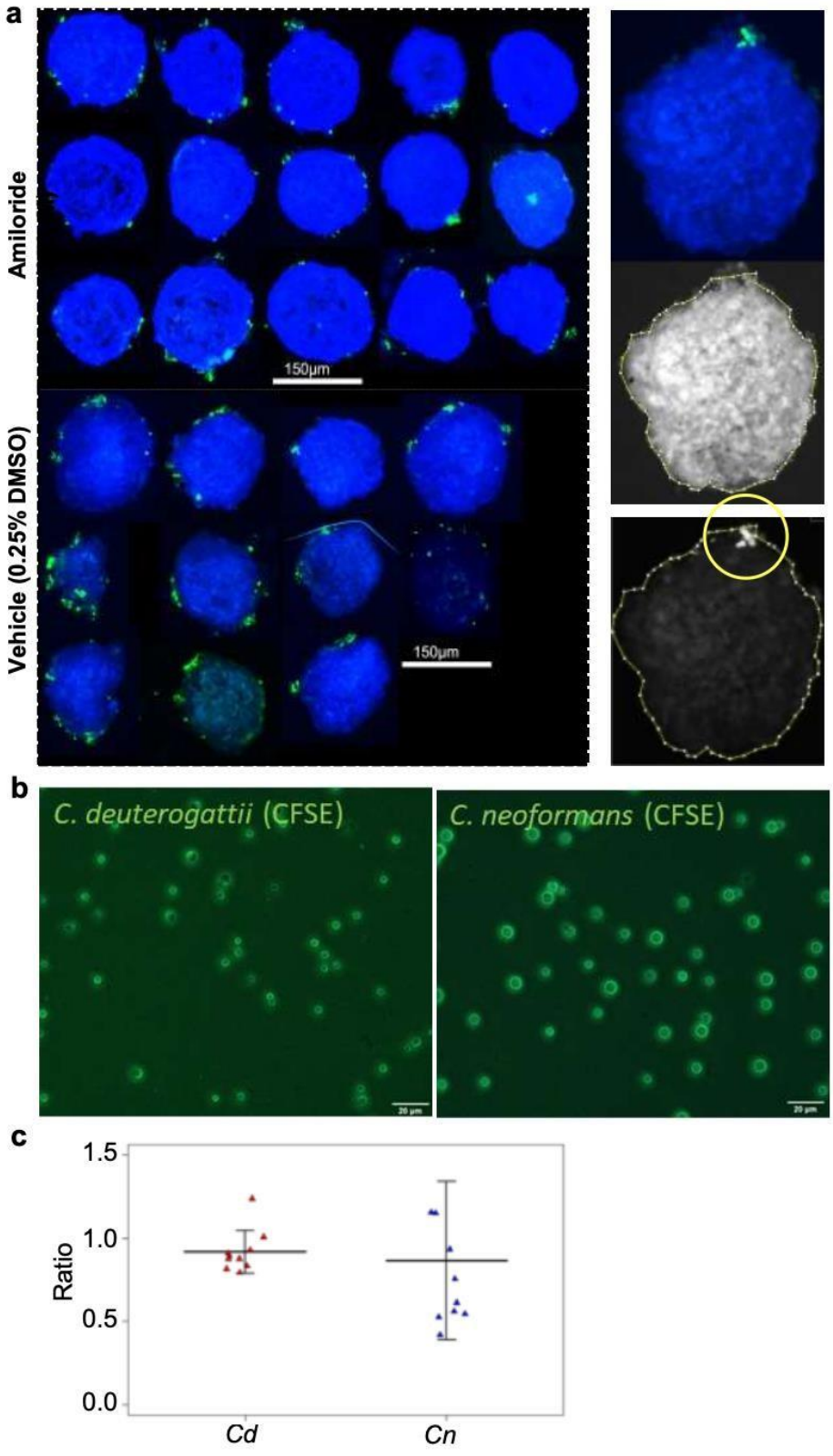

Supplementary Fig. 4. Organoid-based assays to examine the impact of AML treatment on *Cn* BBB-crossing/internalization. a Representative images showing organoids (blue, DAPI) incubated for 24 h with *Cn* (green, CFSE) in media containing either 250 μM amiloride (AML) (top-left) or an equivalent concentration of vehicle control (bottom left). Representative images from the analysis pipeline, with the "input" merged image at top right, border demarked around organoids in the DAPI channel (right middle panel), and this border applied in the CFSE channel to quantify crossing/internalization of fungal cells (bottom right panel, yellow circle). **b, c** Representative fields of view from a control experiment comparing CFSE-stained *Cn* (**b**, right) and *Cd* **(b,** left). Cells were stained with CFSE and incubated under mammalian tissue culture conditions. The ratio of stained (FITC channel) to total cells (transmitted light), as determined by an ImageJ script, does not differ between *Cn* and *Cd* (**c**). Differences in crossing between *Cn* and *Cd* are therefore not attributable to differences in affinity for CFSE. In a few cases, the script undercounted cells in the transmitted light channel, leading to ratios greater than one. *Cd, Cryptococcus deuterogattii; Cn, Cryptococcus neoformans.*

Supplementary Fig. 5

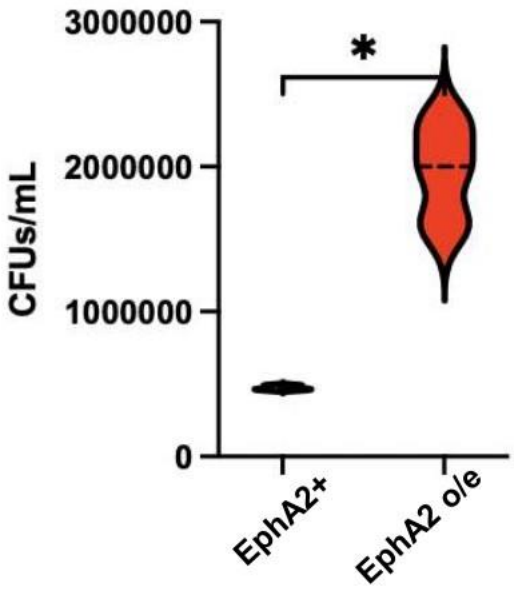

Supplementary Fig. 5. Overexpression of EphA2 in brain endothelial cells increases migration of *Cn* across the brain endothelium in an *in vitro* transwell model of the BBB. Transcytosis assay shows a significant increase in the movement of *Cn* across endothelial cells when brain endothelial cells (iBMECs) overexpress EphA2. EphA2+ iBMECs (wild type) and iBMECs transduced with EphA2 *via* lentivirus were exposed to *Cn* (MOI of 10) that was added to the apical side of the transwell. Following 12 h exposure, fungal cells were collected from the abluminal side of each transwell (well below transwell) and plated onto agar plates for CFU (colony forming units) determination. Each data point represents the fungal count from an individual well (n=3). Statistical analysis was done using a two-tailed, unpaired t-test with Welch correction (p = 0.0178, t= 7.358, df= 2.008)

Supplementary Fig. 6

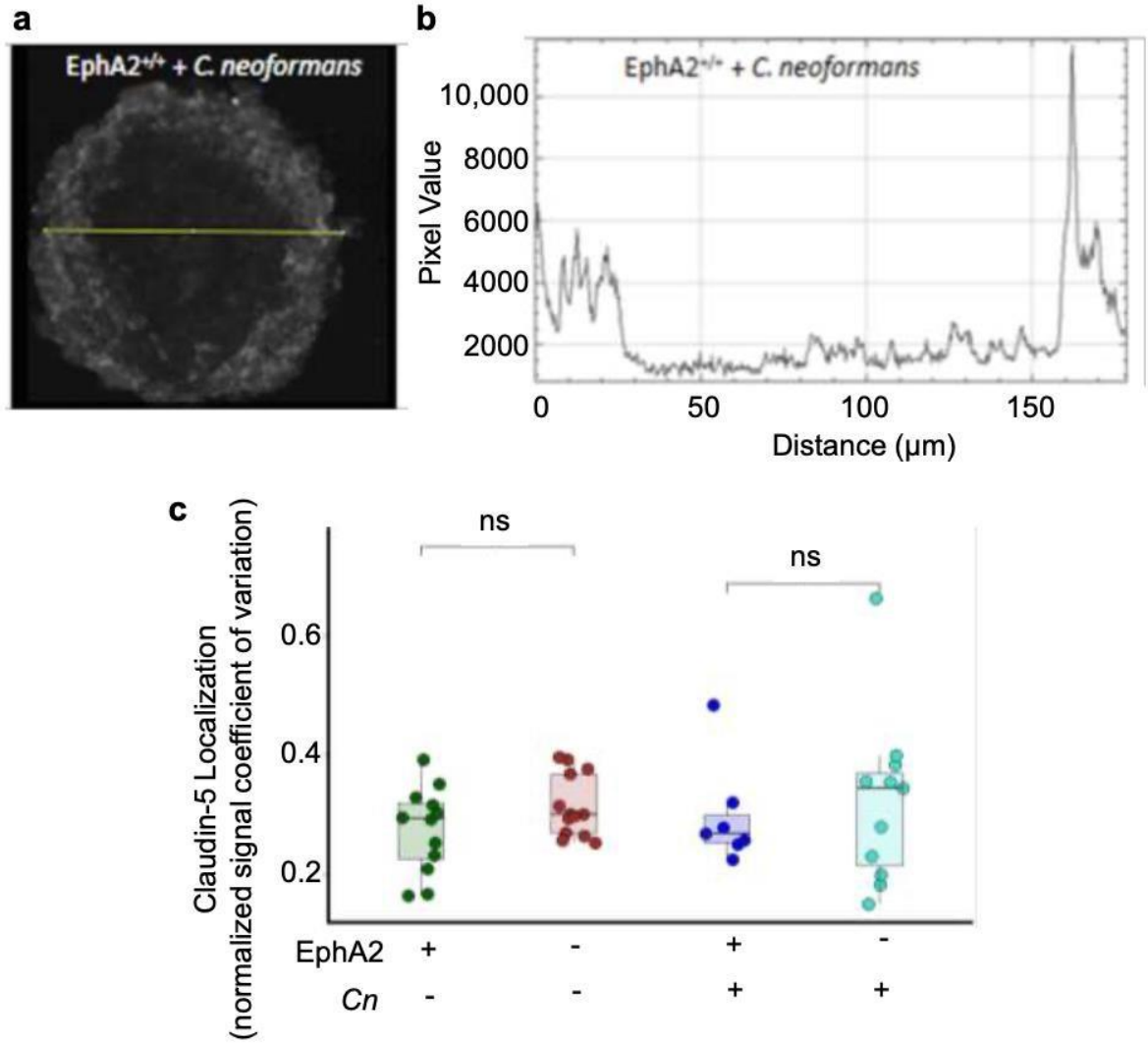

Supplementary Fig. 6. Claudin 5 expression in *EphA2 KO* organoids exposed to *Cn*

a) Claudin5 signal (Cy5 channel) in cross-sections of BBB organoids. Sections were probed with rabbit anti-claudin 5 (1:1000, ab15106, Abcam) primary antibodies and goat anti-rabbit Cy5 (1:1000, ab6565, Abcam) secondary antibodies. **b)** Histograms corresponding to the pixel intensities measured across the diameter of organoids, prior to normalization and downstream analysis. **c)** Claudin 5 localization in organoids from *EphA2*+ or *EphA2 KO* endothelial cells in the presence and absence of *Cn* (24 h coincubation). To create a metric of claudin5 localization within organoids, pixel intensity in the claudin5 (Cy5) channel across the diameter of organoid sections was acquired in ImageJ using the Plot Profile tool, normalized to the maximum value, and the coefficient of variation for each normalized vector was then taken. Points represent the average coefficient of variation across multiple sections for individual organoids. Data drawn from three independent replicates. There is no significant difference between *EphA2*+ and *EphA2 KO* organoids. *Cn, Cryptococcus neoformans.*

Supplementary Fig. 7

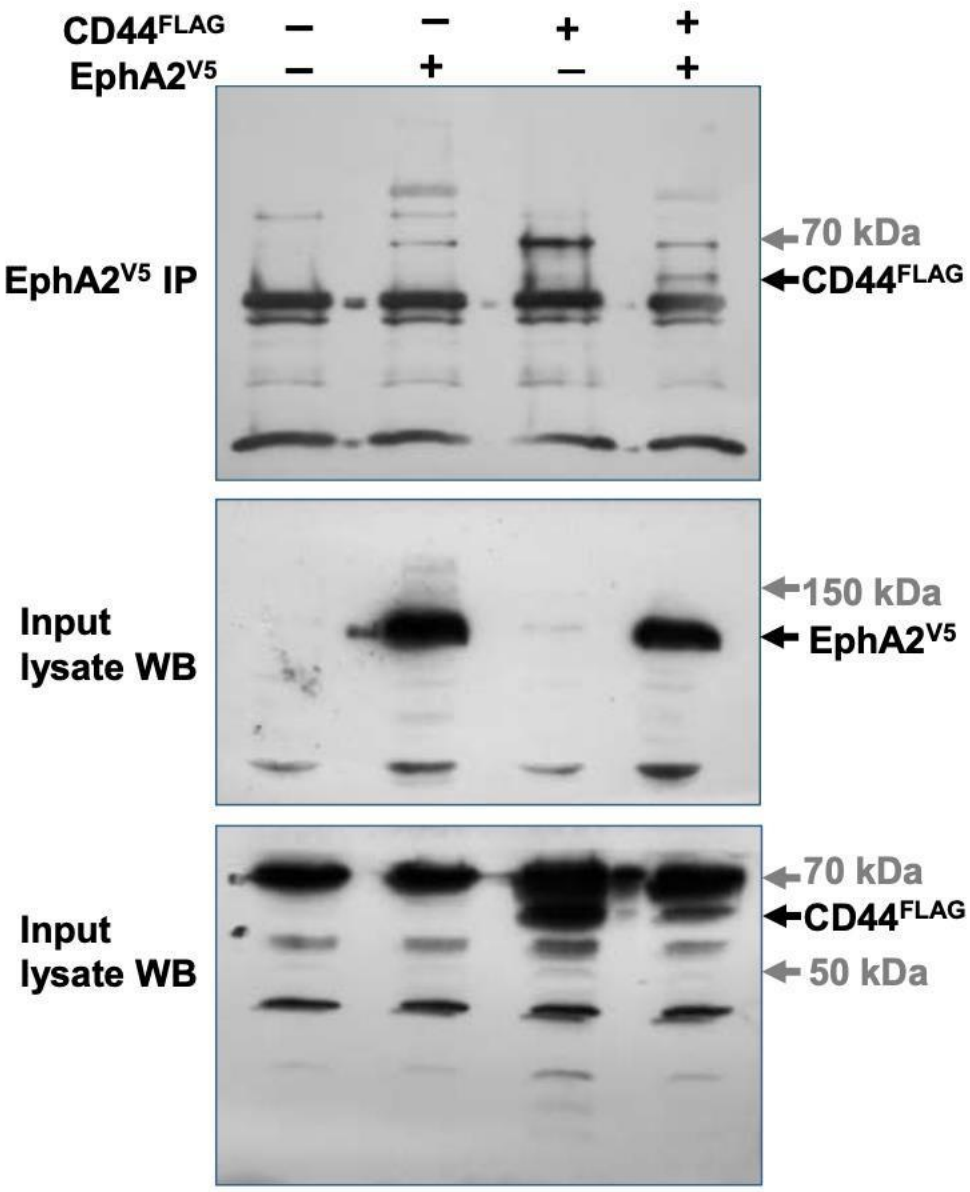

Supplementary Fig. 7. Immunoblots of SDS protein gels from the co- immunoprecipitation studies. HEK293T cells transiently transfected with EphA2V5 and/or CD44FLAG for 48 h were exposed to *Cn* for 2 h then immediately lysed in RIPA buffer supplemented with a protease inhibitor cocktail (with phosphatase inhibitor). Cell lysates were incubated with anti-V5 antibody for 2 h on ice followed by DynaGreen Protein A/G magnetic beads that were subsequently thoroughly washed and added to Laemmli buffer. Denatured proteins were separated by SDS PAGE electrophoresis and transferred to nitrocellulose membranes. Membranes were incubated with mouse primary antibodies (1:800 dilution) of either anti-FLAG or anti- V5 followed by secondary antibodies (1:10,000 IgG H&L HRP) for detection of either EphA2 or CD44 in EphA2V5 pulldown (immunoprecipitation (IP)) and input lysates. Proteins were visualized with enhanced chemiluminescence (ECL) reaction. WB, western blots.

Supplementary Fig. 8

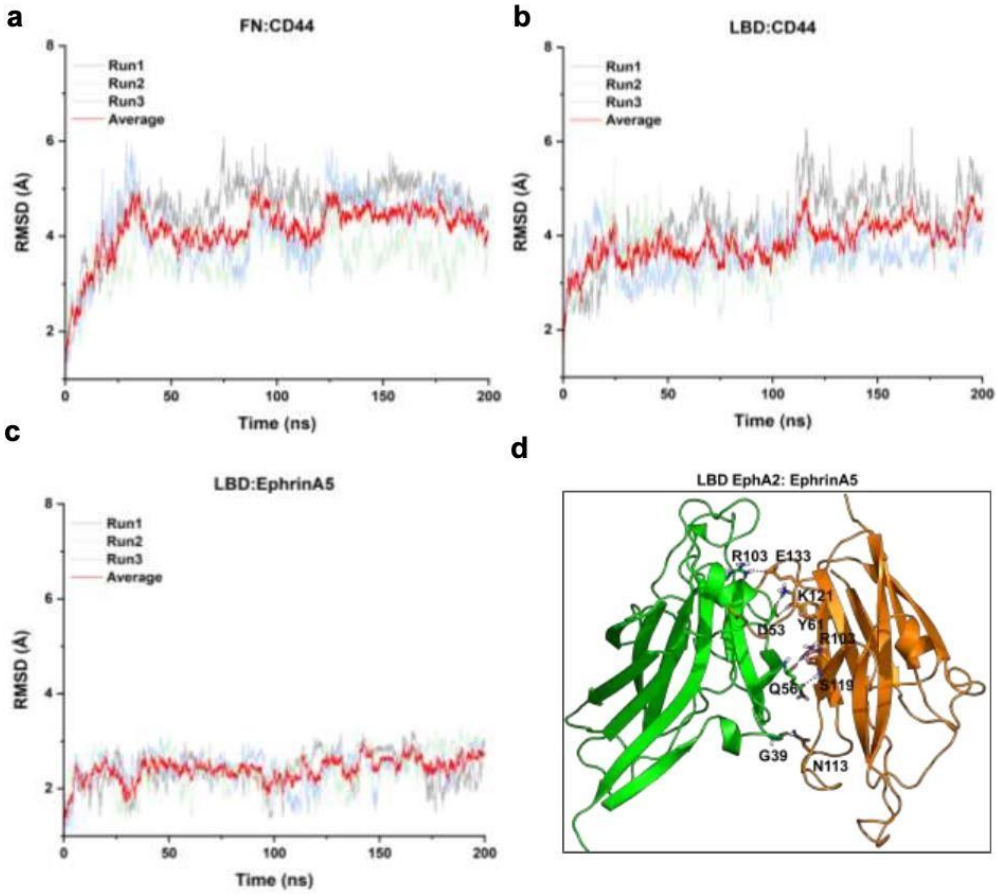

Supplementary Fig. 8. Structural stability and binding conformations of EphA2 complexes. **a–c** Backbone RMSD profiles of the FN: CD44, LBD: CD44, and LBD: ephrinA5 complexes over the course of molecular dynamics simulations. Data from all replica trajectories as well as averaged RMSD values are shown. **d** Representative binding conformation of the LBD: ephrinA5 complex obtained from clustering of all replica trajectories. EphA2 is depicted in green and ephrinA5 in orange cartoon representation. For clarity, only the major interfacial hydrogen bonds are displayed.

Supplementary Fig. 9

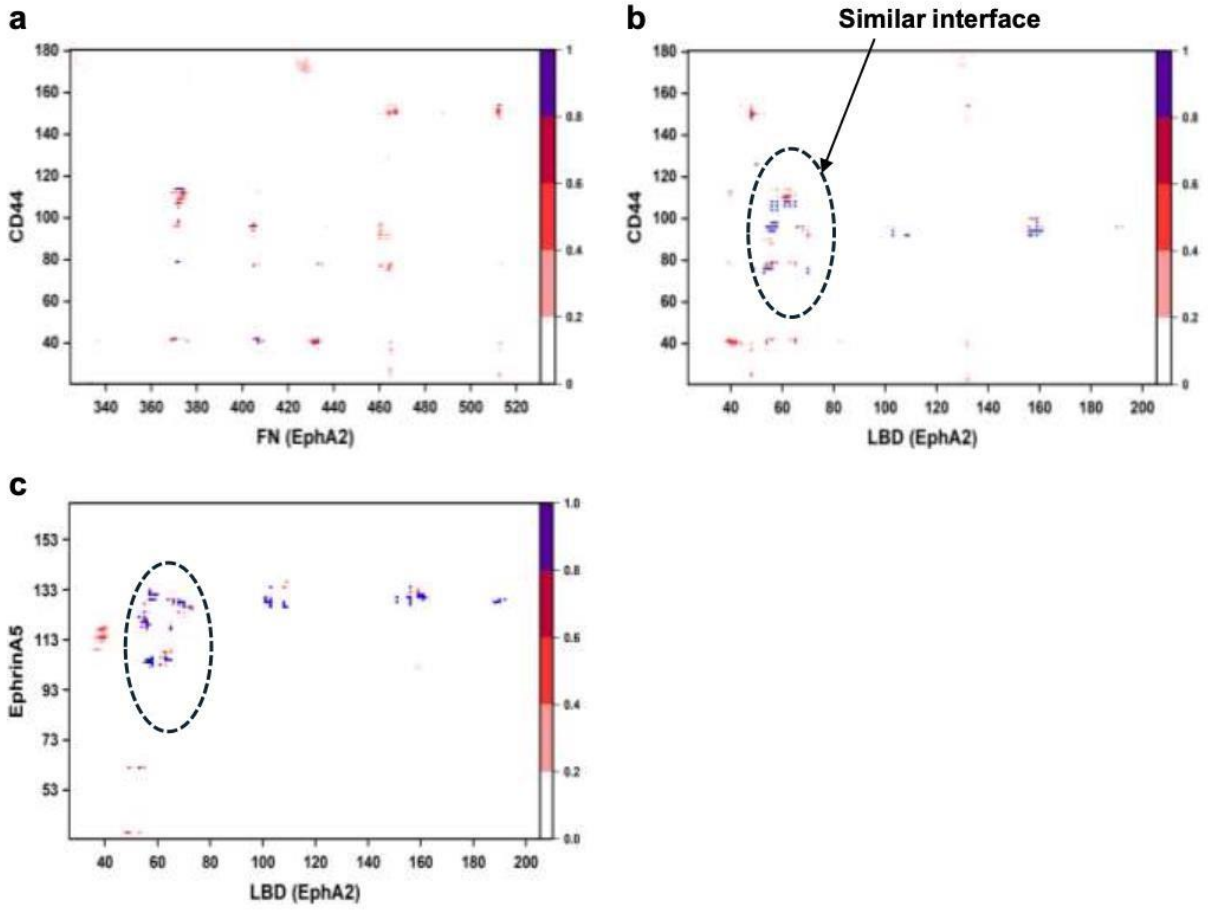

Supplementary Fig. 9. Intermolecular contact interfaces of EphA2 complexes. (**a–c**) Contact maps of the FN: CD44, LBD: CD44, and LBD: ephrinA5 complexes obtained from molecular dynamics simulations. Contacts were calculated using a 5 Å cutoff. The color scale (white to red to blue) represents the fractional occupancy of each contact, ranging from 0 (no contact) to 1 (persistent contact). Data from all replica trajectories were included in the analysis. Notably, CD44 and ephrinA5 engage overlapping interface regions within the EphA2 LBD.

Supplementary Table 1 - Antibodies used in the current study.

Name	Type	Company	Catalog #	Use
mouse anti-CD44	primary	abcam	ab254530	PLA
rabbit anti-EphA2	primary	abcam	ab185156	PLA
mouse anti-Cdc42	primary	Cytoskeleton Inc.	ACD04	WB
rabbit anti-EphA2	primary	Cell signaling	D4A2	WB
goat anti-mouse IgG H&L HRP	secondary	abcam	ab6789	WB
goat anti-rabbit IgG H&L HRP	secondary	abcam	ab6721	WB
rabbit anti-Claudin5	primary	abcam	ab15106	IF
goat anti-rabbit Cy5	secondary	abcam	ab6564	IF
mouse anti-GFAP	primary	Invitrogen	MA5-12023	IF
goat anti-rabbit TexasRed	secondary	abcam	ab6719	IF
goat anti-mouse Cy5	secondary	abcam	ab6563	IF
mouse anti-V5 tag	primary	Santa Cruz Biotechnology	sc271944	IP and WB
mouse anti-FLAG tag	primary	Santa Cruz Biotechnology	sc51590	IP and WB

References

1. Kadry, H., Noorani, B. & Cucullo, L. A blood-brain barrier overview on structure, function, impairment, and biomarkers of integrity. *Fluids Barriers CNS* **17**, 69 (2020).

2. Sloan, D.J. & Parris, V. Cryptococcal meningitis: epidemiology and therapeutic options. *Clin Epidemiol* **6**, 169-182 (2014).

3. Zhou, Y.*, et al.* The pathways and the mechanisms by which Cryptococcus enters the brain. *Mycology* **15**, 345-359 (2024).

4. Enriquez, V.*, et al.* Active Cryptococcus neoformans glucuronoxylomannan production prevents elimination of cryptococcal CNS infection in vivo. *J Neuroinflammation* **22**, 61 (2025).

5. Lee, S.C., Kress, Y., Zhao, M.L., Dickson, D.W. & Casadevall, A. Cryptococcus neoformans survive and replicate in human microglia. *Lab Invest* **73**, 871-879 (1995).

6. Santiago-Tirado, F.H., Onken, M.D., Cooper, J.A., Klein, R.S. & Doering, T.L. Trojan Horse Transit Contributes to Blood-Brain Barrier Crossing of a Eukaryotic Pathogen. *mBio* **8**(2017).

7. Charlier, C.*, et al.* Evidence of a role for monocytes in dissemination and brain invasion by Cryptococcus neoformans. *Infect Immun* **77**, 120-127 (2009).

8. Kechichian, T.B., Shea, J. & Del Poeta, M. Depletion of alveolar macrophages decreases the dissemination of a glucosylceramide-deficient mutant of Cryptococcus neoformans in immunodeficient mice. *Infect Immun* **75**, 4792-4798 (2007).

9. Santangelo, R.*, et al.* Role of extracellular phospholipases and mononuclear phagocytes in dissemination of cryptococcosis in a murine model. *Infect Immun* **72**, 2229-2239 (2004).

10. Sorrell, T.C.*, et al.* Cryptococcal transmigration across a model brain blood-barrier: evidence of the Trojan horse mechanism and differences between Cryptococcus neoformans var. grubii strain H99 and Cryptococcus gattii strain R265. *Microbes Infect* **18**, 57-67 (2016).

11. Kaufman-Francis, K.*, et al.* The Early Innate Immune Response to, and Phagocyte-Dependent Entry of, Cryptococcus neoformans Map to the Perivascular Space of Cortical Post-Capillary Venules in Neurocryptococcosis. *Am J Pathol* **188**, 1653-1665 (2018).

12. Olszewski, M.A.*, et al.* Urease expression by Cryptococcus neoformans promotes microvascular sequestration, thereby enhancing central nervous system invasion. *Am J Pathol* **164**, 1761-1771 (2004).

13. Chen, S.H.*, et al.* Cryptococcus neoformans induces alterations in the cytoskeleton of human brain microvascular endothelial cells. *J Med Microbiol* **52**, 961-970 (2003).

14. Shi, M.*, et al.* Real-time imaging of trapping and urease-dependent transmigration of Cryptococcus neoformans in mouse brain. *J Clin Invest* **120**, 1683-1693 (2010).

15. Vu, K., Eigenheer, R.A., Phinney, B.S. & Gelli, A. Cryptococcus neoformans Promotes Its Transmigration into the Central Nervous System by Inducing Molecular and Cellular Changes in Brain Endothelial Cells. *Infection and Immunity* **81**, 3139-3147 (2013).

16. Chang, Y.C*., et al.* Cryptococcal yeast cells invade the central nervous system via transcellular penetration of the blood-brain barrier. *Infect Immun* **72**, 4985-4995 (2004).

17. Huang, S.H*., et al.* Invasion of Cryptococcus neoformans into human brain microvascular endothelial cells is mediated through the lipid rafts-endocytic pathway via the dual specificity tyrosine phosphorylation-regulated kinase 3 (DYRK3). *The Journal of biological chemistry* **286**, 34761-34769 (2011).

18. Jong, A*., et al.* Invasion of Cryptococcus neoformans into human brain microvascular endothelial cells requires protein kinase C-alpha activation. *Cell Microbiol* **10**, 1854-1865 (2008).

19. Maruvada, R*., et al.* Cryptococcus neoformans phospholipase B1 activates host cell Rac1 for traversal across the blood-brain barrier. *Cell Microbiol* **14**, 1544-1553 (2012).

20. Na Pombejra, S., Salemi, M., Phinney, B.S. & Gelli, A. The Metalloprotease, Mpr1, Engages AnnexinA2 to Promote the Transcytosis of Fungal Cells across the Blood-Brain Barrier. *Front Cell Infect Microbiol* **7**, 296 (2017).

21.Aaron, P.A., Jamklang, M., Uhrig, J.P. & Gelli, A. The blood-brain barrier internalises Cryptococcus neoformans via the EphA2-tyrosine kinase receptor. *Cell Microbiol* **20**(2018).

22. Kim, J*., et al.* Fungal brain infection modelled in a human-neurovascular-unit-on-a-chip with a functional blood-brain barrier. *Nat Biomed Eng* **5**, 830-846 (2021).

23. Chen, Y*., et al.* Quantitative analysis reveals internalisation of Cryptococcus neoformans by brain endothelial cells in vivo. *Cell Microbiol* **23**, e13330 (2021).

24. Davis, J.M., Huang, M., Botts, M.R., Hull, C.M. & Huttenlocher, A. A Zebrafish Model of Cryptococcal Infection Reveals Roles for Macrophages, Endothelial Cells, and Neutrophils in the Establishment and Control of Sustained Fungemia. *Infect Immun* **84**, 3047-3062 (2016).

25. Kerr, M.C. & Teasdale, R.D. Defining macropinocytosis. *Traffic* **10**, 364-371 (2009).

26. Lim, J.P. & Gleeson, P.A. Macropinocytosis: an endocytic pathway for internalising large gulps. *Immunol Cell Biol* **89**, 836-843 (2011).

27. Salloum, G., Bresnick, A.R. & Backer, J.M. Macropinocytosis: mechanisms and regulation. *Biochem J* **480**, 335-362 (2023).

28. Long, M., Huang, S.H., Wu, C.H., Shackleford, G.M. & Jong, A. Lipid raft/caveolae signaling is required for Cryptococcus neoformans invasion into human brain microvascular endothelial cells. *Journal of biomedical science* **19**, 19 (2012).

29. Lanser, D.M., Bennett, A.B., Vu, K. & Gelli, A. Macropinocytosis as a potential mechanism driving neurotropism of Cryptococcus neoformans. *Front Cell Infect Microbiol* **13**, 1331429 (2023).

30. Liu, X.*, et al.* Recent progress on the organoids: Techniques, advantages and applications. *Biomed Pharmacother* **185**, 117942 (2025).

31. Jong, A.*, et al.* Hyaluronic acid receptor CD44 deficiency is associated with decreased Cryptococcus neoformans brain infection. *The Journal of biological chemistry* **287**, 15298-15306 (2012).

32. Jong, A.*, et al.* Involvement of human CD44 during Cryptococcus neoformans infection of brain microvascular endothelial cells. *Cell Microbiol* **10**, 1313-1326 (2008).

33. Jong, A.*, et al.* Identification and characterization of CPS1 as a hyaluronic acid synthase contributing to the pathogenesis of Cryptococcus neoformans infection. *Eukaryot Cell* **6**, 14861496 (2007).

34. Urich, E.*, et al.* Multicellular self-assembled spheroidal model of the blood brain barrier. *Sci Rep* **3**, 1500 (2013).

35. Nzou, G.*, et al.* Human Cortex Spheroid with a Functional Blood Brain Barrier for HighThroughput Neurotoxicity Screening and Disease Modeling. *Sci Rep* **8**, 7413 (2018).

36. Woo, Y.H. & Martinez, L.R. Cryptococcus neoformans-astrocyte interactions: effect on fungal blood brain barrier disruption, brain invasion, and meningitis progression. *Crit Rev Microbiol* **47**, 206-223 (2021).

37. Lee, S.C., Dickson, D.W. & Casadevall, A. Pathology of cryptococcal meningoencephalitis: analysis of 27 patients with pathogenetic implications. *Hum Pathol* **27**, 839-847 (1996).

38. Lee, S.C. & Casadevall, A. Polysaccharide antigen in brain tissue of AIDS patients with cryptococcal meningitis. *Clin Infect Dis* **23**, 194-195 (1996).

39. Koivusalo, M.*, et al.* Amiloride inhibits macropinocytosis by lowering submembranous pH and preventing Rac1 and Cdc42 signaling. *J Cell Biol* **188**, 547-563 (2010).

40. Vu, K., Weksler, B., Romero, I., Couraud, P.O. & Gelli, A. Immortalized human brain endothelial cell line HCMEC/D3 as a model of the blood-brain barrier facilitates in vitro studies of central nervous system infection by Cryptococcus neoformans. *Eukaryot Cell* **8**, 1803-1807 (2009).

41. Weksler, B.B.*, et al.* Blood-brain barrier-specific properties of a human adult brain endothelial cell line. *FASEB journal : official publication of the Federation of American Societies for Experimental Biology* **19**, 1872-1874 (2005).

42. Vu, K.*, et al.* Invasion of the central nervous system by Cryptococcus neoformans requires a secreted fungal metalloprotease. *mBio* **5**, e01101-01114 (2014).

43.Brambillasca, S.*, et al.* Novel selective inhibitors of macropinocytosis-dependent growth in pancreatic ductal carcinoma. *Biomed Pharmacother* **177**, 116991 (2024).

44. Lambies, G.*, et al.* Cell polarity proteins promote macropinocytosis in response to metabolic stress. *Nat Commun* **15**, 10541 (2024).

45. Florey, O. & Overholtzer, M. Macropinocytosis and autophagy crosstalk in nutrient scavenging. *Philos Trans R Soc Lond B Biol Sci* **374**, 20180154 (2019).

46. Le, A.H. & Machesky, L.M. Image-based Quantification of Macropinocytosis Using Dextran Uptake into Cultured Cells. *Bio Protoc* **12**, e4367 (2022).

47.Datta, K.*, et al.* Spread of Cryptococcus gattii into Pacific Northwest region of the United States. *Emerg Infect Dis* **15**, 1185-1191 (2009).

48. Kidd, S.E.*, et al.* A rare genotype of Cryptococcus gattii caused the cryptococcosis outbreak on Vancouver Island (British Columbia, Canada). *Proc Natl Acad Sci U S A* **101**, 17258-17263 (2004).

49. Fonseca, F.L.*, et al.* Immunomodulatory effects of serotype B glucuronoxylomannan from Cryptococcus gattii correlate with polysaccharide diameter. *Infect Immun* **78**, 3861-3870 (2010).

50. Goldman, D.L., Casadevall, A., Cho, Y. & Lee, S.C. Cryptococcus neoformans meningitis in the rat. *Lab Invest* **75**, 759-770 (1996).

51. Ridley, A.J. Rho GTPases and actin dynamics in membrane protrusions and vesicle trafficking. *Trends Cell Biol* **16**, 522-529 (2006).

52. Abramson, J.*, et al.* Accurate structure prediction of biomolecular interactions with AlphaFold 3. *Nature* **630**, 493-500 (2024).

53. Seiradake, E., Harlos, K., Sutton, G., Aricescu, A.R. & Jones, E.Y. An extracellular steric seeding mechanism for Eph-ephrin signaling platform assembly. *Nat Struct Mol Biol* **17**, 398-402 (2010).

54. Alvarez, J.I., Katayama, T. & Prat, A. Glial influence on the blood brain barrier. *Glia* **61**, 19391958 (2013).

55. Prat, A., Biernacki, K., Wosik, K. & Antel, J.P. Glial cell influence on the human blood-brain barrier. *Glia* **36**, 145-155 (2001).

56.Darling, T.K.*, et al.* EphA2 contributes to disruption of the blood-brain barrier in cerebral malaria. *PLoS Pathog* **16**, e1008261 (2020).

57.Thundyil, J.*, et al.* Evidence that the EphA2 receptor exacerbates ischemic brain injury. *PloS one* **8**, e53528 (2013).

58. Almutairi, M.M., Gong, C., Xu, Y.G., Chang, Y. & Shi, H. Factors controlling permeability of the blood-brain barrier. *Cell Mol Life Sci* **73**, 57-77 (2016).

59. Smith, M.W. & Gumbleton, M. Endocytosis at the blood-brain barrier: from basic understanding to drug delivery strategies. *J Drug Target* **14**, 191-214 (2006).

60. Defazio, G.*, et al.* Endocytosis of horseradish peroxidase by brain microvascular and umbilical vein endothelial cells in culture: an ultrastructural and morphometric study. *Brain Res Bull* **43**, 467-472 (1997).

61. Huang, S.H.*, et al.* Escherichia coli invasion of brain microvascular endothelial cells in vitro and in vivo: molecular cloning and characterization of invasion gene ibe10. *Infect Immun* **63**, 4470-4475 (1995).

62. Kim, K.S. E. coli invasion of brain microvascular endothelial cells as a pathogenetic basis of meningitis. *Subcell Biochem* **33**, 47-59 (2000).

63. Nizet, V.*, et al.* Invasion of brain microvascular endothelial cells by group B streptococci. *Infect Immun* **65**, 5074-5081 (1997).

64. Greiffenberg, L., Goebel, W., Kim, K.S., Daniels, J. & Kuhn, M. Interaction of Listeria monocytogenes with human brain microvascular endothelial cells: an electron microscopic study. *Infect Immun* **68**, 3275-3279 (2000).

65. Badger, J.L., Stins, M.F. & Kim, K.S. Citrobacter freundii invades and replicates in human brain microvascular endothelial cells. *Infect Immun* **67**, 4208-4215 (1999).

66. Pujol, C., Eugene, E., de Saint Martin, L. & Nassif, X. Interaction of Neisseria meningitidis with a polarized monolayer of epithelial cells. *Infect Immun* **65**, 4836-4842 (1997).

67. Jong, A.Y., Stins, M.F., Huang, S.H., Chen, S.H. & Kim, K.S. Traversal of Candida albicans across human blood-brain barrier in vitro. *Infect Immun* **69**, 4536-4544 (2001).

68. Liu, N.Q.*, et al.* Human immunodeficiency virus type 1 enters brain microvascular endothelia by macropinocytosis dependent on lipid rafts and the mitogen-activated protein kinase signaling pathway. *J Virol* **76**, 6689-6700 (2002).

69.King, J.S. & Kay, R.R. The origins and evolution of macropinocytosis. *Philos Trans R Soc Lond B Biol Sci* **374**, 20180158 (2019).

70. Lin, X.P., Mintern, J.D. & Gleeson, P.A. Macropinocytosis in Different Cell Types: Similarities and Differences. *Membranes (Basel)* **10**(2020).

71. Mercer, J. & Helenius, A. Vaccinia virus uses macropinocytosis and apoptotic mimicry to enter host cells. *Science* **320**, 531-535 (2008).

72. Mercer, J. & Helenius, A. Virus entry by macropinocytosis. *Nat Cell Biol* **11**, 510-520 (2009).

73. Mercer, J. & Helenius, A. Gulping rather than sipping: macropinocytosis as a way of virus entry. *Curr Opin Microbiol* **15**, 490-499 (2012).

74. Palmulli, R. & Machesky, L.M. Is macropinocytosis more than just a passive gulp? *Curr Opin Cell Biol***94**, 102513 (2025).

75. Liao, Y.N.*, et al.* Progesterone receptor potentiates macropinocytosis through CDC42 in pancreatic ductal adenocarcinoma. *Oncogenesis* **13**, 10 (2024).

76. Egami, Y., Taguchi, T., Maekawa, M., Arai, H. & Araki, N. Small GTPases and phosphoinositides in the regulatory mechanisms of macropinosome formation and maturation. *Front Physiol* **5**, 374 (2014).

77. Bourguignon, L.Y. Hyaluronan-mediated CD44 activation of RhoGTPase signaling and cytoskeleton function promotes tumor progression. *Semin Cancer Biol* **18**, 251-259 (2008).
78. Zhou, Y. & Sakurai, H. Emerging and Diverse Functions of the EphA2 Noncanonical Pathway in Cancer Progression. *Biol Pharm Bull* **40**, 1616-1624 (2017).

79. Gehring, M.P. & Pasquale, E.B. Protein kinase C phosphorylates the EphA2 receptor on serine 892 in the regulatory linker connecting the kinase and SAM domains. *Cell Signal* **73**, 109668 (2020).
80. Preininger, M.K., Zaytseva, D., Lin, J.M. & Kaufer, D. Blood-brain barrier dysfunction promotes astrocyte senescence through albumin-induced TGFbeta signaling activation. *Aging Cell* **22**, e13747 (2023).

81. Manu, D.R.*, et al.* Astrocyte Involvement in Blood-Brain Barrier Function: A Critical Update Highlighting Novel, Complex, Neurovascular Interactions. *International journal of molecular sciences***24**(2023).

82. Heithoff, B.P.*, et al.* Astrocytes are necessary for blood-brain barrier maintenance in the adult mouse brain. *Glia* **69**, 436-472 (2021).

83. Pociute, A., Pivoriunas, A. & Verkhratsky, A. Astrocytes dynamically regulate the blood-brain barrier in the healthy brain. *Neural Regen Res* **19**, 709-710 (2024).

84. Liddelow, S.A. & Barres, B.A. Reactive Astrocytes: Production, Function, and Therapeutic Potential. *Immunity* **46**, 957-967 (2017).

85. Kwon-Chung, K.J.*, et al.* Cryptococcus neoformans and Cryptococcus gattii, the etiologic agents of cryptococcosis. *Cold Spring Harb Perspect Med* **4**, a019760 (2014).

86. O'Hern, J.A.*, et al.* Epidemiology, management and outcomes of Cryptococcus gattii infections: A 22-year cohort. *PLoS Negl Trop Dis* **17**, e0011162 (2023).

87.Chen, S.C., Meyer, W. & Sorrell, T.C. Cryptococcus gattii infections. *Clin Microbiol Rev* **27**, 980-1024 (2014).

88. Barluzzi, R., Brozzetti, A., Delfino, D., Bistoni, F. & Blasi, E. Role of the capsule in microglial cell-Cryptococcus neoformans interaction: impairment of antifungal activity but not of secretory functions. *Med Mycol* **36**, 189-197 (1998).

89. Urai, M.*, et al.* Evasion of Innate Immune Responses by the Highly Virulent Cryptococcus gattii by Altering Capsule Glucuronoxylomannan Structure. *Front Cell Infect Microbiol* **5**, 101 (2015).

90. Harding, A.T., Gehrke, L., Vyas, J.M. & Harding, H.B. Human Brain Organoids: A New Model to Study Neurotropism. *J Fungi* **11**(2025).

91. Lee, J.*, et al.* CHARMM-GUI Input Generator for NAMD, GROMACS, AMBER, OpenMM, and CHARMM/OpenMM Simulations Using the CHARMM36 Additive Force Field. *J Chem Theory Comput***12**, 405-413 (2016).

92. Abraham, M.J., Murtola, T., Schulz, R., Pall, S., Smith, J.C., Hess, B., Lindahl, E. GROMACS: High performance molecular simulations through multi-level parallelism from laptops to supercomputers. *SoftwareX* **1-2**, 19-25 (2015).

93. Huang, J.*, et al.* CHARMM36m: an improved force field for folded and intrinsically disordered proteins. *Nat Methods* **14**, 71-73 (2017).

Acknowledgements. This work was supported by the National Institutes of Health, grant number, R01-NS110800 (AG).

Author contributions. ABB, DML, KV, developed methodology, acquired and analyzed data and wrote/edited the manuscript. ARS and MB performed the in silico protein prediction analysis and data acquisition. AG conceived the project, acquired funding and wrote the manuscript.

Competing interests. Authors declare that they have no competing interests

Materials and correspondence. Requests for materials should be addressed to Angie Gelli.

Chapter 3

Discovery and Characterization of a Potent Antifungal Peptide through One-Bead, One-Compound Combinatorial Library Screening

Authors: Shivani Bansal[1,2], Kiem Vu[3], Ruiwu Liu[1], Yousif Ajena[1], Wenwu Xiao[1], Suvidha M. Menon[3], Amelia Bennett[3], Angie Gelli[3], Kit S. Lam[1,2]

Affiliations:
Department of Pharmacology, School of Medicine, University of California Davis, Davis, CA, 95616, USA.
Department of Biochemistry and Molecular Medicine, University of California Davis, Sacramento, CA, 95817, USA.

*Corresponding author: Kit S. Lam, PhD
Department of Biochemistry and Molecular Medicine, School of Medicine
University of California Davis,
Sacramento, CA, 95817
Email: kslam@ucdavis.edu

Conflict of Interest: The authors have declared that no conflict of interest exists.

Author Contributions: S.B. and K.S.L. conceived and designed the OBOC library and screening experiments. A.G. and K.V. planned and performed all fungal strain MICs. K.V., S.M., and A.B. performed all *in vivo* studies. R.L. sequenced the positives hits. S.B. and Y.A. synthesized and scaled up all positive hits. S.B. performed all synthesis, characterization, and purification. S.B. and W.X. performed biological confirmation like hemolysis and MTT assays. All authors edited and have given approval to the final version of the manuscript.

Abbreviations:

MAP	membrane-active peptide
OBOC	one-bead, one-compound
GUV	giant unilamellar vesicle
AFP	antifungal peptide
SPPS	solid-phase peptide synthesis

Abstract:

This work describes the discovery of a bead-bound membrane-active peptide (MAP), LBF127, that selectively binds fungal giant unilamellar vesicles (GUVs) over mammalian GUVs. LBF127 was re-synthesized in solution form and demonstrated to have antifungal activity with limited hemolytic activity and cytotoxicity against mammalian cells. Through systematic structure–activity relationship studies, including N- and C-terminal truncation, alanine-walk, and D-amino acid substitution, an optimized peptide, K-oLBF127, with higher potency, less hemolytic activity, and cytotoxicity emerged. Compared to the parent peptide, K-oLBF127 is shorter by three amino acids and has a lysine at the N-terminus to confer an additional positive charge. K-oLBF127 was found to have improved selectivity toward the fungal membrane over mammalian membranes by 2-fold compared to LBF127. Further characterizations revealed that, while K-oLBF127 exhibits a spectrum of antifungal activity similar to that of the original peptide, it has lower hemolytic activity and cytotoxicity against mammalian cells. Mice infected with *Cryptococcus neoformans* and treated with K-oLBF127 (16 mg/kg) for 48 h had significantly lower lung fungal burden compared to untreated animals, consistent with K-oLBF127 being active *in vivo*. Our study demonstrates the success of the one-bead, one-compound high-throughput strategy and sequential screening at identifying MAPs with strong antifungal activities.

Introduction:

Multi-drug-resistant infections caused by opportunistic and pathogenic fungi are some of the most dangerous infections in the world.[1,2] Fungal infections can severely affect immunocompromised patients and prove to be fatal for millions of people around the world.[3,4] Current systemic antifungal agents used in the clinic, like amphotericin B and azole drugs such as fluconazole and itraconazole, often have significant side effects. For example, amphotericin B is nephrotoxic and can cause fever, vomiting, headaches, and shortness of breath. Prolonged use of azole drugs, particularly at high dosage, can have serious side effects such as

impotence, mental health issues, and elevated liver enzymes.[5,6] As such, there is a great need to develop efficacious, selective, and less toxic antifungal agents. In recent years, synthetic membrane-active peptides (MAPs) have shown new and exciting antifungal activities against such infections due to their broad spectrum of activity and low resistance rates. [7–12] To address the shortage of effective and non-toxic antifungal agents, we propose the use of one-bead, onecompound (OBOC) combinatorial library methods to develop new membrane-active, fungicidal peptides with selectivity toward fungal membranes over mammalian membranes.

MAPs are short amino acid chains that can interact with the lipid bilayer, perturbing the structure and function of the biological membranes, thus impacting cell functions. Positively charged MAPs interact selectively with negatively charged microbial membranes and disrupt the integrity of the lipid bilayer via several mechanisms, such as through the induction of pore formation, resulting in leakage and cell death.[12–15] MAPs capable of targeting fungal membranes selectively over mammalian membranes due to differing chemical compositions are expected to exhibit antifungal activities. Some MAPs have shown excellent activity against several *Candida*, *Cryptococcus*, and *Aspergillus* species. [12] Due to the ongoing emergence of multi-drug-resistant pathogens, MAPs have become even more relevant as a possible solution to this global health problem.

Membrane-active antifungal peptides (AFPs) have several advantages over current antifungal drugs because they are able to target multiple aspects of the pathogen and reduce the development of drug resistance in organisms that may arise due to a singular target. The progress made in the development of AFPs has been slow over the years. Many AFPs show poor selectivity and toxicity at concentrations used *in vivo* and are often susceptible to proteolysis. Therefore, there is a need to further develop this class of peptides to improve their selectivity, potency, spectrum of activity, and proteolytic stability.

Here we report the successful use of the OBOC combinatorial peptide library synthesis method along with a unique screening platform to discover AFP hits. We then performed structure–activity relationship (SAR) studies by designing and synthesizing a series of peptide analogues in an attempt to discover AFPs with high antifungal activity but low hemolytic activity and low *in vitro* cytotoxicity against mammalian cells.

The first hit, LBF127, showed antifungal effects based on its ability to discriminate between artificially synthesized giant unilamellar vesicles (GUVs) mimicking fungal and mammalian membrane compositions—the screening parameter used to identify peptides with antifungal activities. We systematically modified this peptide to engineer a more effective AFP, K-o-LBF127, that showed 2-fold higher selectivity *in vitro* than the parent peptide LBF127. In addition, K-oLBF127 was found to be less toxic and reduced lung fungal burden in mice infected with 10^4 *Cryptococcus neoformans*.

Results

Sequential Screening and Peptide Discovery

Four OBOC combinatorial linear peptide libraries (8-, 10-, 12-, and 14-mer) were synthesized using 24 building blocks of 16 canonical and 8 non-canonical amino acids according to our previous published method. [16] A subset (∼100 000 beads total) of these libraries were immobilized on a polystyrene plate and sequentially screened for peptide beads binding to fluorescently labeled GUVs of the desired membrane composition. In this case, beads were screened by using a confocal microscope for selective affinity toward fungal membranes over mammalian membranes. The GUVs were prepared using lipid mixtures, which mimic dominant compositions of the mammalian and fungal membranes. The threshold for positive binding to a membrane was defined as any bead that showed punctate fluorescent spots, indicating GUV binding, with sufficient affinity such that the membrane remained attached to the beads during the

washing steps. A control experiment was conducted with naked beads and GUVs, and no binding was seen. A schematic of this screening technique is shown in Figure 1. This sequential screening strategy has enabled us to interrogate every bead for membrane binding properties. Although

~100 000 peptide beads in a screening experiment represent only a small fraction of all possible permutations of the peptide libraries (~2.74×10^{-10}%), we have discovered an entirely new peptide sequence that subsequently showed high selectivity and potency toward fungal cells. Through the subsequent steps of library screening, 11 out of ~100 000 peptides were found to have selective membrane binding toward fungal-like GUVs over mammalian-like GUVs. Since these candidate AFPs were discovered while tethered to the solid support, their conformation and membrane activity in the soluble form might be different. Therefore, we resynthesized all 11 peptides in soluble, C-terminal carboxy-amide form and examined their antifungal activities along with membrane-active polyene controls such as amphotericin B for their ability to interact with fungal cells, mammalian cells, and human red blood cells. Out of 11 positive binding MAPs, 10 were fungal selective. Out of those 10 fungal-selective peptides, 6 peptides were true positive hits—peptides that showed on-bead activity during the retesting phase—and among those, one of the peptides, LBF127, had excellent antifungal properties with a reasonable degree of selectivity, as shown in Table 1. As shown in Figure 1b, LBF127 is a 12-mer peptide in which 5 residues are non-canonical amino acids. It was the most potent peptide and was found to be non-hemolytic at 100 μM and had a minimum inhibitory concentration (MIC) of 25 μM against *Saccharomyces cerevisiae*, a non-pathogenic yeast, after 48 h of incubation. LBF127 was cytotoxic against HEK 293T cells, with an IC_{50} of 160 μM after 72 h. Amphotericin B, in comparison, was found to be hemolytic at 1–2 μM and had a MIC of 20 μM against yeast. While LBF127 had a MIC comparable to that of amphotericin B in an initial yeast kill assay, it was entirely non-hemolytic. These results gave a satisfactory confirmation of our lead peptide and a test of the reliability of our OBOC screening and subsequent biological testing process.

Peptide Activity In Vitro

With the confirmation of the antifungal activity against a non-pathogenic fungi, *S. cerevisiae*, LBF127 was subsequently tested against a number of pathogenic and non-pathogenic fungi to determine the spectrum of activity against different fungal species. Minimum inhibitory concentration (MIC), a measure of the peptides' fungistatic abilities, is summarized in Tables 1 and 2. LBF127 showed excellent antifungal activity against *Cryptococcus* species, including fluconazole-resistant and flucytosine-resistant isolates of *C. neoformans*, while surprisingly having no activity against *Candida* species. We wanted to investigate and further optimize the peptide structure in order to develop a more potent peptide with increased fungal selectivity.

To evaluate LBF127's selectivity toward *Cryptococcus*, the susceptibility of 8 additional ascomycete clinical isolates (*C. auris* and *C. haemulonii*) and 7 basidiomycetes (*R. mucilaginosa*, fluconazole-resistant *C. neoformans* var. H99 and flucytosine-resistant *C. gattii*) were examined. *S. cerevisae* was also tested as a control strain. As shown in Table 2, LBF127 was found to have activities only against basidiomycete isolates. The susceptibility of fluconazole- and flucytosine-resistant clinical isolates of *Cryptococcus* and multi-drug-resistant *R. mucilaginosa* to LBF127 suggested that an optimized version of LBF127 could be an excellent candidate for the treatment of intractable *Cryptococcal* and *Rhodotorula* infections.

Optimization of LBF127

To improve the antifungal potency and spectrum of activity of LBF127, several analogues were designed, synthesized, and tested against *Cryptococcus neoformans* var. grubii (KN99 strain) and red blood cells (RBCs) to assess antifungal potency and hemolytic activity, respectively. These experiments were done in triplicates with at least three repetitions. The most potent candidate AFPs were then selected to undergo a cytotoxic assay with the mammalian cell line, HEK293T (human embryonic kidney cells). The first peptide modifications were N-terminal and

C-terminal truncations, where a single amino acid was deleted one at a time from either end of the peptide. As shown in Table 3, removing Tyr (OMe)1 from the N-terminus had no effect on MIC or hemolytic activity, indicating that this amino acid is not required for antifungal activity.

However, further truncations of the N-terminus resulted in significant loss of activity. Removing N12 and Dpr11 from the C-terminus of LBF127 had minimal effects on activity, while truncating W10 resulted in a 4-fold reduction in activity.

We also performed the alanine scan assay on LBF127 (Table 4), in which every amino acid in the 12-mer peptide was replaced, one by one, with alanine. The result from this systematic structural modification generated a total of 12 alanine-containing peptide analogs. Substituting a single amino acid did not result in a significant change in LBF127's activity, suggesting that no single amino acid is critical for antifungal activity but rather the structure of the entire peptide is crucial for its activity. Results from the alanine scan and truncation assay suggested that Tyr (OMe)1, Dpr11, and N12 were not required for LBF127's activity. These three amino acids were deleted from LBF127 to obtain a 9-mer optimized peptide named oLBF127 (Figure 2, top panel). In addition to amino acid truncation and alanine substitution, we performed additional modifications to systematically optimize the antifungal potency and reduce the hemolysis and cytotoxicity of LBF127 (Table 5). To determine whether dimerizing a peptide could increase its activity, we synthesized a dimeric version of LBF127 by duplicating the sequence of LBF127 to form a linear, 24-mer peptide. The resulting $[LBF127]_2$ dimer had antifungal activity similar to that of LBF127 but was 8 times more hemolytic. To investigate the contribution of a free N-terminus to antifungal activity, the N-terminus of LBF127 was capped with an acetyl group. Acetylating the N-termini of LBF127 and oLBF127 did not result in any changes in their MICs, but the acetylated peptides, Ac-LBF127 and Ac-oLBF127, were 8 times and 2 times more hemolytic than LBF127, respectively. This suggests that a protonated amine at the N-terminus is needed to lower the hemolytic activity.

It is well known that incorporation of a D-amino acid would render the peptides more resistant to proteolysis. We therefore synthesized a version of LBF127 comprising entirely Damino acids, dLBF127. However, it was found to have poor selectivity for fungal cells over RBCs.

A fluorescent-probe-conjugated LBF127 could be a very useful tool for studying mechanisms of action if the antifungal potency and selectivity of LBF127 could be maintained. Conjugating dansylglycine (DG), a fluorescent probe, to the N-terminus of LBF127 and oLBF127 (DG-LBF127, DG-oLBF127 respectively) introduced a tertiary amine at the N-terminus, and the DG-conjugated peptides both had ~2 times more activity against *Cn*KN99. However, compared to LBF127, DGoLBF127 and DG-LBF127 exhibited 4 and 8 times higher hemolytic activity, respectively (Table 5). Conjugating a small amino acid dye, Fmoc-4-aminobenzoic acid (Abz), to the N-terminus of LBF127 also did not prove to be fruitful. While Abz-LBF127 showed no change in hemolytic activity, it had a 4-fold reduction in antifungal activity compared to LBF127.

The challenge for LBF127 optimization is that an improvement in antifungal potency often leads to an increase in hemolytic activity. As shown above, acetylating the N-terminal amine, e.g., Ac-LBF127 and Ac-oLBF127, increased the hemolytic activity without improving the antifungal activity. This suggests that a protonated amine at the N-terminus is needed to lower the hemolytic activity. We therefore added a Lys to the N-terminus of oLBF127 to generate K-oLBF127 (Figure 2, bottom panel). Compared to LBF127, K-oLBF127 had similar antifungal activity but was 2 times less hemolytic, making it 2 times more selective toward fungi (Table 6). This result confirmed our hypothesis that a positive charge at the N-terminus of the peptide was important for its low hemolytic activity while providing an effective template for further optimizations.

A cytotoxicity assay on HEK293T cells was performed to determine the therapeutic index for a number of candidate peptides. The therapeutic index is the ratio of the peptide concentration that is toxic to human cells (IC_{50}) and the concentration that inhibits the growth of *Cn*KN99 (MIC). If mammalian cell cytotoxicity is reduced (higher IC_{50}) and antifungal activity is improved (lower

MIC) for an optimized peptide, then its therapeutic index would be higher. Therefore, candidate AFPs with a higher therapeutic index would be more desirable, as they would be more active against fungi than human cells. Using the IC_{50} and hemolysis data for HEK293T cells and RBCs (Table 6), LBF127 was found to be 17 times more selective toward KN99 over HEK293T cells, and 5 times more selective toward KN99 over RBCs. On the other hand, K-oLBF127 was 36.4 times more selective toward KN99 over HEK293T cells, and 18 times more selective toward KN99 over RBCs. The chemical structure of K-oLBF127, a 10-mer linear peptide, is shown in Figure 2 (bottom panel). In comparison to LBF127, K-oLBF127 had improved antifungal activities against a number of fungal isolates (Table 7), was found to be less toxic to human cells, and had the highest selectivity among all peptide modifications made (Table 6).

To examine the secondary structure of K-oLBF127, the conformations of the peptide were analyzed by circular dichroism (CD) spectroscopy. The CD spectrum of K-oLBF127 showed negative double peaks at 205 and 220 nm at room temperature (Figure 3B), which are well-known characteristics of an α helix (Figure 3C). [17]

Trypan Blue and Propidium Iodide Staining of Cryptococcus and Candida Treated with K-oLBF127

To confirm the effects of K-oLBF127 on membrane integrity, we treated *Cryptococcus neoformans* (KN99 strain), *Candida albicans*, and *Candida auris* strains with the peptide and assessed membrane integrity with both trypan blue and propidium iodide (PI) (Figures 4 and 5). Trypan blue is a negatively charged diazo dye that cannot enter cells unless the membrane is damaged. It has been widely used to identify dead cells and tissues selectively because cells that exclude the dye are considered viable. By contrast, cells with compromised membranes are colored blue and can be readily observed under a microscope. Following 2 h treatment with KoLBF127, virtually all of the KN99 cells were permeable to trypan blue (Figure 4A). Consistent

with the lower susceptibility of ascomycetes to K-oLBF127, only ~35% of *C. albicans* were stained with trypan blue, and no staining was observed for *C. auris* (Figure 4 A,B). Similar to trypan blue, PI is also widely used to assess cell viability and membrane integrity. PI is a nonmembrane-permeable fluorescent agent used to stain DNA and thus can only enter cells with compromised membranes. Nearly 100% of K-oLBF127-treated KN99 cells were found positive for PI, consistent with a major loss of membrane integrity. In contrast, both *C. albicans* and *C. auris* were found to be significantly less permeable to PI (8–18% cells were PI-positive) following K-oLBF127 treatment, echoing the observed resistance of ascomycetes to K-oLBF127 in susceptibility assays (Table 2). Treatment with melittin, a small linear cytolytic peptide known to form pores in the cell membrane, also led to significantly more PI-positive KN99 cells than either PI-positive *C. albicans* or *C. auris*, suggesting that perhaps *C. neoformans*'s membrane is more susceptible to pore formation by both K-o-LBF127 and melittin.

Optimization of the Lead Peptide K-oLBF127

Similar to the observations made with DG-oLBF127, addition of DG to K-oLBF127 dramatically increased both its antifungal activity and HEK293T cell cytotoxicity (Tables 6 and 8), making this peptide analog unsuitable as an AFP candidate. To develop a similarly potent and selective but potentially protease-resistant peptide for *in vivo* testing, three modifications were made on K-oLBF127 using D-amino acid substitutions at strategic positions, as shown in Table 8. In the first modification (kw-oLBF127), four L-tryptophans were replaced with D-tryptophans while conserving the remaining amino acids in order to minimize proteolysis due to chymotrypsin, which is known to target aromatic amino acids like L-tryptophan.[18] For the second modification, an inverse of the peptide was synthesized (ki-oLBF127) where all amino acids were substituted with their D-amino acid versions while the overall sequence was conserved. This modification would give a mirror image of the overall peptide structure. Finally, a retro-inverso version was synthesized (kri-oLBF127) by substituting all L-amino acids with their D-amino acid versions, and

the N- to C-terminus sequence was reversed. A comparison of the D-amino acid peptide analogs with K-oLBF127 and the parent peptide LBF127 is shown in Table 8. The inverse peptide, kioLBF127, was found to be most cytotoxic and hemolytic and was rejected due to its low *in vitro* "therapeutic index". D-Tryptophan-containing and retro-inversed peptides, kw-oLBF127 and kri-oLBF127, were both found to have excellent antifungal activity and reasonable fungal selectivity and therefore were selected for further *in vivo* studies with a mouse model of cryptococcosis.

In Vivo Activity of K-oLBF127, Kri-oLBF127, Kw-oLBF127

Several mouse models of invasive fungal infections exist, including models for *Cryptococcus*, *Candida albicans*, and *Candida auris*. We used the intranasal model of cryptococcal infection as it more closely mimics the natural course of infection, beginning with the inhalation of *C. neoformans* cells, leading to pulmonary disease and followed by dissemination to other organs, especially the brain. We performed lung fungal burden study to assess the efficacy of K-oLBF127 and the two previously selected D-amino acid peptide analogs, Kri-oLBF127 and Kw-oLBF127, in mice infected with *Cn*KN99. We found that animals treated with 16 mg/kg of KoLBF127 by i.p. injection following inoculation with 10^4 *Cn*KN99 had significantly fewer colonyforming units (CFUs) in lung tissue after 48 h of treatment compared to untreated control (Figure 6A). In contrast, no significant difference in lung fungal burden was observed in animals that were treated with either Kri-oLBF127 or Kw-oLBF127 compared to non-peptide vehicle control. Animals treated with all three peptides had significantly lower body weight percentage on the day they were sacrificed for lung fungal burden analysis (Figure 6B), suggesting that all three peptides were mildly toxic. Additional detailed toxicity studies will be needed to fully assess the cytotoxicity of the peptides *in vivo.*

Discussion

The development of membrane-active AFPs is a promising approach to tackle the global health challenge of fungal diseases, because AFPs can interact with fungal membranes directly, show a high degree of selectivity and potency, and are less likely to induce drug resistance in target fungi.

Here, we describe the discovery of a completely novel synthetic AFP, LBF127, which was identified on the basis of its on-bead affinity toward fungal membranes over mammalian membranes. Through sequential screening of OBOC combinatorial peptide libraries with rhodamine-labeled GUVs that mimic either fungal or mammalian biological membranes, we have succeeded in the identification of linear MAPs with preferential affinity toward fungal membranes. Unlike other combinatorial library methods such as phage-display, yeast-display, and mRNAdisplay peptide libraries, the OBOC method allows the inclusion of many non-canonical amino acids, thus enabling us to greatly expand on previously published MAPs. The sequential screening method applied to an immobilized OBOC library has allowed us to interrogate each and every peptide library bead with different GUVs under different conditions. Such a screening approach has not been possible with other available combinatorial library methods.

The observed on-bead affinity of LBF127 toward fungal membranes was translatable to antifungal effects on live microbes. Using standard susceptibility assays with various fungal strains, we found that LBF127 was active against primarily basidiomycetes,
including *Cryptococcus* and *Rhodotorula* and drug-resistant isolates. Interestingly, although LBF127 is active against *S. cerevisiae*, a non-pathogenic yeast, it appears to have little to no activity against several *Candida* species, including the multi-drug-resistant *C. auris*. The observed weak activities toward ascomycetes suggest that perhaps there are distinct differences in the membrane compositions between different fungi. After systematic modifications to optimize LBF127, a 10-mer linear peptide—K-oLBF127—emerged as the leading candidate AFP. While the antifungal activity of K-oLBF127 did not dramatically improve, the optimized AFP had 2-fold higher selectivity toward fungal cells over mammalian cells compared to the original peptide, LBF127.

Mice treated with K-oLBF127 40 h post-infection showed a significantly lower fungal burden compared to untreated animals, confirming that K-oLBF127 was also active *in vivo*. To further improve the stability of K-oLBF127 *in vivo*, we synthesized several D-amino acid versions of our lead peptide and examined their activity in mice that had been infected with 10^4 *C. neoformans*. No reduction in lung fungal burden was found in animals treated with either 16 mg/kg of Kri-oLBF127 or 16 mg/kg of Kw-o-LBF127, suggesting that D-amino acid substitutions did not enhance *in vivo* antifungal activity.

Conclusion

Fungal infections are an ongoing global problem. Deaths and morbidities due to fungal infections are alarmingly high, as treating fungal infections has become more difficult due to significant side effects of current drugs and the emergence of drug resistance. Most of the deaths from fungal diseases are caused by *Cryptococcus*, *Candida*, and *Aspergillus* species. The current repertoire of antifungal drugs is limited, and the emergence of multi-drug-resistant strains is highly problematic. As such, there is a dire need for the development of novel, potent, nontoxic, and highly selective antifungal drugs with activity against drug-resistant fungi.

In this study, we propose that the use of OBOC technology and GUVs mimicking membrane compositions of microbes can lead to the discovery of novel antimicrobial MAPs. Since these peptides are discovered on the basis of their binding to membranes with lipid composition mimicking fungal membrane, they are likely to display high selectivity toward fungi over mammalian cells. MAPs that target fungal membranes directly are also less likely to develop resistance in target fungi, unlike many conventional antifungals that target specific glycan, ergosterol, or DNA synthesis pathways. Since the OBOC technology affords a high degree of chemical control, peptides can be easily modified to the desired length and conformation with both canonical and non-canonical amino acids. Interestingly, K-oLBF127 has a non-canonical amino acid, aminoisobutyric acid (Aib), which has been found in known AFPs such as trichogin.

[19] As demonstrated in this study, OBOC also proves to be an excellent tool in the discovery of AFPs, as this technique was demonstrated to be highly translatable to biological systems; i.e., peptides discovered using this technique exhibited activities against a number of fungal pathogens. Work to identify a further optimized AFP using a focused OBOC library approach is underway. Future work to examine the mechanisms of action underlying the observed antifungal activities of KoLBF127 and longer term animal studies will be necessary to fully characterize this new AFP.

Methods

Peptide Synthesis and Modifications

PEGA beads (0.4 mmol/g, 150–300 μm) were purchased from Agilent Technologies (Santa Clara, CA). HATU, trifluoroacetic acid (TFA), phenol, Rink-Amide MBHA beads, ammonium acetate, triisopropylsilane, and thioanisole were purchased from Sigma-Aldrich (St. Louis, MO). Ethyl ether, diisopropylethylamine (DIEA), dimethylformamide (DMF), methanol, and methylene chloride (DCM) were purchased from Fischer Scientific (Hampton, NH). 4Methylpiperidine was purchased from Spectrum (New Brunswick, NJ). Natural L-amino acids were purchased from p3BioSystems (Louisville, KY). Fmoc-Hyp(tBu)-OH, Fmoc-Nva-OH, FmocDpr(Boc)-OH, Fmoc-Nle-OH, and Fmoc-Abu-OH were purchased from Chem Impex (Wood Dale, IL), and Fmoc-Aib-OH was purchased from ChemPep (Wellington, FL). Fmoc-Tyr(OMe)-OH, Fmoc-Cha-OH, and Fmoc-Orn(Boc)-OH were purchased from Ark Pharm (Arlington House, IL). Matrix-assisted laser desorption/ionization time-of-flight mass spectrometry (MALDI-TOF-MS) analysis was performed on a Bruker UltraFlextreme mass spectrometer (Billerica, MA, USA). High-performance liquid chromatography was performed on a Waters 2996 HPLC system equipped with a 4.6 × 150 mm Waters Xterra MS C18 5.0 μm column, and it employed a 20 min gradient from 100% aqueous H_2O (0.1% TFA) to 100% CH_3CN (0.1% TFA) at a flow rate of 1.0 mL/min. OBOC combinatorial peptide libraries were synthesized according to our previously

published methods. [16,20–22] PEGA beads (2 g) were washed thoroughly to duly deprotect any existing Fmoc group. Molar excesses (6–7 equiv) of each unique Fmoc-protected amino acid were added to each column of beads, along with a carbodiimide activating agent (Oxyma) and a base (DIC). The Oxyma activated the carboxylic acid, while the base promoted amide bond formation. The columns were shaken for 45 min at 40 °C, and a ninhydrin test [23]was performed on bead samples to ensure completion of reaction. If any unreacted amine group remained on the beads, the test would appear bright blue. Following coupling, the beads were mixed together and washed copiously in a fritted tube with DMF, MeOH and DCM.

The Fmoc-protecting group was then removed with 20% 4-methylpiperidine/DMF for 20 min at room temperature; a fresh solution was used during the last 5 min to ensure complete deprotection. These steps were then repeated for the desired length of the peptide. At the end of peptide synthesis, a global deprotection was carried out using a cocktail of 82.5% TFA, 5% phenol, water, thioanisole, and 2.5% triisopropylsilane in order to cleave the acid-labile groups protecting the side chains of the amino acid. This step would also cleave the peptide from the bead. The acid cocktail was then added to the peptides and shaken at room temperature for 4–6 h, depending on the individual amino acids. In the case of global deprotection, the solution was drained and washed with DMF and then washed again with MeOH and DCM. In the case of cleavage from Rink resin, the solution was drained and saved in a 50 mL tube, as all the peptides were then in solution. Excess solvent was removed by evaporation, and the compound was precipitated using anhydrous diethyl ether. The product was collected as a white powder, which was then purified by reverse-phase HPLC, and its identity was confirmed with MALDI-TOF-MS.

OBOC Library Design and Synthesis

OBOC combinatorial linear peptide libraries were synthesized according to our previously reported method. [24] Twenty-four Fmoc-amino acids, both canonical and non-canonical, were used to prepare the 8-, 10-, 12-, and 14-mer OBOC libraries.

OBOC Peptide Library Screening

Sequential screening is a technique which enables the interrogation of a single immobilized bead against different conditions. In the context of membrane binding, each immobilized bead can be treated with a GUV, then washed away, then treated with another type of GUV. Immobilization of beads was carried out in 8-well polystyrene plates using a 90% DMF in water solution to soften the plastic and reversibly fix each bead at the plate surface. [24] GUVs were diluted to 2 mL with buffer, added to plated beads, and incubated for 30 min. Any nonbinding GUVs were washed away. Screening was performed using confocal laser scanning microscopy (CLSM, Carl Zeiss LSM 800). GUV-binding bead-bound peptides were physically isolated by a micropipet, washed, and sequenced with an automatic peptide microsequencer. Screening of about 100 000 library beads could be achieved in 45 min, which included the time of incubation and image acquisition. Bound GUVs could be washed off and treated with another type of GUV to observe the binding of a single peptide under different conditions.

GUV Synthesis

1-Palmitoyl-2-oleoyl-*sn*-glycero-3-phosphocholine (POPC), 1,2-dioleoyl-*sn*-glycero-3phosphocholine (DOPC), egg sphingomyelin (egg SM), lissamine rhodamine B 1,2-dioleyl-*sn*glycero-3-phosphoethanolamine (Rhodamine-B DOPE), cholesterol (Ch, ovine), and dehydroergosterol (erg) were acquired from Avanti Polar Lipids (Alabaster, AL). 2-(*N*-(7Nitrobenz-2-oxa-1,3-diazol-4-yl)amino)-2-deoxyglucose (2-NBDG, or NBD-glucose) was purchased from

ThermoFisher Scientific (Eugene, OR). Sucrose was obtained from EMD Chemicals (Philadelphia, PA). Chloroform was purchased from Fisher Scientific (Fair Lawn, NJ). Ninety-six-well glass bottom plates were obtained from MatTek Corporation (Ashland, MA).

Indium tin oxide (ITO)-coated glass slides with busbars (resistance 70–100 Ω) were obtained from SPI Supplies (West Chester, PA), and Grace Bio-Laboratories press-to-seal silicone isolators (PSA both sides, 20 mm diameter × 1 mm depth) were obtained from Sigma-Aldrich (St. Louis, MO). All chemicals were used without further purification. GUVs were prepared using a classic electroformation protocol from Angelova and Dimitrov [25] and were prepared using processes from a previously published study. [26] Two separate stock solutions—fungal GUV and mammalian GUV—were used, mammalian consisting of a 1.5:1:1.5 ratio of DOPC, CM, and Ch with 1% rhodamine-B-DOPE in chloroform, and fungal consisting of a 2:1:1.3 ratio of DOPC, erg, and SM. [27,28] Small droplets of stock solution were spread on the conductive side of ITO-coated slides to deposit 0.2 µg/well and allowed to dry under vacuum overnight. [29] The dried film was then directly hydrated with 100 mM aqueous sucrose. The solution droplet was contained using a 1 mm thick adhesive silicone isolator (~20 mm diameter). A water-tight chamber was then created by sealing the second ITO slide over the ring, ensuring that no visible air bubbles were trapped inside. Using a function generator, a 3 V_{pp} AC sine-wave was then applied across the two slides at 10 Hz for ~ 2 h. During the formation, the ITO sandwich was covered with aluminum foil to protect it from light. Following the formation, a 3 mL syringe was used to suck the vesicle solution out of the slides. The GUVs were either used immediately or stored in small centrifuge tubes at 4 °C and used within 36 h of preparation.

Peptide Modifications

Some peptide modifications were made: (i) Truncation series, a type of modification where individual amino acids are “chopped”, one-by-one, from the N-terminus or the C-terminus. In this

assay, information about important active motifs within a longer peptide can be inferred. For Nterminus modifications (chopping amino acids from N-terminus), the base peptide was synthesized using standard solid-phase peptide synthesis (SPPS). For subsequent truncations, a small amount of the beads were removed before additional SPPS steps. This enabled the synthesis of incremental truncations in a single synthesis set-up. For C-terminus truncations, each truncation was synthesized individually since SPPS was performed starting from the C-terminus to the N-terminus. (ii) Alanine walks, a type of modification where every amino acid in the peptide is replaced, one-by-one, with a small amino acid like alanine. This assay provided information about whether an individual amino acid might be important or unimportant for activity. In combination with truncations, alanine walks can be a powerful technique to develop a highly optimized peptide.

In Vitro Activity and Selectivity

The hemolysis of peptides was analyzed using fresh citrated blood from healthy Balb/C mice. Red blood cells (RBCs) were collected via centrifugation at 1000 rpm for 10 min, washed three times with PBS, and then brought to a final concentration of 2% in PBS. Next, 180 μL of erythrocyte suspension was mixed with 20 μL portions of different concentrations of drugs and incubated for 4 h at 37 °C. The mixture was centrifuged at 1000 rpm for 5 min, and 100 μL of supernatant from each sample was transferred to a 96-well plate. Free hemoglobin in the supernatant was measured by the absorbance at 540 nm using a micro-plate reader (SpectraMax M2, Molecular Devices, USA). RBCs were incubated with Triton-100 (0.1%) and PBS as the positive and negative controls, respectively. The MTS assay was used to evaluate the potential cytotoxicity of peptides against normal HEK293 cells. Briefly, 3×10^3 HEK293 cells in 100 μL of media per well were seeded in the 96-well tissue culture plates, and analysis was performed 72 h after treatment with different concentrations of drugs by adding 10 μL per well of the mixture of the compound 3-(4,5-dimethylthiazol-2-yl)-5-(3-carboxymethoxyphenyl)-2-(4-sulfophenyl)-

2*H*tetrazolium (MTS) and an electron-coupling reagent called phenazine methosulfate (PMS) at 20:1 for 2 h at 37 °C. The 96-well plates were read at 490 nm using the SpectraMax M2 reader (Molecular Devices, USA).

Fungal Strains and Susceptibility Testing

Fungal strains were either clinical isolates or lab strains and originated from either the American Type Culture Collection (ATCC) or the Fungus Testing Laboratory (University of Texas Health, San Antonio). Basidiomycete representative strains include *Cryptococcus neoformans* var. *grubii* (H99, clinical isolate and KN99, lab strain), *Cryptococcus gattii* (clinical isolate), *Cryptococcus neoformans* var. *neoformans* (JEC21, lab strain), and *Rhodotorula mucilaginosa* (clinical isolate). Ascomycete representative strains include *Candida albicans*, *Candida auris*, *Candida glabrata*, *Candida haemulonii*, *Candida kruisei*, *Candida parapsilosis*, and *Candida tropicalis*. Fluconazole-resistant isolates (*C. neoformans* var. *grubii*, H99 strain) and flucytosine-resistant isolates (*C. gattii* and *S. cerevisiae*) were also included in this study. The susceptibility of fungal strains to LBF126 and LBF127 was determined according to the Clinical and Laboratory Standards Institute (CLSI). *In vitro* testing was carried out in RPMI 1640 medium containing L-glutamine without sodium bicarbonate and buffered to pH 7.0 with MOPS in 96-well plates (round-bottom, Costar). Inocula of *C. neoformans* (10 µL) were prepared in accordance with the CLSI standard (M27-A3), added to the 96-well plates, and incubated for 48 h (*Candida*) or 72 h (*Cryptococcus*) at 35 °C without shaking. Readings were determined via visual inspections. The minimum inhibitory concentration (MIC) of the candidate peptides was defined as the lowest peptide concentration in a well at which a 100% reduction in optical density was observed compared to the no-peptide control well. Minimum fungicidal concentrations (MFCs) were determined by plating 100 µL from each well onto YPD plates that were then incubated at 30 °C for 72 h. The lowest concentration that yielded three or fewer colonies was recorded (>99.99% killing) as the MFC. [30]

In Vivo Testing of Three Lead AFP Candidates in the Mouse Inhalation Model of Cryptococcal Disease

Seven-week-old A/J mice were inoculated with 10^4 *C. neoformans* (KN99 lab strain) and treated 40 h later with 16 mg/kg of peptides (K-o-LBF127, Kri-o-LBF127, or Kw-o-LBF127) every 8 h for 2 days (six treatments total). Immediately prior to fungal inoculation, the animals were anesthetized with 5% isoflurane. To do this, a mask was placed over the nose and mouth, and 5% (flow-rate) isoflurane was administered until the heart beat slowed down to about 1 beat per second. To prevent the animals from waking up, 2.5% of isoflurane gas was applied as necessary. Once anesthetized, the animals were inoculated with 10^4 fungal cells (resuspended in 50 µL of PBS) through the nares using a 100 µL pipet. The control groups (un-infected animals treated with 16 mg/kg of candidate peptides) were similarly inoculated with 50 µL of 1X PBS in place of fungal cells. Inoculation via the nares was achieved by holding the scruff of the neck in an upright position in order to extend the animal's neck, thus ensuring that the inoculum was inhaled smoothly with minimal obstruction After applying the inoculum through the animals' nares, they were held for another 10 s to ensure that all of the inoculums had been inhaled. Following 40 h post-infection, mice were treated with 16 mg/kg of candidate peptides in a 400 µL volume via intraperitoneal (i.p.) injection every 8 h for a period of 2 days (six injections total). The control group that did not receive peptide treatments was treated with 400 µL of water instead via i.p. injection. Mice were then closely monitored on a daily basis to assess changes in weight and/or changes in physical behavior or appearance. At the conclusion of the experiment, the animals were euthanized, and lungs were removed for CFU enumerations. Homogenized lung tissues were plated on yeast peptone dextrose (YPD) agar plates supplemented with 100 µg/mL of ampicillin for 2 days until colonies appeared.

Circular Dichroism

All the samples were scanned on a Jasco 715 CD spectrometer. A sample with a volume of 250 mL was loaded on a 1 mm path length quartz cuvette, and spectra were recorded in a wavelength range from 260 to 190 nm. All the spectra were obtained with a continuous scanning mode with 20 nm/min speed. The “steady-state” CD spectra were obtained with a response time constant of 2 s, a scan rate of 20 nm/min, accumulation of three scans, and a bandwidth of 1 nm. The Origin graphic software was used to subtract the buffer background for normalization. The graphs were plotted using the same software. Initially all the CD measurements were made at room temperature for all the samples and later according to the temperature requirement and pH studies. The predicted structural details were calculated using the online-available software BESTSEL (http://bestsel.elte.hu/index.php).

Trypan Blue Staining of *Cn*KN99, *C. albicans*, and *C. auris* Pre-treated with K-oLBF127

Fungal cells (*Cn*KN99, *C. albicans*, and *C. auris*) were cultured in YPD overnight and diluted to 1.5×10^6 cells/mL in 50 mL of RPMI. The cultures were then treated with 16 μg/mL of K-oLBF127 for 2 h at 35 °C prior to staining with trypan blue. A second set of cultures were processed in a similar manner but without K-oLBF127 treatment. The cultures were subsequently stained with 20% trypan blue. Brightfield images of treated and untreated cells were obtained from a conventional microscope.

Propidium Iodide Staining Analysis by Flow Cytometry

Fungal cells (*Cn*KN99, *C. albicans*, and *C. auris*) were cultured in YPD overnight and diluted to 3000 cells/mL in 50 mL of RPMI. The cultures were then treated with either 16 μg/mL of K-o-LBF127 peptide or 3 μg/mL of melittin for 30 min at 35 °C. Separately, a second set of cultures were incubated at 99 °C for 10 min to serve as a positive control for PI staining. Treated cultures

were then concentrated to 1 mL and brought to the flow cytometry core at UC Davis (Davis Campus Shared Flow Cytometry Resource) for analysis. A 4 µL volume of PI (1 mg/mL) was added to 1 mL culture immediately prior to inputting the samples into the flow cytometer (Beckman Coulter “Cytoflex” 13-color cytometer).

Abstract figure.

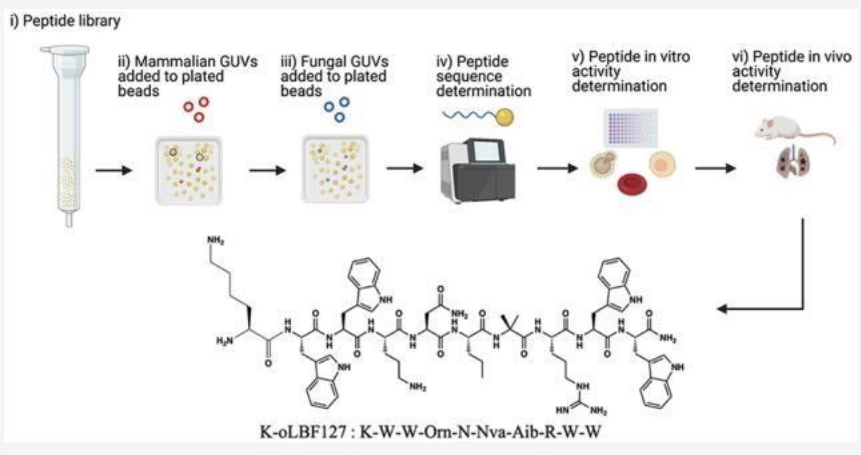

Figure 1.

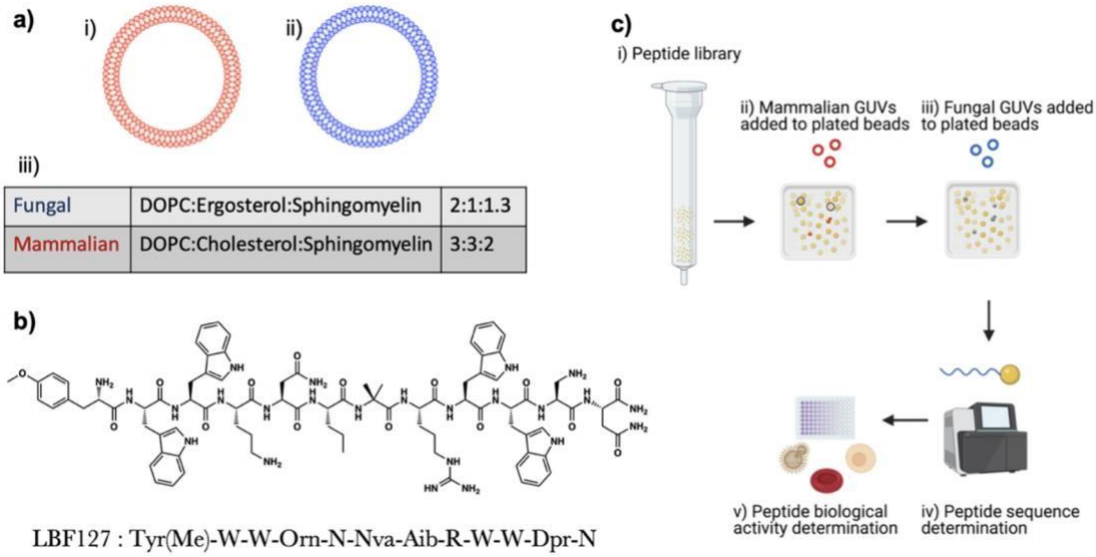
a)
i)
ii)
iii)
Fungal
DOPC:Ergosterol:Sphingomyelin
2:1:1.3
Mammalian
DOPC:Cholesterol:Sphingomyelin
3:3:2
b)
LBF127 : Tyr(Me)-W-W-Orn-N-Nva-Aib-R-W-W-Dpr-N
c)
i) Peptide library
ii) Mammalian GUVs added to plated beads
iii) Fungal GUVs added to plated beads
iv) Peptide sequence determination
v) Peptide biological activity determination

Figure 1. High-throughput sequential screening of bead-bound peptides using giant unilamellar vesicles (GUVs). (a) Vesicle type and membrane lipid concentrations: (i) mammalian vesicles are coded red as depicted in the scheme to the left, (ii) fungal vesicles are coded blue as depicted in the scheme to the right, and (iii) fungal membrane and mammalian membrane lipid composition are given as ratios of phospholipid, sterol, and sphingomyelin. Each GUV also contained 1% rhodamine-DOPE, a membrane dye used in fluorescence microscopy. (b) LBF127 is a linear peptide comprised of 12 amino acids, including non-canonical L-amino acids such as Tyr(OMe), Orn, Nva, Dpr, and Aib. Molecular weight = 1708 g/mol. (c) Schematic representation of the sequential screening strategy with two different GUVs to identify MAPs from the OBOC combinatorial peptide library: (i) the OBOC peptide library was immobilized on the plate; (ii) immobilized beads were incubated with “mammalian GUVs” (in red), and unbound GUVs were washed away. Positive hits (beads with visibly bound GUVs) were identified, and their position on the plate was recorded. Bound GUVs were eventually removed by washing with ethanol to prepare the plate for screening with another type of GUV. (iii) Immobilized beads were incubated with “fungal GUVs” (in blue), unbound GUVs were washed away, and positively bound hits were identified and recorded. Positively bound beads of interest were identified and isolated (circled beads in c-ii depict peptide beads that bound fungal GUVs selectively, i.e., fungal-specific binding). (iv) Selected beads were microsequenced via automatic Edman chemistry. (v) Lead compounds were resynthesized in soluble form to confirm their membrane activity in relevant biological systems. Peptide biological effects on yeast (*S. cerevisiae*), HEK 293 kidney cells, and red blood cells were determined.

Table 1. Biological Profile of Fungal- Selective Peptides Identified from the OBOC Screen with GUVs

peptide	*S. cerevisiae* MIC (μM)	hemolysis (μM)	HEK293T IC_{50} (μM)	therapeutic index [a]
LBF127	25	50	160	6
LBF126	20	200	160	8
LBF124	75	12.5	100	1
LBF121	50	25	50	1
LBF82	50	100	200	4
LBF89	200	100	200	1
LBF14	50	25	25	1
amphotericin B	1.0	1	40	40.0

[a]Therapeutic index = (IC_{50} HEK293/MIC *S. cerevisiae*).

Table 2. Antifungal Profile LBF127

fungal genus and strain name	MIC (μM)
Cryptococcus neoformans (KN99)	9.4
Cryptococcus neoformans (JEC21)	4.7
Cryptococcus gattii	4.7
Cryptococcus neoformans H99 (fluconazole-resistant, fluconazole MIC = 64 μg/mL)	9.4–18.7
Cryptococcus gattii (flucytosine-resistant, 5FC MIC > 64 μg/mL)	9.4–18.7
Rhodotorula mucilaginosa isolate 1-2	4.7–9.4
Candida albicans	18.7
Candida glabrata	>37.5
Candida auris isolate 1-5	>37.5
Candida haemulonii isolate 1-3	>37.5

Table 3. Truncation series of LBF127

peptide sequence	peptide name	*Cn*KN99 MIC (μM)	hemolysis (μM)
Aib-R-W-W-Dpr-N	LBF127-tr6	>37.4	>200
Nva-Aib-R-W-W-Dpr-N	LBF127-tr7	>37.4	>200
N-Nva-Aib-R-W-W-Dpr-N	LBF127-tr8	>37.4	>200
Orn-N-Nva-Aib-R-W-W-Dpr-N	LBF127-tr9	>37.4	>200
W-Orn-N-Nva-Aib-R-W-W-Dpr-N	LBF127-tr10	>37.4	200
W-W-Orn-N-Nva-Aib-R-W-W-Dpr-N	LBF127-tr11	10.5	100
Tyr(oMe)-W-W-Orn-N-Nva-Aib-R-W-W-Dpr-N	LBF127	10.5	100
Tyr(oMe)-W-W-Orn-N-Nva-Aib-R-W-W-Dpr	LBF127-ctr1	5.0	6.25
Tyr(oMe)-W-W-Orn-N-Nva-Aib-R-W-W	LBF127-ctr2	10.6	6.25
Tyr(oMe)-W-W-Orn-N-Nva-Aib-R-W	LBF127-ctr3	48.5	200

Table 4. Alanine Scan of LBF127

peptide sequence	peptide name	*Cn*KN99 MIC (μM)	hemolysis (μM)
A-W-W-Orn-N-Nva-Aib-R-W-W-Dpr-N	AJ-1	5.0	12.5
Tyr(oMe)-**A**-W-Orn-N-Nva-Aib-R-W-W-Dpr-N	AJ-2	20.1	>200
Tyr(oMe)-W-**A**-Orn-N-Nva-Aib-R-W-W-Dpr-N	AJ-3	20.1	>100
Tyr(oMe)-W-W-**A**-N-Nva-Aib-R-W-W-Dpr-N	AJ-4	9.6	25
Tyr(oMe)-W-W-Orn-**A**-Nva-Aib-R-W-W-Dpr-N	AJ-5	4.8	12.5
Tyr(oMe)-W-W-Orn-N-**A**-Aib-R-W-W-Dpr-N	AJ-6	19.0	200
Tyr(oMe)-W-W-Orn-N-Nva-**A**-R-W-W-Dpr-N	AJ-7	9.4	50
Tyr(oMe)-W-W-Orn-N-Nva-Aib-**A**-W-W-Dpr-N	AJ-8	9.9	50
Tyr(oMe)-W-W-Orn-N-Nva-Aib-R-**A**-W-Dpr-N	AJ-9	20.1	200
Tyr(oMe)-W-W-Orn-N-Nva-Aib-R-W-**A**-Dpr-N	AJ-10	20.1	50
Tyr(oMe)-W-W-Orn-N-Nva-Aib-R-W-W-**A**-N	AJ-11	18.9	50
Tyr(oMe)-W-W-Orn-N-Nva-Aib-R-W-W-Dpr-**A**	AJ-12	4.8	6.25

Figure 2.

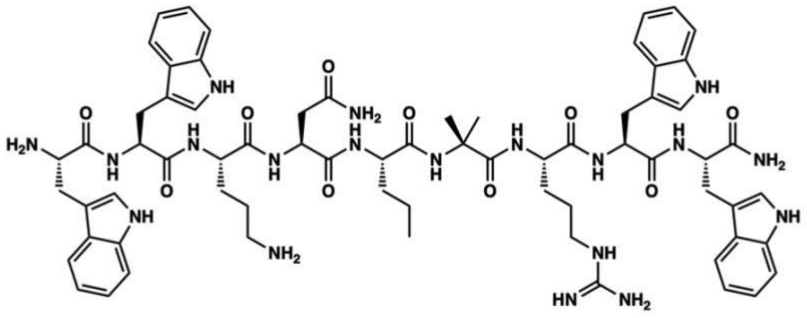

oLBF127 : W-W-Orn-N-Nva-Aib-R-W-W

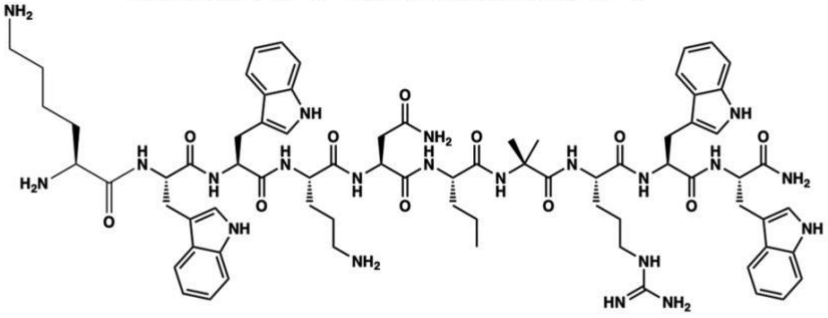

K-oLBF127 : K-W-W-Orn-N-Nva-Aib-R-W-W

Figure 2. Chemical structures of oLBF127 and K-oLBF127

Table 5. Structure-Activity Relationships of LBF127 Analogs

fungal genus and strain name	MIC (μM)
Cryptococcus neoformans (KN99)	9.4
Cryptococcus neoformans (JEC21)	4.7
Cryptococcus gattii	4.7
Cryptococcus neoformans H99 (fluconazole-resistant, fluconazole MIC = 64 μg/mL)	9.4–18.7
Cryptococcus gattii (flucytosine-resistant, 5FC MIC > 64 μg/mL)	9.4–18.7
Rhodotorula mucilaginosa isolate 1-2	4.7–9.4
Candida albicans	18.7
Candida glabrata	>37.5
Candida auris isolate 1-5	>37.5
Candida haemulonii isolate 1-3	>37.5

Table 6. Biological Activities of K-oLBF127 and its $_{D}$ -Amino Acid- Containing Analogues

peptide name	*Cn*KN99 MIC (μM)	hemolysis (μM)	HEK293T IC_{50} (μM)	therapeutic index
LBF127	9.4	50	160	17.0
oLBF127	12.0	50	84	7.0
DG-oLBF127	4.9	12.5	48	9.7
K-oLBF127	5.5	100	200	36.4
amphotericin B	1.0	1	40	40.0

Table 7. Antifungal Susceptibility Data for K-oLBF127 and LBF127

	MIC (μM)	
strain name (1)	**LBF127**	**K-oLBF127**
Cryptococcus neoformans (KN99)	9.4	5.5
Cryptococcus neoformans (JEC21)	4.7	5.5
Cryptococcus gattii (NIH444)	4.7–9.4	11.0
Rhodotorula mucilaginosa	4.7–9.4	5.5
Cryptococcus neoformans (H99, fluconazole-resistant, fluconazole MIC = 64 μg/mL)	9.4–18.7	5.5
Cryptococcus gattii (flucytosine-resistant, 5FC MIC > 64 μg/mL)	9.4–18.7	5.5
Candida albicans	18.7–37.4	22
Candida glabrata	>37.4	>44
Candida auris	>37.4	>44
Candida haemulonii	>37.4	>44
Candida kruisei	18.7	11–22
Candida parapsilosis	>37.4	>44
Candida tropicalis	9.4	5.5

Figure 3.

A

K-oLBF127
K-W-W-Orn-N-Nva-Aib-R-W-W

B

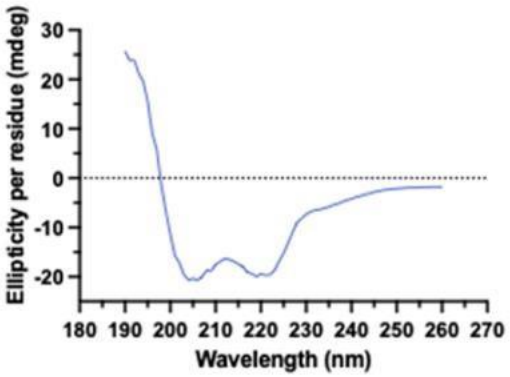

C

Peptide	Helix	Antiparallel	Parallel	Turn	Others
K-oLBF127	76.9	10.4	1.4	0.0	11.4

Figure 3. Secondary structure of K-oLBF127 peptide. (A) Amino acid sequence of K-oLBF127. (B) CD spectrum of K-oLBF127 in acetonitrile at RT. (C) Secondary structure analysis of KoLBF127 suggests a predominant helix form.

Figure 4.

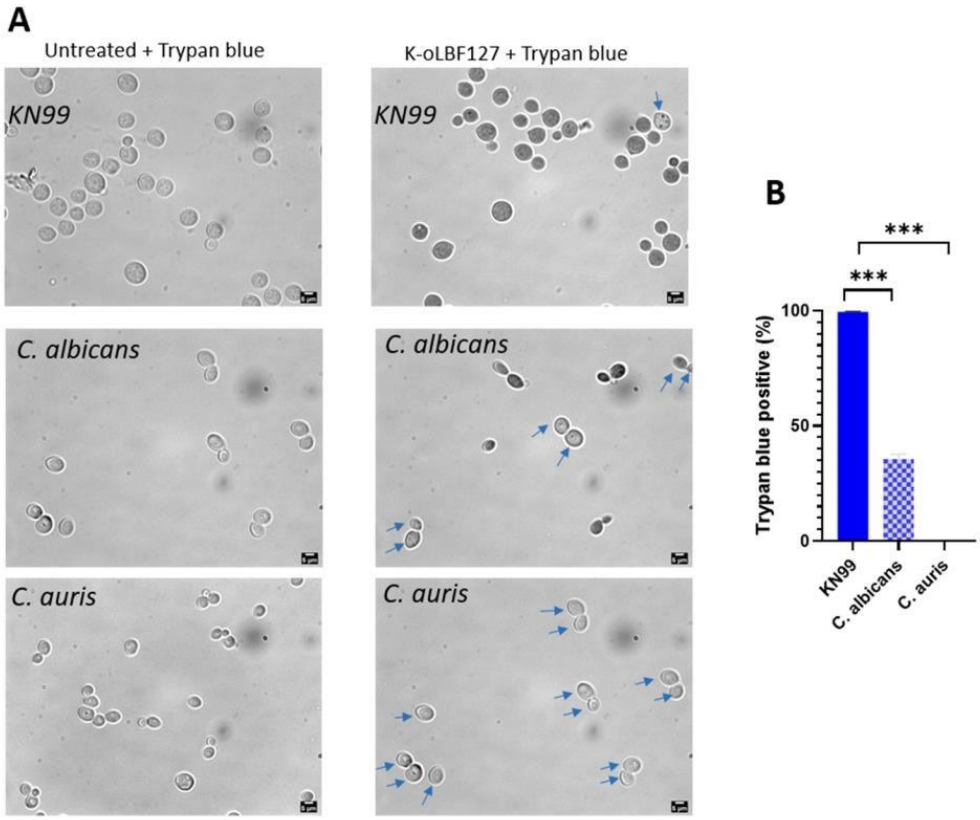

Figure 4. Trypan blue staining of *Cryptococcus neoformans*, *Candida albicans*, and *Candida auris* cells following K-o-LBF127 treatment. (A) The three fungal strains were treated with 16 µg/mL of K-oLBF127 for 2 h at 35 °C. Blue arrows point to unstained cells in K-oLBF127-treated samples. (B) Quantification of percentage of cells stained with trypan blue. Error bars represent the standard deviation of over 100 counted cells from at least six images (***$P < 0.0001$).

Figure 5.

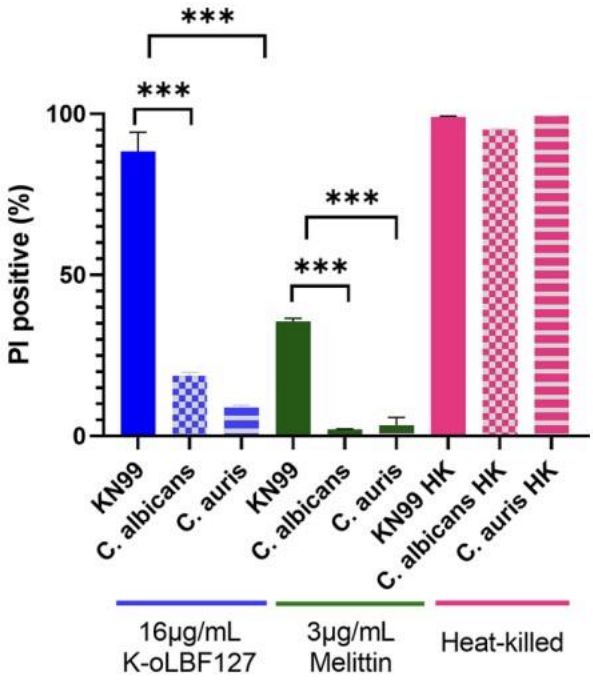

Figure 5. Flow cytometry analysis of propidium iodide (PI)-positive *Cryptococcus neoformans*, *Candida albicans*, and *Candida auris* cells after K-o-LBF127, melittin, and heatkilled (HK) treatments. The three fungal strains were treated for 30 min at 35 °C. Flow cytometry was performed as described in the methods section. Each experiment used around 150 000 cells per treatment. Error bars represent the standard deviation of three trials (***P < 0.0001). **Table 8. Modifications of K-oLBF127**

peptide sequence	peptide name	*Cn*KN99 MIC (μM)	hemolysis (μM)	HEK293T IC_{50} (μM)	therapeutic index
Tyr(oMe)-W-W-Orn-N-Nva-Aib-R-W-W-Dpr-N	LBF127	9.4	50	160	17.0
K-W-W-Orn-N-Nva-Aib-R-W-W	K-oLBF127	5.5	100	200	36.4
(DG)-K-W-W-Orn-N-Nva-Aib-R-W-W	DG-K-oLBF127	2.3	25	39	17.0
k-w-w-orn-n-nva-Aib-r-w-w	ki-oLBF127	9.4	20	30	10.9
k-w-w-r-Aib-nva-n-orn-w-w	kri-oLBF127	8.9	>200	70	12.7
K-w-w-Orn-N-Nva-Aib-R-w-w	kw-oLBF127	4.7	80	160	14.6

Figure 6.

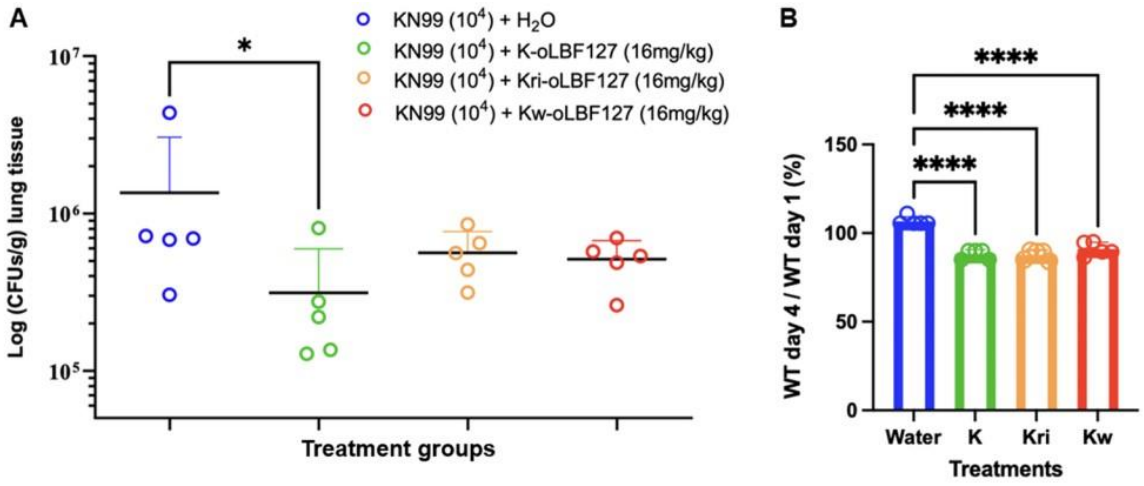

Figure 6. Treatment with K-oLBF127 reduces fungal burden in the lungs of mice intranasally inoculated with 10^4*C. neoformans*. (A) Mice were treated with K-oLBF127, Kri-oLBF127, or KwoLBF127 (16 mg/kg, 3× per day for 2 days) via intraperitoneal injection following 40 h postinoculation of *Cn*KN99 strain. The animals were euthanized on day 4 following 2 days of treatment, and lung tissue was processed for CFU determination. For each treatment group n = 5. Significance was determined by a Welch's t test. *$P < 0.05$. (B) Percent body weight relative to day 1 after fungal inoculation and peptide treatments, ****$P < 0.0001$. Abbreviations: WT, weight; K, K-oLBF127; Kri, Kri-oLBF127; Kw, Kw-oLBF127.

References

1. Bongomin F, Gago S, Oladele RO, Denning DW. Global and Multi-National Prevalence of Fungal Diseases—Estimate Precision. *J Fungi*. 2017;3(4):57. doi:10.3390/jof3040057

2. Fisher MC, Hawkins NJ, Sanglard D, Gurr SJ. Worldwide emergence of resistance to antifungal drugs challenges human health and food security. *Science*. 2018;360(6390):739-742. doi:10.1126/science.aap7999

3. Rautemaa-Richardson R, Richardson MD. Systemic fungal infections. *Medicine (Baltimore)*. 2017;45(12):757-762. doi:10.1016/j.mpmed.2017.09.007

4. Kaushik N, Pujalte GGA, Reese ST. Superficial Fungal Infections. *Prim Care Clin Off Pract*. 2015;42(4):501-516. doi:10.1016/j.pop.2015.08.004

5. Lo Re V, Carbonari DM, Lewis JD, et al. Oral Azole Antifungal Medications and Risk of Acute Liver Injury, Overall and by Chronic Liver Disease Status. *Am J Med*. 2016;129(3):283291.e5. doi:10.1016/j.amjmed.2015.10.029

6. Sabra R, Branch RA. Amphotericin B Nephrotoxicity. *Drug Saf*. 1990;5(2):94-108. doi:10.2165/00002018-199005020-00003

7. Fernández de Ullivarri M, Arbulu S, Garcia-Gutierrez E, Cotter PD. Antifungal Peptides as Therapeutic Agents. *Front Cell Infect Microbiol*. 2020;10:105. doi:10.3389/fcimb.2020.00105

8. Buda De Cesare G, Cristy SA, Garsin DA, Lorenz MC. Antimicrobial Peptides: a New Frontier in Antifungal Therapy. *mBio*. 2020;11(6):10.1128/mbio.02123-20. doi:10.1128/mbio.02123-20

9. Landy M, Warren GH, RosenmanM SB, Colio LG. Bacillomycin: An Antibiotic from Bacillus subtilis Active against Pathogenic Fungi∗. *Proc Soc Exp Biol Med*. 1948;67(4):539-541. doi:10.3181/00379727-67-16367

10. Hancock REW, Chapple DS. Peptide Antibiotics. *Antimicrob Agents Chemother*. 1999;43(6):1317-1323. doi:10.1128/aac.43.6.1317

11. Fosgerau K, Hoffmann T. Peptide therapeutics: current status and future directions. *Drug Discov Today*. 2015;20(1):122-128. doi:10.1016/j.drudis.2014.10.003

12. Matejuk A, Leng Q, Begum MD, et al. Peptide-based Antifungal Therapies against Emerging Infections. *Drugs Future*. 2010;35(3):197. doi:10.1358/dof.2010.035.03.1452077

13. Avci FG, Sariyar Akbulut B, Ozkirimli E. Membrane Active Peptides and Their Biophysical Characterization. *Biomolecules*. 2018;8(3):77. doi:10.3390/biom8030077

14. Rautenbach M, Troskie AM, Vosloo JA. Antifungal peptides: To be or not to be membrane active. *Biochimie*. 2016;130:132-145. doi:10.1016/j.biochi.2016.05.013

15. Mode of action of membrane active antimicrobial peptides - Shai - 2002 - Peptide Science - Wiley Online Library. Accessed March 6, 2026. https://onlinelibrary.wiley.com/doi/full/10.1002/bip.10260?casa_token=W8AYr2W9EOAAAAAA%3ANJu6OYGoQkG4C2_y_VqRFMNjgzOtzJMBHjJonddchj0to995v0wnporpSDEr0UdggIRzzuR_70QUxE4

16. Bansal S, Su WC, Budamagunta M, et al. Discovery and mechanistic characterization of a structurally-unique membrane active peptide. *Biochim Biophys Acta BBA - Biomembr*. 2020;1862(10):183394. doi:10.1016/j.bbamem.2020.183394

17. Sani MA, Le Brun AP, Separovic F. The antimicrobial peptide maculatin self assembles in parallel to form a pore in phospholipid bilayers. *Biochim Biophys Acta BBA - Biomembr*. 2020;1862(5):183204. doi:10.1016/j.bbamem.2020.183204

18. Arias M, Piga KB, Hyndman ME, Vogel HJ. Improving the Activity of Trp-Rich Antimicrobial Peptides by Arg/Lys Substitutions and Changing the Length of Cationic Residues. *Biomolecules*. 2018;8(2):19. doi:10.3390/biom8020019

19. De Zotti M, Sella L, Bolzonello A, et al. Targeted Amino Acid Substitutions in a Trichoderma Peptaibol Confer Activity against Fungal Plant Pathogens and Protect Host Tissues from Botrytis cinerea Infection. *Int J Mol Sci*. 2020;21(20):7521. doi:10.3390/ijms21207521

20. Carney RP, Thillier Y, Kiss Z, et al. Combinatorial Library Screening with Liposomes for Discovery of Membrane Active Peptides. *ACS Comb Sci*. 2017;19(5):299-307. doi:10.1021/acscombsci.6b00182

21. Lam KS, Liu R, Miyamoto S, Lehman AL, Tuscano JM. Applications of one-bead onecompound combinatorial libraries and chemical microarrays in signal transduction research. *Acc Chem Res*. 2003;36(6):370-377. doi:10.1021/ar0201299

22. Lam KS, Salmon SE, Hersh EM, Hruby VJ, Kazmierski WM, Knapp RJ. A new type of synthetic peptide library for identifying ligand-binding activity. *Nature*. 1991;354(6348):82-84. doi:10.1038/354082a0

23. Sarin VK, Kent SBH, Tam JP, Merrifield RB. Quantitative monitoring of solid-phase peptide synthesis by the ninhydrin reaction. *Anal Biochem*. 1981;117(1):147-157. doi:10.1016/0003-2697(81)90704-1

24. Lam KS, Lebl M. Synthesis of a One-Bead One-Compound Combinatorial Peptide Library. In: Cabilly S, ed. *Combinatorial Peptide Library Protocols*. Humana Press; 1998:1-6. doi:10.1385/0-89603-392-9:1

25. Angelova MI, Dimitrov DS. Liposome electroformation. *Faraday Discuss Chem Soc*. 1986;81(0):303-311. doi:10.1039/DC9868100303

26. Su WC, Gettel DL, Chabanon M, Rangamani P, Parikh AN. Pulsatile Gating of Giant Vesicles Containing Macromolecular Crowding Agents Induced by Colligative Nonideality. *J Am Chem Soc*. 2018;140(2):691-699. doi:10.1021/jacs.7b10192

27. van Meer G, Voelker DR, Feigenson GW. Membrane lipids: where they are and how they behave. *Nat Rev Mol Cell Biol*. 2008;9(2):112-124. doi:10.1038/nrm2330

28. van Meer G, de Kroon AIPM. Lipid map of the mammalian cell. *J Cell Sci*. 2011;124(1):58. doi:10.1242/jcs.071233

29. Collins MD, Gordon SE. Giant Liposome Preparation for Imaging and Patch-Clamp Electrophysiology. *J Vis Exp JoVE*. 2013;(76):50227. doi:10.3791/50227

30. Espinel-Ingroff A, Fothergill A, Peter J, Rinaldi MG, Walsh TJ. Testing Conditions for Determination of Minimum Fungicidal Concentrations of New and Established Antifungal Agents for Aspergillus spp.: NCCLS Collaborative Study. *J Clin Microbiol*. 2002;40(9):3204-3208.
doi:10.1128/jcm.40.9.3204-3208.2002

Chapter 4 Conclusion and Future directions

Despite fungal pathogens being responsible for 3.8 million deaths annually, research on fungal pathogenesis receives only 1.5% of all infectious disease research funding. [1,2] This disproportionately low funding for fungal pathogen research is a significant problem because (1) it hinders the ability to combat rising mortality rates from invasive fungal infections, (2) there is a surge in drug-resistant strains and (3) the existing drug arsenal that we have for these infections are limited, toxic and largely ineffective. In this dissertation we use *Cryptococcus neoformans* (*Cn*) as a model fungal pathogen and propose that gaining a mechanistic understanding of how *Cn* infiltrates the central nervous system can elucidate novel host and pathogen targets for new antifungal therapeutics.

Investigating the pathogenesis of *Cn* is crucial because it is the leading cause of fatal meningoencephalitis in immunocompromised populations. People living with HIV/AIDS are the primary and leading risk factor for Cryptococcal meningoencephalitis (CM). Annually, this opportunistic fungal pathogen causes approximately 220,000 cases of HIV- associated CM and 180,000 deaths. Additionally, *Cn* has detrimental effects on other immunocompromised populations including organ transplant patients, cancer patients and those on immunosuppressants, causing high long-term morbidity and 20-30% mortality. [3,4]

Beyond the established threat to immunocompromised individuals, there is a possibility that *Cn* can evolve to establish infection in immunocompetent hosts as well. Research indicates this fungal pathogen is undergoing rapid adaptation, enhancing its pathogenic potential. Not only are strains of *Cn* developing drug resistance to fluconazole, but it is increasingly found in patients alongside the bacterial pathogen *Mycobacterium tuberculosis* with pathoadaptive mutations resulting in higher mortality rates. [5–7,10] Furthermore, global warming is driving the evolution of fungal pathogens by selecting for increased thermal tolerance, accelerating genetic mutations,

enhancing drug resistance and enhancing reproduction of fungi, leading to higher spore counts and increased infection rates in humans. [8]

This dissertation provides complementary strategies to better understand and therapeutically target cryptococcal disease by identifying the host protein complex that facilitates the transcellular crossing of *Cn* into the central nervous system and advancing the development of selective antifungal membrane-active peptides.

Overview of each chapter

In chapter 1 we aimed to provide the reader with an overview of how the exchange between the brain parenchyma and the blood is regulated and how pathogens have developed mechanisms to infiltrate the CNS. We discussed the impact of the neuropathogenic fungi, *Cn* and the inadequacy of the current treatment options for the disease it causes, CM. We provided the reader with an overview of the neuropathogenesis of *Cn* and the gaps in knowledge concerning the molecular mechanisms that facilitate *cryptococcal* invasion of the BBB. Lastly, we proposed that the tyrosine kinase receptor, EphA2 could serve as a potential therapeutic target to block the transcellular crossing of *Cn* into the CNS and a new de novo antifungal peptide, k-oLBF127 that targets the membrane of *Cn*.

Our aim in chapter 2 was to use a BBB organoid model along with traditional 2D models of the BBB to evaluate how the EphA2 receptor facilitates the transcellular crossing of *Cn* across the BBB. In a previous study, our lab established that the EphA2, plays a vital role in the transcytosis of *Cn* into the CNS.[9] Here, we propose how EphA2 becomes activated during *Cn* infection, and how its downstream signaling pathway leads to an endocytic event that could cause BMECs to engulf *Cn*.

We began with validating a novel BBB organoid model for neural cryptococcosis that we use throughout this study. To better replicate the 3D, multicellular and physiological microenvironment, we generated BBB organoids that consisted of a 1:1:1 ratio of brain

microvascular endothelial cells (BMECs), pericytes and astrocytes. We validated these organoids by using immunofluorescence and fluid phase marker, FITC dextran, to show expression of cellular markers of the BBB and to assess the integrity of the organoid endothelium respectively. Next, we recapitulated what has been observed in previous *Cn* studies using the traditional 2D monolayer of BMECs to establish that the BBB organoids is a robust neuropathogenic tool. Using transmission electron microscopy, we demonstrated membrane ruffling of the BMECs in organoids exposed to *Cn* and the transcytosis of *Cn* into the organoids. Conversely, we also show that no transcytosis occurs in organoids exposed to *Saccharomyces cerevisiae* (a nonneuropathogenic fungi) or in organoids with BMECs lacking EphA2.

Due to the size of *Cn* and its ability to induce membrane ruffling of BMECs, we hypothesized that macropinocytosis was the endocytic mechanism responsible for the transcellular crossing of *Cn* across the BBB. Macropinocytosis is an actin-dependent, nonselective endocytic mechanism where cells engulf large amounts of extracellular fluid and solutes. We proved that EphA2 signaling stimulates macropinocytosis to facilitate cryptococcal entry into immortalized BMECs (iBMECs). We demonstrated that the transcytosis of Cn was sensitive to amiloride (a sodium/proton inhibitor known to specifically inhibit macropinocytosis), that EphA2 downstream signaling activates rho GTPase, cdc42 (a known required enzyme for macropinocytosis), and that *Cn* induces large fluid uptake in iBMECs (another unique hallmark of macropinocytosis). In contrast, in iBMECs lacking EphA2, we did not see an increase in active cdc42, nor did we see any fluid uptake in cells in the presence nor absence of *Cn*.

Furthermore, we provide evidence that receptor cross talk between EphA2 and host glycoprotein CD44 is what facilitates the transcellular uptake of *Cn*. The evidence gathered implies that *Cn* activates CD44 via HA, and activated CD44 transactivates EphA2 to facilitate BBB crossing. iBMECs exposed to mutant *Cn* cells unable to produce HA, were unable to stimulate an activation of GTPase cdc42, using Alphafold3 we found plausible binding sites on CD44 and EphA2 that could facilitate an interaction, and we used biochemical assays including proximity

ligation assay and co-immunoprecipitation assay to confirm their interaction in *Cn* infected iBMECs.

Altogether, the evidence gathered in chapter 2, elucidates the initial molecular pathway that permits the transcellular migration of *Cn* into the CNS and we have identified EphA2 as a potential therapeutic target for novel antifungal drugs. EphA2 is known for inducing cytoskeletal rearrangements and prior to this study, has only been linked to stimulating clathrin-mediated endocytosis. In addition to its effect on the cytoskeleton, EphA2 has also been noted to affect the arrangement of junction proteins between cells. Given its high expression on BMECs, and a previous study suggesting that EphA2 contributes to BBB degradation during cerebral malaria pathogenesis, it is possible that *Cn* uses EphA2 to permit a transcellular and paracellular opening for it to infiltrate the BBB. However, before we can consider EphA2 as a serious therapeutic target, additional studies are needed. Future studies should: evaluate the contribution of EphA2 in *Cn* pathogenesis in vivo, identify the specific sites where EphA2 and CD44 interact, determine if EphA2 activation has an impact on junction proteins of the BBB during *Cn* infection and track migration of macropinosomes once *Cn* has been engulfed by BMECS.

In Chapter 3, we transition to the development of a novel antifungal peptide. Antifungal peptides offer rapid, direct action, and multifaceted mechanisms. In chapter 3, we proposed the use of a one-bead, one-compound (OBOC) combinatorial library method to develop new membrane active, fungicidal peptides that demonstrate selectivity toward fungal membranes over mammalian membranes. We used this method to assess the activity of a peptide library against giant unilamellar vesicles (GUVs) either with fungal membrane composition or mammalian membrane composition and identified one membrane active peptide that was fungal selective, called LBF127. Next, we made a series of modifications to optimize the peptide including N and C terminus truncations, alanine substitutions and lysine additions. After using minimum inhibitory concentration assays, IC50 and flow cytometry analysis of propidium iodide, we found that the modified peptide, k-oLBF127 had increased antifungal potency and decreased hemolytic activity.

Finally, we also tested the peptide in vivo and found that k-oLBF127 reduces the fungal burden in the lungs of *Cn* infected mice.

Our studies in chapter 3 propose a more efficient screening method for antimicrobial peptide drug development and identifies a promising new membrane active antifungal peptide, koLBF127. While k-oLBF127 is an attractive potential drug candidate for CM, more research is required. Future studies should include: identifying the specific fungal membrane target of koLBF127, the long-term systemic effects of the peptide, determining if it can be used in conjunction with the current therapeutics of CM and determine if it can reduce fungal burden in the brain.

References

1. Rodrigues ML, Nosanchuk JD. Fungal diseases as neglected pathogens: A wake-up call to public health officials. *PLoS Negl Trop Dis*. 2020;14(2):e0007964. doi:10.1371/journal.pntd.0007964

2. Tan C, Wu A, Li C. Forty years of global research on WHO's four critical priority fungal pathogens: Advances and prospects. *J Infect Public Health*. 2025;18(11):102947. doi:10.1016/j.jiph.2025.102947

3. Mourad A, Perfect JR. The war on cryptococcosis: A Review of the antifungal arsenal. *Mem Inst Oswaldo Cruz*. 2018;113(7):e170391. doi:10.1590/0074-02760170391

4. Wang F, Wang Y, He J, et al. Clinical Characteristics and Risk Factors for Mortality in Cryptococcal Meningitis: Evidence From a Cohort Study. *Front Neurol*. 2022;13:779435. doi:10.3389/fneur.2022.779435

5. Mondon P, Petter R, Amalfitano G, et al. Heteroresistance to Fluconazole and Voriconazole inCryptococcus neoformans. *Antimicrob Agents Chemother*. 1999;43(8):18561861. doi:10.1128/aac.43.8.1856

6. Chen YC, Chang TY, Liu JW, et al. Increasing trend of fluconazole-non-susceptible Cryptococcus neoformans in patients with invasive cryptococcosis: a 12-year longitudinal study. *BMC Infect Dis*. 2015;15(1):277. doi:10.1186/s12879-015-1023-8

7. Nguyen MH, Barchiesi F, McGough DA, Yu VL, Rinaldi MG. In vitro evaluation of combination of fluconazole and flucytosine against Cryptococcus neoformans var. neoformans. *Antimicrob Agents Chemother*. 1995;39(8):1691-1695. doi:10.1128/aac.39.8.1691

8. Williams SL, Toda M, Chiller T, Brunkard JM, Litvintseva AP. Effects of climate change on fungal infections. *PLOS Pathog*. 2024;20(5):e1012219. doi:10.1371/journal.ppat.1012219

9. Aaron PA, Jamklang M, Uhrig JP, Gelli A. The blood–brain barrier internalises Cryptococcus neoformans via the EphA2-tyrosine kinase receptor. *Cell Microbiol*. 2018;20(3):e12811. doi:10.1111/cmi.12811

10. Ross O, Liliane M, Dambuza I. Cryptococcus neoformans responds to presence of mycobacterium by 2 diversifying its morphologies and remodelling its capsular material. bioRxiv. 2025. [Preprint].doi:10.1101/2025.11.16.687457

.